INL/RPT-22-69040
Revision 0

Comparison of AGR-3/4 Fission Product Transport Model to Measurements and Extraction of Diffusivities via Analytical Fits

September 2022

Adriaan A. Riet
John D. Stempien

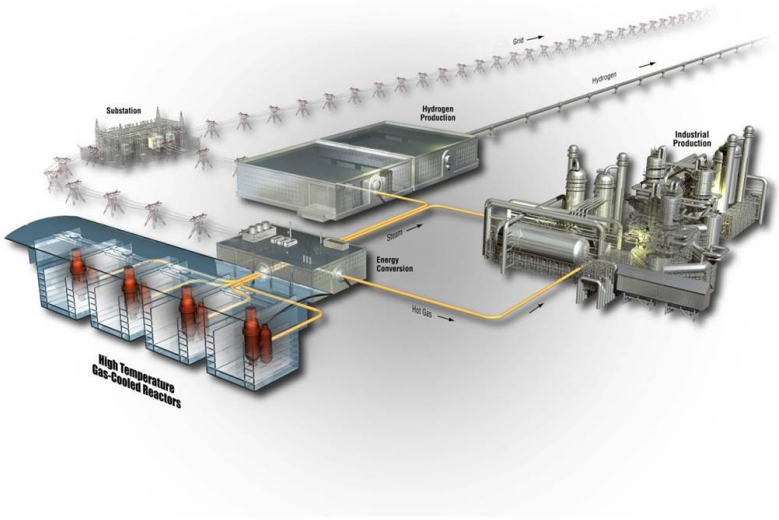

Changing the World's Energy Future

Idaho National Laboratory

INL/RPT-22-69040
Revision 0

Comparison of AGR-3/4 Fission Product Transport Model to Measurements and Extraction of Diffusivities via Analytical Fits

Adriaan A. Riet
John D. Stempien

September 2022

Idaho National Laboratory
Advanced Reactor Technologies
Idaho Falls, Idaho 83415

http://www.ART.INL.gov

Prepared for the
U.S. Department of Energy
Office of Nuclear Energy
Under DOE Idaho Operations Office
Contract DE-AC07-05ID14517

Page intentionally left blank

INL ART Program

Comparison of AGR-3/4 Fission Product Transport Model to Measurements and Extraction of Diffusivities via Analytical Fits

INL/RPT-22-69040
Revision 0

September 2022

Technical Reviewer: (Confirmation of mathematical accuracy, and correctness of data and appropriateness of assumptions.)

William F. Skerjanc — 9/13/2022
William Skerjanc — Date

Approved by:

Travis Mitchell — 9/13/2022
Travis R. Mitchell — Date
ART Program Manager

Paul Demkowicz — 9/13/2022
Paul A. Demkowicz — Date
AGR Program Technical Director

Michelle Sharp — 9/13/2022
Michelle T. Sharp — Date
INL Quality Assurance

ABSTRACT

A one-dimensional (1D) finite-element model based on the Multiphysics Object-Oriented Simulation Environment (MOOSE) framework has been constructed, and overall transport estimates are predicted based on available diffusivities and sorption isotherms in the extant literature. The predicted transport profiles are compared to experimental results, where such results are available, including total inventory analysis of gamma emitters, liquid scintillation results for Sr-90 concentrations, radial deconsolidation leach-burn-leach within compacts, tomographic reconstructions based on detailed gamma scanning and destructive physical sampling of several rings. The magnitude of expected transport to the sink ring is generally predicted by the model for silver and cesium; however, the modeled detailed concentration profiles are not consistent with experimental results. Strontium and europium transport is not well characterized by model results.

Page intentionally left blank

CONTENTS

ABSTRACT iv
ACRONYMS xiv
1. OVERVIEW 1
1.1 Overall Program Purpose 1
1.2 Purpose of AGR-3/4 1
1.3 AGR-3/4 Fuel Description 1
1.4 AGR-3/4 Test Train, Irradiation, Graphite, and Graphitic Rings 3
2. METHODS 5
2.1 Inventory Analysis 5
2.2 Physical Sampling 6
2.3 Fuel Compact Radial Deconsolidation 6
2.4 Finite-Element Method Model 6
3. COMPARISON OF MODEL PREDICTIONS AND PIE MEASUREMENTS 10
3.1 Capsule 1 11
3.1.1 Cesium 12
3.1.2 Silver 12
3.1.3 Strontium 13
3.1.4 Europium 13
3.2 Capsule 2 14
3.2.1 Cesium 14
3.2.2 Silver 15
3.2.3 Strontium 16
3.2.4 Europium 16
3.3 Capsule 3 17
3.3.1 Cesium 17
3.3.2 Silver 18
3.3.3 Strontium 18
3.3.4 Europium 19
3.4 Capsule 4 20
3.4.1 Cesium 20
3.4.2 Silver 21
3.4.3 Strontium 21
3.4.4 Europium 22
3.5 Capsule 5 22
3.5.1 Cesium 23
3.5.2 Silver 23

3.5.3 Strontium 24
3.5.4 Europium 25
3.6 Capsule 6 26
3.6.1 Cesium 26
3.6.2 Silver 26
3.6.3 Strontium 27
3.6.4 Europium 28
3.7 Capsule 7 28
3.7.1 Cesium 28
3.7.2 Silver 29
3.7.3 Strontium 30
3.7.4 Europium 30
3.8 Capsule 8 31
3.8.1 Cesium 31
3.8.2 Silver 32
3.8.3 Strontium 32
3.8.4 Europium 33
3.9 Capsule 9 34
3.9.1 Cesium 34
3.9.2 Silver 35
3.9.3 Strontium 35
3.9.4 Europium 36
3.10 Capsule 10 36
3.10.1 Cesium 37
3.10.2 Silver 37
3.10.3 Strontium 38
3.10.4 Europium 38
3.11 Capsule 11 39
3.11.1 Cesium 40
3.11.2 Silver 40
3.11.3 Strontium 41
3.11.4 Europium 41
3.12 Capsule 12 42
3.12.1 Cesium 42
3.12.2 Silver 43
3.12.3 Strontium 44
3.12.4 Europium 44
4. DISCUSSION 45
4.1 Cesium 50

4.2 Silver 51
4.3 Strontium 51
4.4 Europium 51
5. CONCLUSIONS AND FUTURE WORK 52
6. REFERENCES 53
Appendix A Custom MOOSE InterfaceKernel 57

FIGURES

Figure 1. Image of an AGR-3/4 fuel compact (left) and x-ray side view image (right) (Hunn, Trammell, and Montgomery 2011) 2
Figure 2. Axial cutaway diagram of a standard AGR-3/4 irradiation capsule. 3
Figure 3. Geometry of the finite-element model. The designed-to-fail region and driver particle region are modeled as homogenous volumes with a defined source term. Gas gaps are modeled explicitly. 7
Figure 4. General layout of figures. Results for compacts and each ring are given in Figures 5–52. A representative average diffusion-weighted average temperature across the compact and each ring are shown on the top of the figure. Gas gaps are visible as vertical lines between the capsules (regions of zero concentration). Tomographic reconstruction data are semi-transparent, and where multiple tomographic measurements of the same ring are available, a filled region between concentration estimates is shown. 11
Figure 5.: Capsule 1 cesium concentration profile. Experimental results are on the order of modeled behavior from literature transport parameters. The partially obscured Cs-137 OR inventory measurement overlaps the green line modeling results using transport parameters from (Hoinkis 1994; Hayashi and Fukuda 1989). 12
Figure 6. Capsule 1 silver concentration profile. Model predictions using literature transport parameters are compared against available measurements. Open symbols denote a value derived from an MDA. 13
Figure 7. Capsule 1 strontium concentration profile. Model predictions using literature transport parameters are compared against available measurements. 13
Figure 8. Capsule 1 europium concentration profile. Model predictions using literature transport parameters for strontium are compared against available measurements. Open symbols denote values derived from MDAs. 14
Figure 9. Capsule 2 cesium concentration profile. Model predictions using literature transport parameters are compared against available measurements. 15
Figure 10. Capsule 2 silver concentration profile. Model predictions using literature transport parameters are compared against available measurements. Open symbols denote a value derived from an MDA. 15
Figure 11. Capsule 2 strontium concentration profile. Model predictions using literature transport parameters are compared against available measurements. 16

Figure 12. Capsule 2 europium concentration profile. Model predictions using literature transport parameters are compared against available measurements. Open symbols denote a value derived from an MDA. 17

Figure 13. Capsule 3 cesium concentration profile. Model predictions using literature transport parameters are compared against available measurements. The diamond symbols represent the inventory in small nubs on the OR outer surface that were used to center the OR inside the sink ring during irradiation. 18

Figure 14. Capsule 3 silver concentration profile. Model predictions using literature transport parameters are compared against available measurements. The diamond symbol represents the inventory in small nubs on the OR outer surface that were used to center the OR inside the sink ring during irradiation. 18

Figure 15. Capsule 3 strontium concentration profile. Model predictions using literature transport parameters are compared against available measurements. The diamond symbol represents the inventory in small nubs on the OR outer surface that were used to center the OR inside the sink ring during irradiation. 19

Figure 16. Capsule 3 europium concentration profile. Model predictions using literature transport parameters for strontium are compared against available measurements. An open symbol denotes a value derived from an MDA. 20

Figure 17. Capsule 4 cesium concentration profile. Model predictions using literature transport parameters are compared against available measurements. 21

Figure 18. Capsule 4 silver concentration profile. Model predictions using literature transport parameters are compared against available measurements. 21

Figure 19. Capsule 4 strontium concentration profile. Model predictions using literature transport parameters are compared against available measurements. 22

Figure 20. Capsule 4 europium concentration profile. Model predictions using literature transport parameters for strontium are compared against available measurements. Open symbols denote values derived from MDAs. 22

Figure 21. Capsule 5 cesium concentration profile. Model predictions using literature transport parameters are compared against available measurements. The Cs-134 and Cs-137 inventory measurements in the sink ring are within 1% of each other and the markers overlap. 23

Figure 22. Capsule 5 silver concentration profile. Model predictions using literature transport parameters are compared against available measurements. Open symbols denote values derived from MDAs. 24

Figure 23. Capsule 5 strontium concentration profile. Model predictions using literature transport parameters are compared against available measurements. Open symbols denote values derived from MDAs. 25

Figure 24. Capsule 5 europium concentration profile. Model predictions using literature transport parameters for strontium are compared against available measurements. Open symbols denote values derived from MDAs. 25

Figure 25. Capsule 6 cesium concentration profile. Model predictions using literature transport parameters are compared against available measurements. 26

Figure 26. Capsule 6 silver concentration profile. Model predictions using literature transport parameters are compared against available measurements. Open symbols denote a value derived from an MDA. 27

Figure 27. Capsule 6 strontium concentration profile. Model predictions using literature transport parameters are compared against available measurements. 27

Figure 28. Capsule 6 europium concentration profile. Model predictions using literature transport parameters for strontium are compared against the available measurement. Open symbols denote a value derived from an MDA. 28

Figure 29. Capsule 7 cesium concentration profile. Model predictions using literature transport parameters are compared against available measurements. The diamond symbols represent the inventory in small nubs on the OR outer surface that were used to center the OR inside the sink ring during irradiation. 29

Figure 30. Capsule 7 silver concentration profile. Model predictions using literature transport parameters are compared against available measurements. The diamond symbol represents the inventory in small nubs on the OR outer surface that were used to center the OR inside the sink ring during irradiation. 29

Figure 31. Capsule 7 strontium concentration profile. Model predictions using literature transport parameters are compared against available measurements. The diamond symbol represents the inventory in small nubs on the OR outer surface that were used to center the OR inside the sink ring during irradiation. 30

Figure 32. Capsule 7 europium concentration profile. Model predictions using literature transport parameters for strontium are compared against available measurements. The diamond symbol represents the inventory in small nubs on the OR outer surface that were used to center the OR inside the sink ring during irradiation. 31

Figure 33. Capsule 8 cesium concentration profile. Model predictions using literature transport parameters are compared against available measurements. 32

Figure 34. Capsule 8 silver concentration profile. Model predictions using literature transport parameters are compared against available measurements. The open symbol denotes a value derived from an MDA. 32

Figure 35. Capsule 8 strontium concentration profile. Model predictions using literature transport parameters are compared against available measurements. 33

Figure 36. Capsule 8 europium concentration profile. Model predictions using literature transport parameters are compared against available measurements. Open symbols denote values derived from an MDA. 34

Figure 37. Capsule 9 cesium concentration profile. Model predictions using literature transport parameters are compared against available measurements. 35

Figure 38. Capsule 9 silver concentration profile. Model predictions using literature transport parameters are compared against available measurements. Open symbols denote values derived from an MDA. 35

Figure 39. Capsule 9 strontium concentration profile. Model predictions using literature transport parameters are compared against available measurements. 36

Figure 40. Capsule 9 europium concentration profiles. Model predictions for europium use literature transport parameters from strontium. The open symbol denotes a value derived from an MDA. 36

Figure 41. Capsule 10 cesium concentration profile. Model predictions using literature transport parameters are compared against available measurements. The diamond symbols represent the inventory in small nubs on the OR outer surface that were used to center the OR inside the sink ring during irradiation. 37

Figure 42. Capsule 10 silver concentration profile. Model predictions using literature transport parameters are compared against available measurements. Open symbols denote values derived from MDAs..... 38

Figure 43. Capsule 10 strontium concentration profile. Model predictions using literature transport parameters are compared against available measurements. The diamond symbol represents the inventory in small nubs on the OR outer surface that were used to center the OR inside the sink ring during irradiation. Open symbols denote values derived from MDAs..... 38

Figure 44. Capsule 10 europium concentration profile. Model predictions using literature transport parameters for strontium are compared against available measurements. Open symbols denote values derived from MDAs..... 39

Figure 45. Capsule 11 cesium concentration profile. Model predictions using literature transport parameters are compared against available measurements..... 40

Figure 46. Capsule 11 silver concentration profile. Model predictions using literature transport parameters are compared against available measurements..... 40

Figure 47. Capsule 11 strontium concentration profile. Model predictions using literature transport parameters are compared against available measurements. 41

Figure 48. Capsule 11 europium concentration profile. Model predictions for europium used literature transport parameters from strontium. Only the sink ring was measured from this FB, and its europium-154 content was below the MDA. The MDA is depicted using an open symbol. 42

Figure 49. Capsule 12 cesium concentration profile. Model predictions using literature transport parameters are compared against available measurements. The diamond symbols represent the inventory in small nubs on the OR outer surface that were used to center the OR inside the sink ring during irradiation. 43

Figure 50. Capsule 12 silver concentration profile. Model predictions using literature transport parameters are compared against available measurements. The diamond symbol represents the inventory in small nubs on the OR outer surface that were used to center the OR inside the sink ring during irradiation. Open symbols denote values derived from an MDA (in this case, all measured values)..... 43

Figure 51. Capsule 12 strontium concentration profile. Model predictions using literature transport parameters are compared against available measurements. The diamond symbol represents the inventory in small nubs on the OR outer surface that were used to center the OR inside the sink ring during irradiation. 44

Figure 52. Capsule 12 europium concentration profile. Model predictions using literature transport parameters for strontium are compared against available measurements. The diamond symbol represents the inventory in small nubs on the OR outer surface that were used to center the OR inside the sink ring during irradiation. Open symbols denote values obtained from an MDA..... 45

TABLES

Table 1. As-fabricated particle dimensions and standard deviations from Table A-2 of Collin (2015a). 3

Table 2. AGR-3/4 capsule types, ring materials, and ring dimensions from PIE (Stempien et al. 2016). Complete sets of dimensions and uncertainties are available in Stempien (et al. 2016). 4

Table 3. Freundlich sotherm parameters used in this study. 8

Table 4. Literature diffusion parameters used to model transport through matrix and graphite materials within the AGR 3/4 capsules. 9

Table 5. Calculated to measured ratio of total capsule inventories for the IR of selected capsules. Predictions with agreement to within a factor of ten are highlighted. 46

Table 6. Calculated to measured ratio of ring inventories for the OR of selected capsules. Predictions with agreement to within a factor of ten are highlighted. 47

Table 7. Ratio of calculated to measured inventories for the sink ring of selected capsules. Predictions in agreement to within a factor of ten are highlighted. 49

Page intentionally left blank

ACRONYMS

1D	one-dimensional
2D	two-dimensional
AGR	Advanced Gas Reactor Program
DTF	Designed-to-fail
FB	Fuel Body
FIMA	fissions per initial metal atom
HTGR	High Temperature Gas-Cooled Reactor
IAEA	International Atomic Energy Agency
IPyC	pyrolytic carbon (inner layer)
IR	Inner ring
MDA	Minimum Detectable Activity
MOOSE	Multiphysics Object-Oriented Simulation Environment
OPyC	pyrolytic carbon (outer layer)
OR	Outer ring
ORNL	Oak Ridge National Laboratory
PGS	Precision Gamma Scanner
PIE	Post-irradiation examination
R-DLBL	Radial deconsolidation leach, burn, leach
SiC	Silicon Carbide
TAVA	time-average-volume-average
TRISO	Tristructural isotopic nuclear fuel particle

Page intentionally left blank

Comparison of AGR-3/4 Fission Product Transport Model to Measurements and Extraction of Diffusivities via Analytical Fits

1. OVERVIEW

1.1 Overall Program Purpose

The Advanced Gas Reactor (AGR) Fuel Development and Qualification Program was established to perform research and development on tristructural isotropic (TRISO)-coated particle fuel to support deploying a high-temperature gas-cooled reactor (HTGR). This work continues as part of the Advanced Reactor Technologies Program. To achieve these goals, the program includes the elements of fuel fabrication, irradiation, post-irradiation examination (PIE), safety/heating testing, fuel performance modeling, and fission product transport (Mitchell and Demkowicz 2020). Several fuel-irradiation experiments have been performed at the Advanced Test Reactor (ATR) at Idaho National Laboratory (Mitchell and Demkowicz 2020), and AGR-5/6/7, the fourth and final irradiation, was completed on July 22, 2020. These experiments are intended to provide data on fuel performance under irradiation, support fuel fabrication process development, qualify fuel for operating and accident conditions, provide irradiated fuel for accident testing, and support the development of fuel performance and fission product transport models.

1.2 Purpose of AGR-3/4

The AGR-1, AGR-2, and AGR-5/6/7 experiments focused on the performance of high-quality TRISO fuel, and PIE focused on quantifying the very small rates of Silicon Carbide (SiC) and TRISO coating failures. In contrast, the AGR-3/4 experiment was primarily a fission product transport experiment focused on observing the migration of fission products throughout the fuel, graphitic matrix material, and nuclear-grade graphites in the presence of exposed fuel kernels (Collin et al. 2018). The experiment consisted of fuel compacts containing TRISO-coated driver-fuel particles similar to AGR-1 baseline fuel (Collin 2015a; Hunn and Lowden 2007; Hunn et al. 2014) and designed-to-fail (DTF) particles that are designed to release fission products during irradiation to migrate through the surrounding cylindrical rings of graphitic matrix and nuclear-grade graphite. Following irradiation, PIE measurements of the fission inventories and spatial distributions (axially and radially) within AGR-3/4 samples (primarily the graphite rings and compacts) were completed (Harp, Stempien, and Demkowicz 2020; Riet 2022; Stempien 2021). These data will be used to support refinement of fission product transport models and HTGR source-term analyses.

1.3 AGR-3/4 Fuel Description

A feature of AGR-3/4 fuel that sets it apart from AGR-1 and AGR-2 was the incorporation of 20 DTF particles in each compact in addition to the approximately 1,898 TRISO-coated “driver” fuel particles. DTF fuel kernels were coated only with a thin (20-μm-thick) pyrocarbon layer. This layer was intentionally fabricated with high anisotropy, so it would be likely to fail during the irradiation (Collin 2015a; Hunn and Miller 2009; Kercher et al. 2011), resulting in up to 20 exposed fuel kernels per compact. As shown on the right in Figure 1, the DTF particles (highlighted in red) were aligned roughly along the compact radial centerline. DTF particles provided a known source of fission products to migrate radially outward in the compacts and into the surrounding concentric rings of graphite and/or matrix material. It was expected that intact DTF particles would behave like TRISO particles with SiC layer failures (e.g., releasing substantial Cs but retaining fission gases), and failed DTF particles (DTF particles with breached pyrocarbon layers) would behave like TRISO particles with failed TRISO coatings (e.g., releasing both Cs and fission gases).

The white particles in Figure 1 are the driver particles. AGR-3/4 driver particle fuel kernels were fully TRISO-coated with a buffer layer, inner pyrolytic carbon (IPyC) layer, SiC layer, and outer pyrolytic carbon (OPyC) layer with characteristics similar to the "baseline" variant from the AGR-1 experiment (Collin 2015b; Hunn and Lowden 2007). Both the AGR-3/4 driver and DTF fuel particles contain UCO fuel kernels (approximately 350 µm in diameter) manufactured at BWX Technologies (BWXT) Nuclear Operations Group (Lynchburg, VA). The U-235 enrichment was 19.7 wt%. The DTF pyrocarbon coating and the driver-fuel TRISO coatings were applied to the kernels at Oak Ridge National Laboratory (ORNL). Driver particle and DTF particle properties are summarized in (Collin 2015a). Complete kernel and particle characterization and fabrication data are compiled in several reports and papers (Hunn and Kercher 2006; Hunn and Lowden 2007; Hunn and Miller 2009; Kercher et al. 2011). Driver-fuel particles and DTF particles had average dimensions, as summarized in Table 1.

AGR-3/4 driver and DTF particles were overcoated with a precursor to graphitic matrix material and formed into cylindrical fuel compacts at ORNL. The compact graphitic matrix material is composed of graphite and a carbonized phenolic resin. Compacts were nominally 12.3 mm in diameter and 12.5 mm long (in contrast to the AGR-1 and AGR-2 compacts, which were approximately 12.3 mm in diameter and 25 mm long). A summary of AGR-3/4 fuel compact properties is provided in the AGR-3/4 Final As-Run Report (Collin 2015a). Detailed characterization data of the as-fabricated compacts were compiled in an ORNL report (Hunn, Trammell, and Montgomery 2011).

In the X-Y compact naming convention, X denotes the capsule number, and Y denotes the level of the compact within the capsule (with level 1 at the bottom and level 4 at the top of the capsule). In AGR-3/4, there were four compacts per capsule. Thus, for example, Compact 3-3 is the third compact from the bottom of Capsule 3, and Compact 12-1 is the bottom compact from Capsule 12.

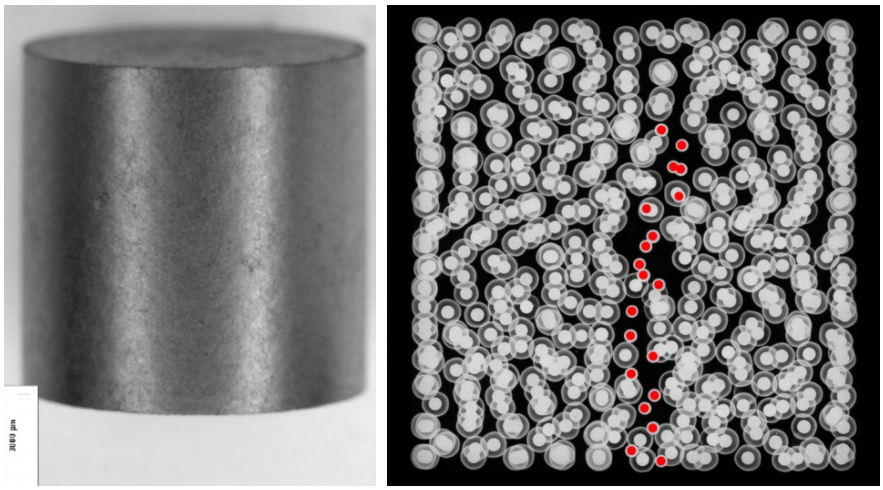

Figure 1. Image of an AGR-3/4 fuel compact (left) and x-ray side view image (right) (Hunn, Trammell, and Montgomery 2011). DTF particles are highlighted with red dots in the x-ray image.

Table 1. As-fabricated particle dimensions and standard deviations from Table A-2 of Collin (2015a).

DTF Particle Properties	
Kernel diameter (µm)	357.3 ± 10.5
DTF pyrocarbon thickness (µm)	20.0 ± 9
DTF particle overall diameter (µm)	400.0 ± 9.2
Driver Particle Properties	
Kernel diameter (µm)	357.3 ± 10.5
Buffer thickness (µm)	109.7 ± 7.7
IPyC thickness (µm)	40.4 ± 2.3
SiC thickness (µm)	33.5 ± 1.1
OPyC thickness (µm)	41.3 ± 2.1
Driver particle overall diameter (µm)	818.9 ± 14.2

1.4 AGR-3/4 Test Train, Irradiation, Graphite, and Graphitic Rings

The AGR-3/4 irradiation test train consisted of 12 capsules numbered 1 through 12 from the bottom to the top of the ATR core (Collin et al. 2018). Each capsule contained four fuel compacts. Figure 2 shows a cross section of an AGR-3/4 irradiation capsule. The compacts were stacked vertically in the center of concentric rings made from graphitic matrix material and/or structural graphite (IG-110 and PCEA). Toyo Tanso IG-110 is an isostatically molded graphite with fine grains, and GrafTech PCEA is an extruded graphite. The matrix rings were produced at ORNL using a recipe similar to the historic German A3-27 formulation (Hunn, Trammell, and Montgomery 2011). These matrix rings were fabricated with a blend of natural and synthetic graphite flake mixed with Hexion SD-1708 novolac resin. BWXT provided this blend of graphite flake and resin to ORNL.

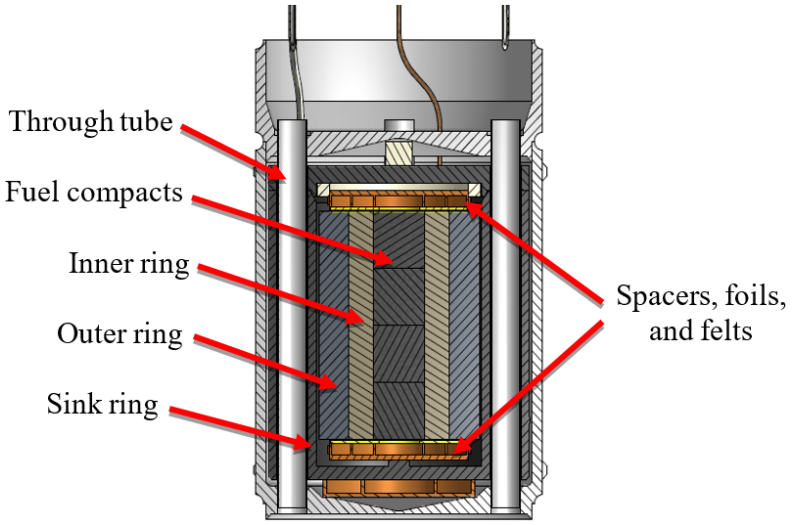

Figure 2. Axial cutaway diagram of a standard AGR-3/4 irradiation capsule.

Table 2 lists the materials, types of capsules, and PIE measurement diameters for each ring. There were two types of capsules: "standard" and "fuel body (FB)." The standard capsule type is depicted in Figure 2 where the outer ring (OR) is open on its top and bottom. Fuel bodies, on the other hand, had floors and a lid that screwed on to the top of the OR. Each capsule also included several small spacers of various materials (graphite, zirconia, or zircaloy-4) and graphite foils to separate components and act as thermal barriers to control temperature in the compacts. Compact lengths were measured as part of PIE, but ring lengths were not measured. All inner rings (IRs) had as-fabricated lengths of 50.8 mm (2.0 in.). In standard capsules, OR lengths were 50.8 mm (2.0 in.). In fuel bodies, the ORs had a sealed bottom and a lid for a total overall length of about 61.0 mm (2.4 in.). Sink ring lengths were generally about 63.5 mm (2.5 in.); however, some sink rings were about 71.1 mm (2.8 in.) long. All sink rings had lids and sealed bottoms. Sink rings had intentionally cold irradiation temperatures to stop further radial transport of fission products during the experiment.

Table 2. AGR-3/4 capsule types, ring materials, and ring dimensions from PIE (Stempien et al. 2016). Complete sets of dimensions and uncertainties are available in Stempien (et al. 2016).

Capsule No.	Capsule Type	Ring Material			IR Diameters (mm)		OR Diameters (mm)		Sink Ring Diameters (mm)	
		Inner	Outer	Sink	ID	OD	ID	OD	ID	OD
1	Std	Matrix	PCEA	PCEA	12.55	23.61	24.53	33.50	41.21	61.59
2	FB	Matrix	PCEA	PCEA	N/A	N/A	N/A	36.72	39.33	62.05
3	Std	PCEA	PCEA	PCEA	12.62	24.03	24.86	33.08	41.42	63.56
4	FB	Matrix	PCEA	PCEA	12.71	23.87	24.70	39.24	39.48	63.32
5	Std	Matrix	PCEA	PCEA	12.67	23.89	24.68	39.39	39.54	63.61
6	FB	Matrix	PCEA	PCEA	N/A	N/A	N/A	39.33	39.48	63.30
7	Std	Matrix	PCEA	PCEA	12.75	23.67	24.93	37.35	39.53	63.63
8	Std	IG-110	IG-110	PCEA	12.60	24.07	24.77	38.55	39.57	63.64
9	FB	Matrix	IG-110	PCEA	N/A	N/A	N/A	39.27	39.46	63.08
10	Std	PCEA	PCEA	PCEA	12.58	24.04	24.83	37.48	39.40	63.43
11	FB	Matrix	PCEA	PCEA	N/A	N/A	N/A	33.29	N/A	N/A
12	Std	Matrix	PCEA	PCEA	12.47	24.23	24.51	34.98	39.34	61.60

Std: standard capsule
N/A: not available

2. METHODS

2.1 Inventory Analysis

To determine the fission product mass balance, each of the 12 irradiation capsules was disassembled, and their component parts were analyzed via gamma spectrometry, mass spectrometry, and gas proportional counting (Stempien 2021). The most commonly detected radionuclides were gamma-emitting Ag-110m, Cs-134, Cs-137, Eu-154, Eu-155, and beta-emitting Sr-90. In "standard" capsules (Capsules 1, 3–5, 7–-8, 10, and 12), IR, OR, sink rings, spacers, foils, felts, and through tubes were all analyzed. The metallic hardware was acid leached, and that leachate was analyzed for gamma-emitting nuclides and Sr-90. Small non-metallic hardware (e.g., spacers, foils, and felts) and the large graphite sink rings were gamma counted using common high-purity germanium detectors before leaching (of ceramic spacers) or burn-leaching (of carbonaceous samples like felts and sink rings) was performed to allow measurement of Sr-90 in the leachate.

The precision gamma scanner (PGS) was used to measure the inventory of gamma-emitting fission products in the compacts and IRs and ORs (Harp, Stempien, and Demkowicz 2020). Select rings were also subjected to tomographic gamma scans on the PGS, and subsequent tomographic reconstructions of those scans was used to produce 1D radial and 2D representations of the fission product spatial distributions in the rings (Riet 2022). In addition to non-destructive gamma spectrometry of entire rings, portions of the IRs and ORs from Capsules 3, 5, 7, 8, 10 and 12 were destructively analyzed for both gamma-emitting nuclides and beta-emitting Sr-90 (see Section 2.2). "FB" Capsules 2, 6, 9, and 11 were retained intact for future heating tests; thus, the compacts, smaller non-metallic items (e.g., spacers), and IR and ORs from these capsules were not measured.

Summing the fission product inventory measured on each capsule component made it clear that the presence of 80 DTF particles in each capsule resulted in noticeably higher releases of cesium (Cs-134 and Cs-137) from AGR-3/4 fuel when compared to AGR-1 and AGR-2 fuel, which did not have DTF particles. Greater than 30 particles' worth of cesium was measured outside of the fuel compacts in Capsules 3-5, 7, 8, and 10. In Capsule 11 (an intact FB for which the IRs and ORs were not measured), 26 particle equivalents of cesium were measured outside of the OR. Based on experience from AGR-1, it is very unlikely that any driver particles failed during the irradiation (Demkowicz et al. 2015); therefore, this cesium is assumed to be overwhelmingly dominated by release from DTF particles (Stempien 2021).

Higher levels of europium and strontium release were also observed in AGR-3/4 when compared to AGR-1, and when compared to most capsules from AGR-2. Tens of particles worth of Eu-154 or Eu-155 were typically measured outside of the fuel compacts (even in the FB capsules for which the mass balance is incomplete). This is largely due to the DTF particles.

When analysis of the data from physical sampling of portions of the IRs and ORs of Capsules 3, 7, 8, and 10 was completed, a Sr-90 balance for the entirety of those rings was estimated and added to the Sr-90 balance contributed from other components of those capsules (e.g., spacers, foils, and metallic hardware). Currently, the estimated AGR-3/4 Sr-90 balances give one to two orders of magnitude higher release than the entire in-pile Sr-90 releases from AGR-1. As in the case of europium, this is due substantially to the DTF particles. More details can be found in INL/EXT-18-46049 (Stempien et al. 2018).

2.2 Physical Sampling

Physical sampling of the rings involved milling material from around the circumference of the rings, collecting that material, and analyzing it for gamma-emitting fission products and beta-emitting Sr-90. The fines from milling each step were collected in individual vials, and those were sent to Pacific Northwest National Laboratory (PNNL) where they were gamma counted for key isotopes such as Ag-110m, Cs-134, Cs-137, Ce-144, Eu-154, and Eu-155. After gamma counting the solid samples (i.e., the fines from milling), the samples were transferred to fused silica beakers and oxidized in a muffle furnace at 750°C for 24 hours. The ash and residue remaining in the beaker was dissolved with HNO_3. In instances where solids did not dissolve using only HNO_3, small amounts of concentrated HF in HNO_3 were used. PNNL reported that solutions with residual solids were centrifuged, the supernate was decanted, and HF and HNO_3 were added. This process was repeated until all solids were dissolved. All the solutions for a given sample were combined. A Sr-90 separation process using an Eichrom strontium resin was then performed for the solutions. After the Sr-90 separation, Sr-90 was quantified by liquid scintillation counting. Knowing the thickness and location of material removed from the ring in each milling step and the fission product inventory in the material collected from each milling step, the radial fission product concentration profiles in the rings were constructed. Further details can be found in INL/EXT-21-62863 (Stempien 2021).

2.3 Fuel Compact Radial Deconsolidation

Selected fuel compacts have been subjected to electrolytic radial deconsolidation-leach-burn-leach (R-DLBL) (Stempien 2017). Radial deconsolidation sequentially removes radial segments of compacts from the outside in so that each segment can be analyzed separately for fission products and a fission product concentration profile can be constructed. In regions of the compact away from the DTF particles, this method gives the fission product inventory in the fuel compact matrix and the OPyC of the driver-fuel particles. In the central region of the compact, where the DTF particles reside, this method gives the fission product inventory retained in the DTF particles, plus that in the fuel compact matrix, and the OPyC of driver-fuel particles surrounding the DTF particles. Radioanalytical work is still in progress on a number of R-DLBLs, and reports detailing the radial deconsolidation work are in progress.

2.4 Finite-Element Method Model

We modeled transport of fission products through the rings in each capsule with the Multiphysics Object-Oriented Simulation Environment (MOOSE) finite-element framework. The capsule dimensions were obtained from post-irradiation metrology (Stempien et al. 2016) where available. Where post-irradiation metrology was not available, dimensions were taken from capsule design documents. The finite-element model simplifies the design of the experiment to a 1D radially symmetric transport problem, as shown in Figure 3 with the center of the capsule on the left and the outer surface of the graphite sink ring on the right.

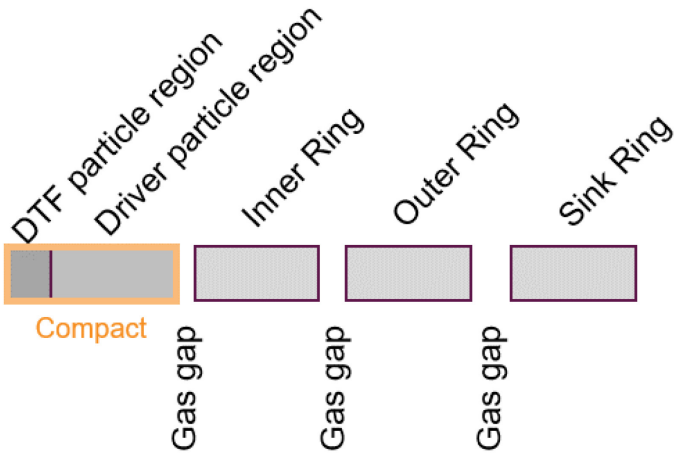

Figure 3. Geometry of the finite-element model. The designed-to-fail region and driver particle region are modeled as homogenous volumes with a defined source term. Gas gaps are modeled explicitly.

The finite-element mesh was generated for each region in Figure 3 by taking linearly spaced samples on the interval [0,1] from a sigmoid cumulative distribution function shown in (1), and scaling for the size of the modeled region. To ensure stability, the total number of mesh elements in each region was adjusted such that the inequality (2) was satisfied for all elements in the simulation.

$$cdf(x) = \frac{\frac{1}{1+\exp(5-10x)}}{\tanh\left(\frac{5}{2}\right)} \tag{1}$$

$$\min\left(\frac{D_0\, exp\left(-\frac{E_a}{RT(x)}\right)}{\Delta x^2}\right) > 1 \tag{2}$$

The temperature at each ring interface was determined as a diffusion-weighted average using the As-Run Thermal report 15-minute-resolution temperature data as a reference (Hawkes 2016). Though the temperature was, strictly speaking, time-dependent, taking a steady-state approximation of the temperature simplified the implementation of the Freundlich isotherm and improved model stability. In practice, during irradiation, temperatures within the capsules were effectively constant for most of the duration of the experiment, with transients only at startup and a temperature increase in the final round of irradiation (Hawkes 2016). The diffusion weighting at each interface was determined with (3), where D_0 and E_a are the pre-exponential factor and activation energy of diffusion in the relevant compact or ring, R is the ideal gas constant, and $T(t)$ is the temperature of the edge of the compact or ring at a given time. The summation is done over time, t.

$$T_{avg} = \frac{\sum\left(D_0\, exp\left(-\frac{E_a}{RT(t)}\right)T(t)\Delta t\right)}{\sum\left(D_0\, exp\left(-\frac{E_a}{RT(t)}\right)\Delta t\right)} \tag{3}$$

The heat generation from the TRISO-coated driver particles and DTF particles was not time-averaged, which may lead to some minor inconsistency in transport within the interior of the compact.

Transport into the gas gaps was accounted for using the Freundlich isotherm (4), where P_{gas} is the vapor-phase pressure in pascals, C_{int} is the concentration of the isotope at the interface in mol/m^3, ρ is the density of the graphite material in g/cm^3 (this converts the concentration to mmol/kg carbon, which are the units in which the isotherm correlation is derived) and A, B, D, E, d_1, and d_2 are experimentally determined. The values of the experimentally determined constants are material dependent, and those used in this work are listed in Table 3.

$$P_{gas} = \begin{cases} \frac{C_{int}}{\rho} exp\left(\left(A + \frac{B}{T}\right) + \left(D - 1 + \frac{E}{T}\right)(d_1 - d_2 T)\right), & C_{int} < (d_1 - d_2 T) \\ \left(\frac{C_{int}}{\rho}\right)^{D+\frac{E}{T}} exp\left(A + \frac{B}{T}\right), & C_{int} > (d_1 - d_2 T) \end{cases} \quad (4)$$

Table 3. Freundlich sotherm parameters used in this study.

	Material Measured	Used to Model	A	B [K]	D	E [K]	d_1	d_2 [1/K]	Reference
Ag	NBG-17	Matrix & Graphite	1.253	-0.1343	-5.594	-0.1579	6.305	4.3445×10^{-3}	(Walton et al. 2021)
Cs	Fuel rod Matrix Material (Ashland A-240)	Matrix	19.3	-47300	1.51	4340	3.4	6.15×10^{-4}	(Myers, et al., 1979)
Cs	Unirradiated H-451	Graphite	24	-35700	-1.56	6120	2.04	1.79×10^{-3}	(Myers, et al., 1979)
Sr		Matrix	54.3	-149000	-8.52	28500	3.13	0	(IAEA 1997)
Sr	H-451 and H-327	Graphite	19.4	-40100	-0.32	4090	-2.12	0	(Myers, et al., 1974)

Many of the values in Table 3 were determined from historical nuclear graphites, so they may vary somewhat from the properties of modern graphites (for example: IG-110, PCEA, NBG-17). There are no experimentally determined values for silver sorption on matrix material, so NBG-17 graphite parameters from (Walton et al. 2021) were used.

The source terms for the model in the DTF and driver regions were obtained using PARticle Fuel ModEl (PARFUME) particle release calculations (Skerjanc 2016). As an input to PARFUME, and for the DTF particle releases, total production of fission products was calculated with JMOCUP (Sterbentz 2015). The boundary conditions on the center of the compact and on the outside of the sink ring are both insulating (i.e., Neumann) boundary conditions with transport across the boundary set to zero. A zero-concentration boundary condition was also investigated on the outside of the sink ring, and no practical difference was observed between the two.

The International Atomic Energy Agency (IAEA) TECDOC-978 (IAEA 1997) provides reference values for diffusion coefficients in historical graphites (see Table 4), which were used to generate a reference set of comparisons against the measured AGR-3/4 PIE data.

Table 4. Literature diffusion parameters used to model transport through matrix and graphite materials within the AGR 3/4 capsules.

Isotope	Material Measured	Used to Model	D_0 [m^2/s]	E_a [kJ/mol]	Reference
Cs	Unirradiated A3-3	Matrix	3.6×10^{-4}	-189	(Hoinkis 1983) as referenced in (IAEA 1997)
Cs		Matrix	3.5×10^{-7}	-116	(IAEA 1997)
Cs	In-pile (Compilation)	Graphite	1.7×10^{-6}	-149	(Myers and Bell 1979)
Cs	IG-110	Graphite	9.0×10^{-6}	-157	(Hayashi et al. 1987)
Cs	IG-110	Graphite	1.2×10^{-4}	-112	(Hayashi and Fukuda 1989)
Cs	In-pile IG-110 (OGL-1)	Graphite	1.7×10^{-4}	-95	(Hayashi et al. 1987)
Cs		Graphite	5.8×10^{-2}	-151	(IAEA 1997)
Ag	A3-3 Unirradiated	Matrix	6.8×10	-262	(Hoinkis 1994)
Ag	A3-27	Matrix	1.3	-246	(Hoinkis 1994)
Ag	A3-3 Irradiated	Matrix	1.6	-258	(Hoinkis 1994; 1983)
Ag		Matrix	8.7×10^{7}	-414	(IAEA 1997)
Ag	H-451	Graphite	1.6	-258	(Causey and Wichner 1981)

Ag	IG-110	Graphite	6.3×10^{-3}	-264	(Hayashi et al. 1987)
Ag		Graphite	1.6×10^{2}	-364	(IAEA 1997)
Sr	A3-3	Matrix	1.0×10^{-2}	-303	(Hensel and Hoinkis 1991)
Sr	"VHTR Matrix graphite"	Matrix	2.8×10^{-4}	-210	(Fukuda, Sawai, and Ikawa 1984)
Sr		Matrix	5.6×10^{-2}	-312	(IAEA 1997)
Sr	(Compilation)	Graphite	1.7×10^{-2}	-268	(Myers and Bell 1974)
Sr		Graphite	8.3×10^{-1}	-324	(IAEA 1997)

Europium was not modeled directly, because relevant transport parameters for Eu are not available, so no PARFUME transport predictions (governing release from the TRISO particles) could be made. We assume instead that strontium and europium share the same transport parameters, and scale the results from strontium transport predictions by the total production of strontium calculated by JMOCUP (Sterbentz 2015). A sample input file, as well as files related to custom MOOSE classes, can be found in Appendix A

3. COMPARISON OF MODEL PREDICTIONS AND PIE MEASUREMENTS

The AGR-3/4 fission product transport model results were compared to measured fission product inventories and spatial distributions for each capsule in the experiment. There are three primary types of measurements obtained in PIE which can be compared against:

1. Total radionuclide inventories – totals measured outside of the fuel compacts and total inventory in individual parts of the test such as the inner, outer, and sink rings.
2. Spatial radionuclide concentrations – gamma tomography provided 2D maps of gamma-emitter distributions at specific axial locations in the IRs and ORs. These have also been used to construct radial fission product concentration profiles. Destructive sampling of selected IRs and ORs has produced radial fission product concentration profiles for both gamma-emitting nuclides and Sr-90. In some cases, rings were sampled at multiple axial locations (Stempien 2021). We compare only against samples at the axial center of the rings here except in the case of silver, which exhibited large axial variations in concentration. These are represented by square ■ or star ☆ markers. On some ORs, small "nubs", protrusions on the surface intended to aid in centering the ring in the cavity, were large enough that a separate sample of fission product concentration was taken at the nubs. These are shown where available and are represented by filled diamond ◊ markers. Nubs were features exclusive to the edge of the rings, so some inconsistency corresponding to the difference in axial location may be expected.
3. Radionuclide inventories in fuel compacts – selected AGR-3/4 fuel compacts were subjected to radial deconsolidation, which gives fission product concentrations in the compact matrix outside the SiC layer of the TRISO-coated driver-fuel as a function of radius in the compact.

Figures 5–52 depict the results of the model described in Section 2.4 using transport parameters recommended in IAEA TECDOC-978. Most were verified from the source publication, with the exception of the work of Nabielek (1981). Each concentration profile has a corresponding cross (×) marker indicating the average modeled concentration within a given ring. The cross markers may be directly compared against the mass-balance report measurements (denoted by a filled circle ● or + symbol) (Stempien et al. 2018) as both show the average inventory for a given ring. In some cases, the measurement of a particular isotope's concentration yielded a result not statistically distinct from zero. For these measurements, an open symbol is shown, denoting the minimum detectable activity (MDA) of that isotope. As such, open symbols denote only an upper bound on the measured concentration. Because the transport calculations were performed in terms of elements, and the measurements quantified specific isotopes, the isotopic measurements are scaled to the modeled overall elemental concentrations using as-calculated isotopic abundances for the two compacts in the center of each capsule. Isotopic abundances were obtained from (Sterbentz 2015). This allows for direct comparisons between the modeled results and the measurement results. Because the diffusion-weighted average temperature varies based on the modeled parameters, each diffusion parameter had a unique temperature profile associated with it (See Section 2.4 and equation (3)). For reference, the average (diffusion-weighted) temperature of the compact, and of each ring as modeled with one set of transport parameters is plotted across the top of Figures 5–52. Figure 4 shows the general layout of Figures 5–52.

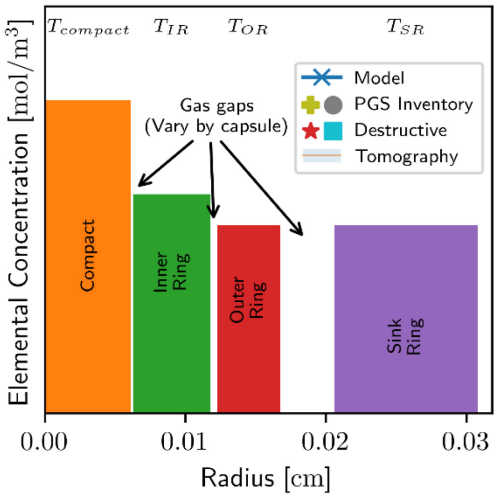

Figure 4. General layout of figures. Results for compacts and each ring are given in Figures 5–52. A representative average diffusion-weighted average temperature across the compact and each ring are shown on the top of the figure. Gas gaps are visible as vertical lines between the capsules (regions of zero concentration). Tomographic reconstruction data are semi-transparent, and where multiple tomographic measurements of the same ring are available, a filled region between concentration estimates is shown.

3.1 Capsule 1

The four Capsule 1 compacts had burnups ranging from 5.43 to 6.85% fissions per initial metal atom (FIMA), with compact fast neutron fluences of 1.42-2.10 (10^{25} n/m^2, E > 0.18 MeV) at the end of irradiation (Collin et al. 2018). The time-average peak temperature within the compacts was 978°C. The time-average-volume-average (TAVA) temperature of the compacts, inner, outer, and sink rings were 927, 853, 765 and 517°C, respectively (Hawkes 2016). The calculated axial variation in temperature was

less than 131°C for the compacts[a], 82°C for the IR and 28°C for the OR. Capsule 1 is a standard capsule, with a matrix media IR, PCEA outer ring, and PCEA sink ring.

3.1.1 Cesium

The total inventories predicted by the model in Section 2.4 for cesium, plotted in Figure 5, are consistent with the overall concentrations measured by Stempien (et al. 2019) for Capsule 1.

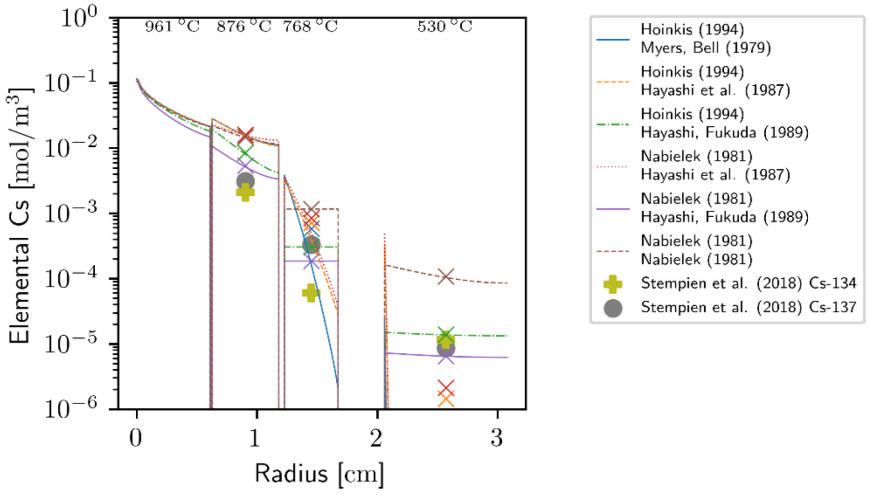

Figure 5.: Capsule 1 cesium concentration profile. Experimental results are on the order of modeled behavior from literature transport parameters. The partially obscured Cs-137 OR inventory measurement overlaps the green line modeling results using transport parameters from (Hoinkis 1994; Hayashi and Fukuda 1989).

3.1.2 Silver

The physics captured in the transport model for silver are not sufficient to explain the transport of silver observed experimentally for Capsule 1, as shown in Figure 6. Though there is no detailed concentration profile data, there is significantly higher transport out of the compacts to the sink ring than was predicted by the modeled literature parameters. This could be due to an underestimation of silver transport at low temperatures and at low concentrations; for example, the referenced paper from Hoinkis (Hoinkis 1994) used a loading of 10^{-4} atomic %, approximately two orders of magnitude higher than the 10^{-6} atomic % measured in the IR. Because the Ag-110m activity in the rings was too low to be reliably measured, the silver concentrations in the IR and ORs were derived from MDAs, so the values shown on Figure 6 are only upper bounds. The measured concentration of silver in the IR is thus between zero and 2.1×10^{-3} mol/m^3, and that of the OR is between zero and 1.6×10^{-3} mol/m^3.

[a] The axial temperature difference is across all four compacts, and was calculated from Figures 56-67 of Hawkes (2016). It was estimated by taking the largest maximum difference in temperature at each radial position for each cycle-average temperature distribution.

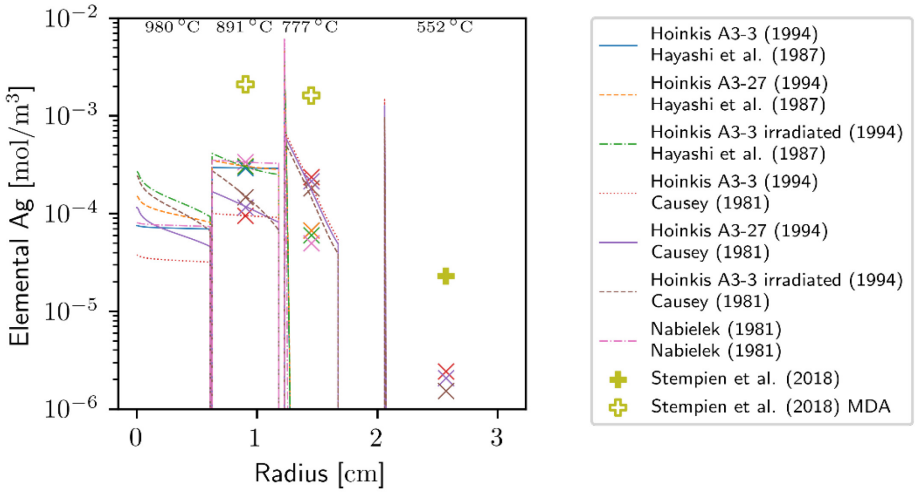

Figure 6. Capsule 1 silver concentration profile. Model predictions using literature transport parameters are compared against available measurements. Open symbols denote a value derived from an MDA.

3.1.3 Strontium

As strontium is not a gamma-emitter, its measurement in carbonaceous materials in the AGR-3/4 experiment must be accomplished via destructive burn-leach methods. The Capsule 1 IR and OR were not subjected to destructive exams, so the only experimental measurement of concentration in a Capsule 1 ring is in the sink ring. Figure 7 shows that the experimentally determined concentration of strontium is much higher than expected from a radially diffusive model employing literature transport parameters. It is possible that the strontium (or a gaseous precursor such as Kr-90 or Rb-90) traveled through gas gaps between the rings, allowing it to deposit on the cool sink ring, and elevating the concentration there.

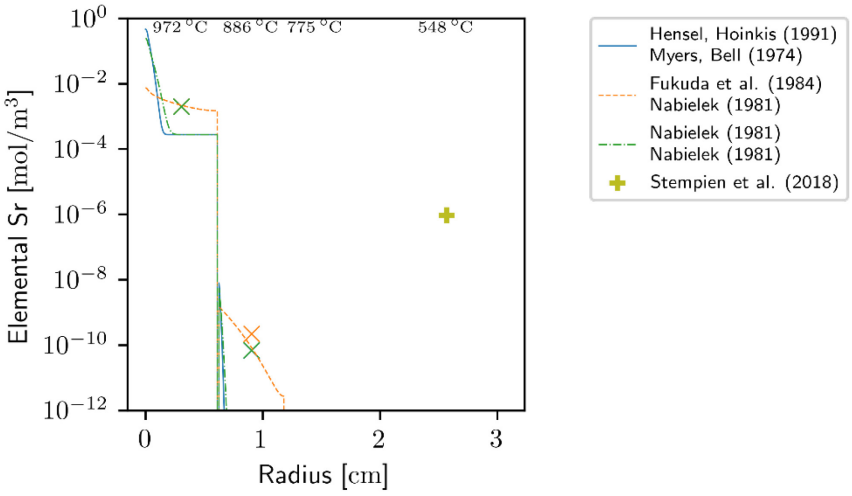

Figure 7. Capsule 1 strontium concentration profile. Model predictions using literature transport parameters are compared against available measurements.

3.1.4 Europium

As noted at the end of Section 2.4, europium transport in Capsule 1 was not modeled directly. Instead, it was assumed that europium transport is similar to strontium transport, and the modeled predictions for

strontium transport were scaled to the total amount of europium calculated to be produced in AGR-3/4. Using literature parameters for strontium to model europium transport underpredicts the amount of europium transport to the IR.

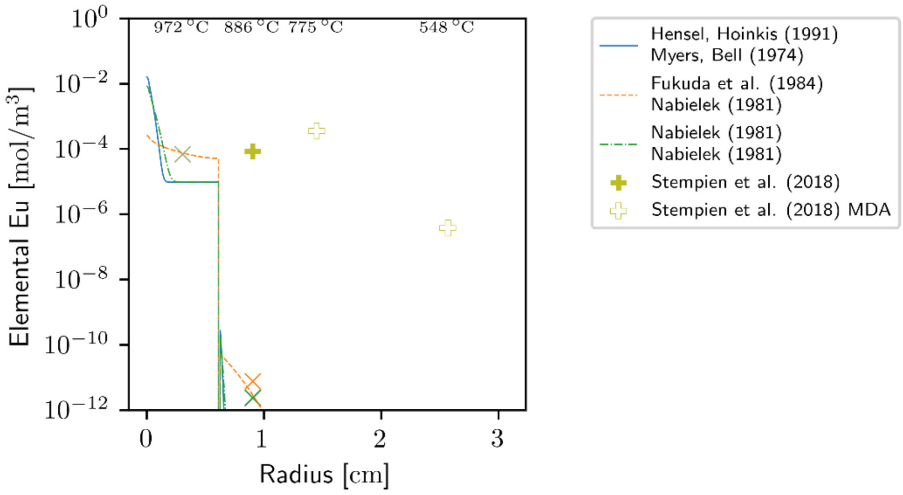

Figure 8. Capsule 1 europium concentration profile. Model predictions using literature transport parameters for strontium are compared against available measurements. Open symbols denote values derived from MDAs.

3.2 Capsule 2

Capsule 2 is a FB capsule with a matrix IR and PCEA outer and sink rings. The OR of this FB was not opened; thus, only the sink ring and some capsule internals were measured for fission products. Capsule 2 had compact burnups of 9.43–10.65% FIMA, with compact fast neutron fluences of 2.95-3.44 (10^{25} n/m^2, E > 0.18 MeV) at the end of irradiation (Collin et al. 2018). The time-average peak temperature within the compacts was 1113°C. The TAVA temperatures of the compacts, inner, outer and sink rings were 1057, 934, 859 and 609°C respectively (Hawkes 2016), and the calculated axial variation in temperature was less than 116°C for the compacts, 50°C for the IR and 30°C for the OR.

3.2.1 Cesium

The experimentally determined average concentration of the sink ring from the mass-balance report (Stempien et al. 2018) is consistent with model predictions using literature parameters, as shown in Figure 9. Generally, Cs-134 is deemed more reliable in the measurements because it is less susceptible to hot-cell contamination than is the longer-lived Cs-137 isotope and because Cs-134 does not have a gaseous precursor complicating the concentration profile.

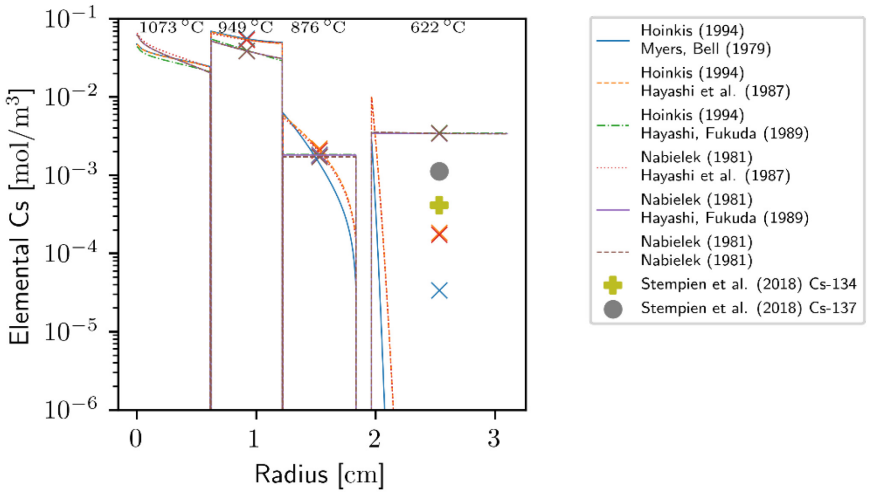

Figure 9. Capsule 2 cesium concentration profile. Model predictions using literature transport parameters are compared against available measurements.

3.2.2 Silver

For Capsule 2, the measured silver concentration in the sink ring shown in Figure 10 is lower than expected from using the literature parameters in the transport model, leading to a conservative estimate. The experimental value for silver concentration in the sink ring is derived from an MDA and, as such, is only a bounding upper limit, not a true concentration measurement (Stempien et al. 2018). The true concentration of silver in the sink ring is thus somewhere between zero and 4.6×10^{-5} mol/m^3.

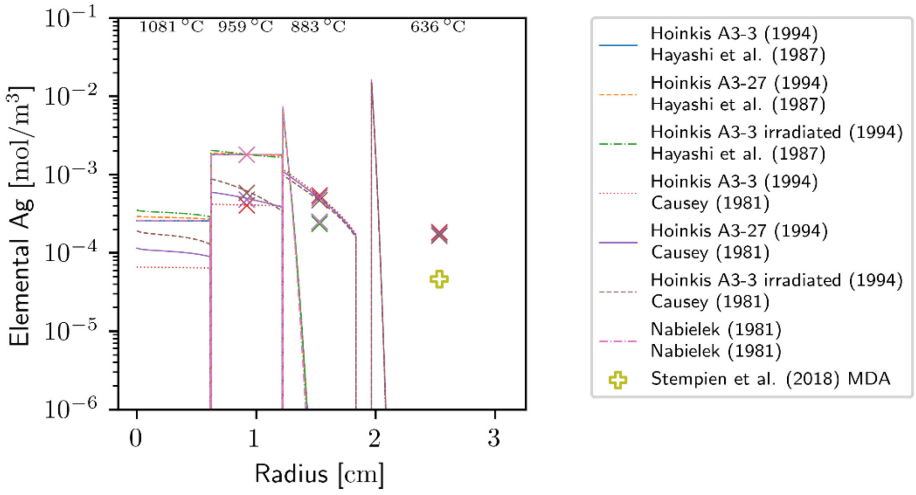

Figure 10. Capsule 2 silver concentration profile. Model predictions using literature transport parameters are compared against available measurements. Open symbols denote a value derived from an MDA.

3.2.3 Strontium

As in Capsule 1, Figure 11 shows that strontium transport in Capsule 2 is significantly underpredicted by every set of literature parameters available. Again, it is possible that there are short-circuit diffusion pathways around the rings that would be available to Sr-90 and its gaseous precursors, which would allow for an increase in the concentration of strontium at the inner edge of the sink ring.

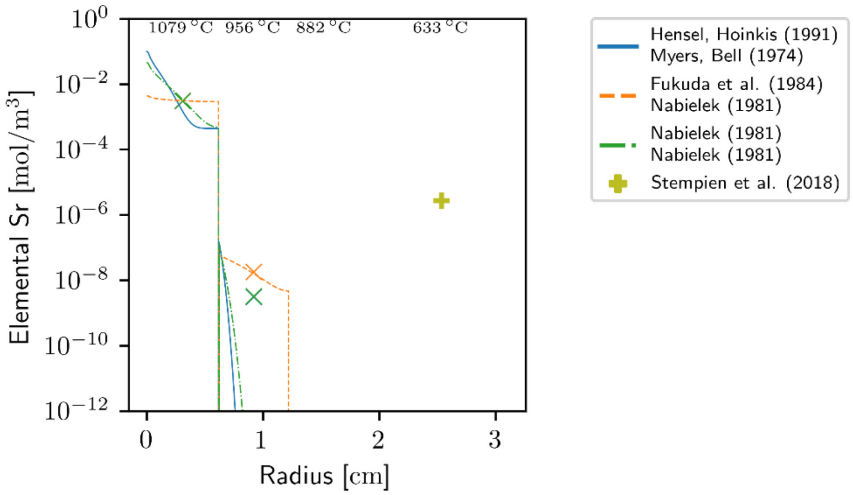

Figure 11. Capsule 2 strontium concentration profile. Model predictions using literature transport parameters are compared against available measurements.

3.2.4 Europium

Because the Capsule 2 FB was not disassembled, only the sink ring was assessed via PIE for its fission product content. No europium-154 was detected in the sink ring. The open symbol denotes a value derived from the MDA for europium-154 in the sink ring. There are no experimental measurements to compare with the europium model prediction in Capsule 2 (Figure 12).

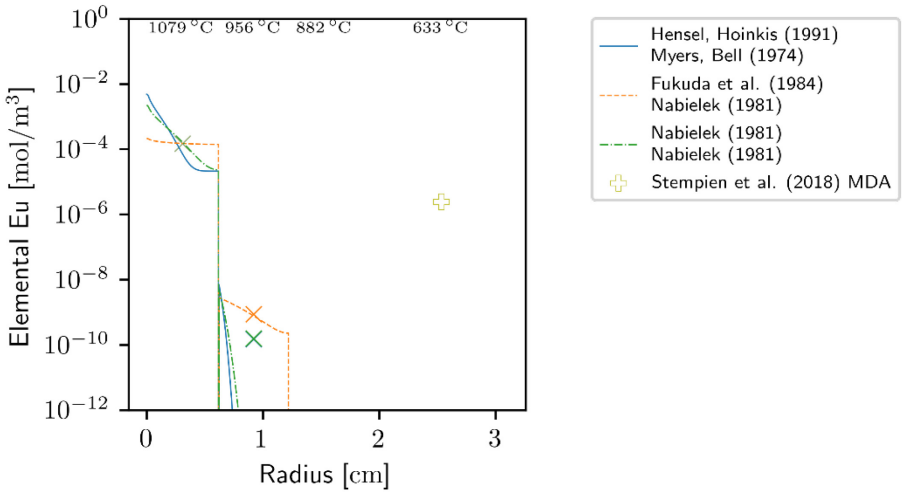

Figure 12. Capsule 2 europium concentration profile. Model predictions using literature transport parameters are compared against available measurements. Open symbols denote a value derived from an MDA.

3.3 Capsule 3

Capsule 3 is a standard capsule, and all the Capsule 3 rings were made from PCEA. Capsule 3 had compact burnups of 12.16–12.93% FIMA, with compact fast neutron fluences of 4.04–4.38 (10^{25} n/m^2, E > 0.18 MeV) at the end of irradiation (Collin et al. 2018). The time-average peak temperature within the compacts was 1242°C. The TAVA temperatures of the compacts, inner, outer, and sink rings were 1177, 1026, 962, and 539°C, respectively (Hawkes 2016). The calculated axial variation in temperature was less than 177°C for the compacts, 54°C for the IR, and 24°C for the OR. The IR and OR of Capsule 3 were subjected to destructive physical sampling to generate radial fission product concentration profiles (Stempien 2021). These data points are included here using star and square symbols in the following plots.

3.3.1 Cesium

Overall transport of cesium in Capsule 3 is well-predicted with models based on literature parameters, which bracket the experimentally determined concentrations. However, there does appear to be more complex phenomena within the compact than a simple diffusive transport model predicts, and the elevated concentration of cesium at the outer surface of the rings is not predicted by the models. This is a possible indicator of unaccounted for transport *around* the rings, possibly through the gaps between the rings which allow for the sweep gas to be carried in and through, see Figure 13.

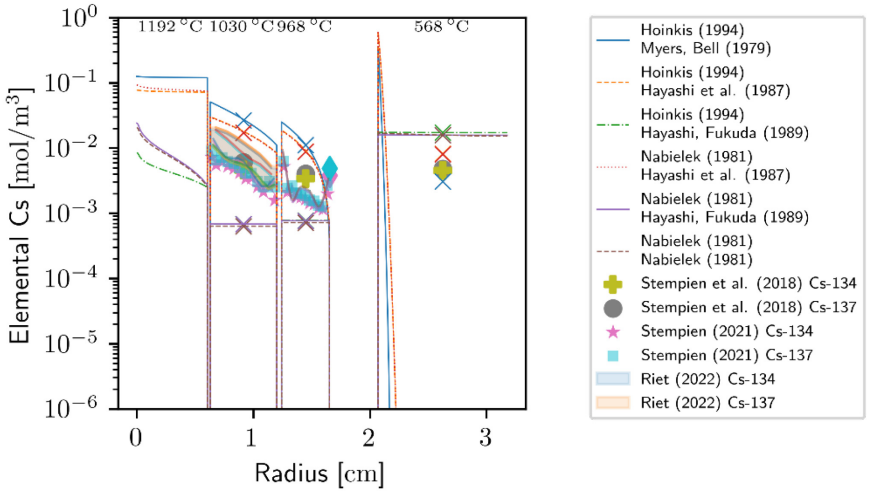

Figure 13. Capsule 3 cesium concentration profile. Model predictions using literature transport parameters are compared against available measurements. The diamond symbols represent the inventory in small nubs on the OR outer surface that were used to center the OR inside the sink ring during irradiation.

3.3.2 Silver

Experimentally measured silver transport in Capsule 3 follows a concentration profile that does not closely resemble diffusive transport. Despite the shape of the concentration profile, the overall transport of silver to the sink ring is predicted to within a factor of ten by the diffusivities found within the literature, suggesting that it may be possible to determine overall silver transport with a diffusion model, though classical diffusion does not seem to be the dominant mode of transport, see Figure 14.

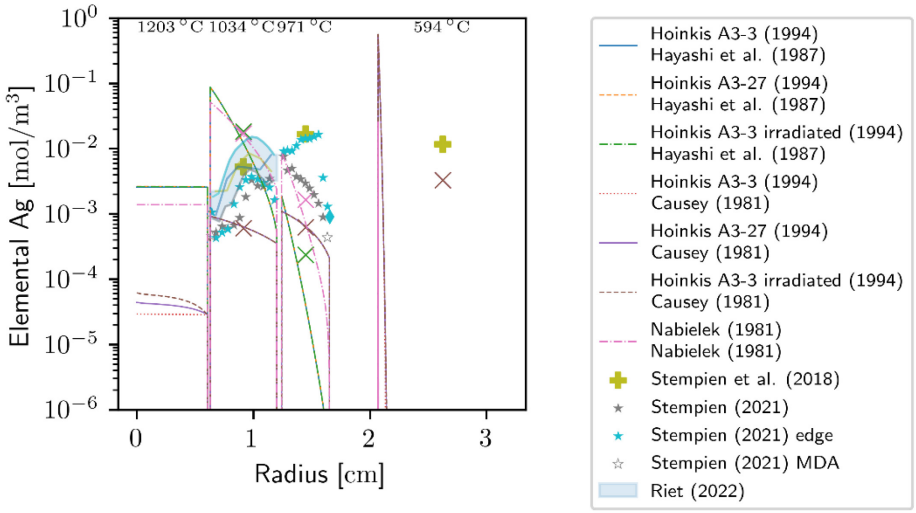

Figure 14. Capsule 3 silver concentration profile. Model predictions using literature transport parameters are compared against available measurements. The diamond symbol represents the inventory in small nubs on the OR outer surface that were used to center the OR inside the sink ring during irradiation.

3.3.3 Strontium

The experimentally determined concentration profiles shown in Figure 15 show that the modeled release of strontium from the particles is smaller than the actual release, as every experimentally

measured concentration of strontium is larger than the model-predicted value. In the case of the sink ring, the difference is severe (the modeled sink ring average concentration is not significant relative to numerical precision). The experimentally determined concentration profiles indicate that there is significant transport around the rings, and possibly a fast-transport regime through the rings, but the profile as a function of radial distance is smooth enough that it may be possible to obtain an effective diffusion coefficient within the ring materials, separate from the overall transport.

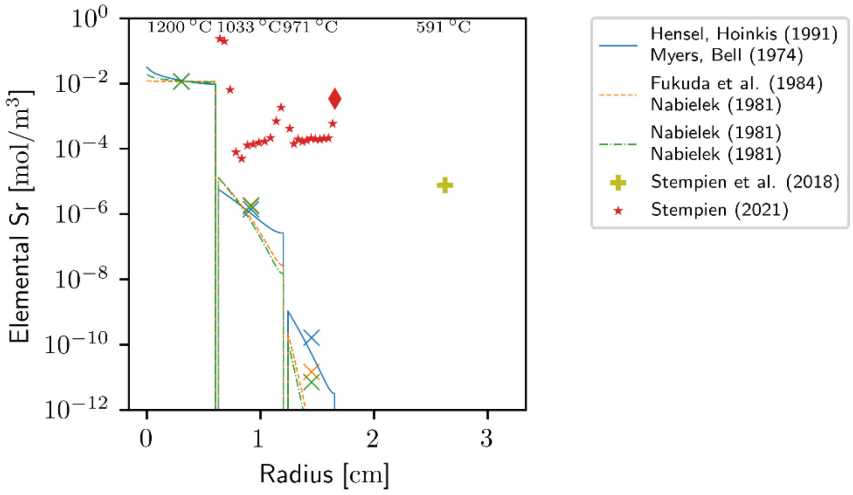

Figure 15. Capsule 3 strontium concentration profile. Model predictions using literature transport parameters are compared against available measurements. The diamond symbol represents the inventory in small nubs on the OR outer surface that were used to center the OR inside the sink ring during irradiation.

3.3.4 Europium

Modeled europium transport through Capsule 3 is in better agreement with experimental results than the modeled transport of strontium through Capsule 3, though transport to the rings is still underpredicted. Note that the physical sampling method is a little more sensitive than the non-destructive gamma scanning method employed for the OR. In the OR, the radial profile determined from the physical sampling is real, with concentrations just below the MDA from the gamma scanned inventory analysis, see Figure 16.

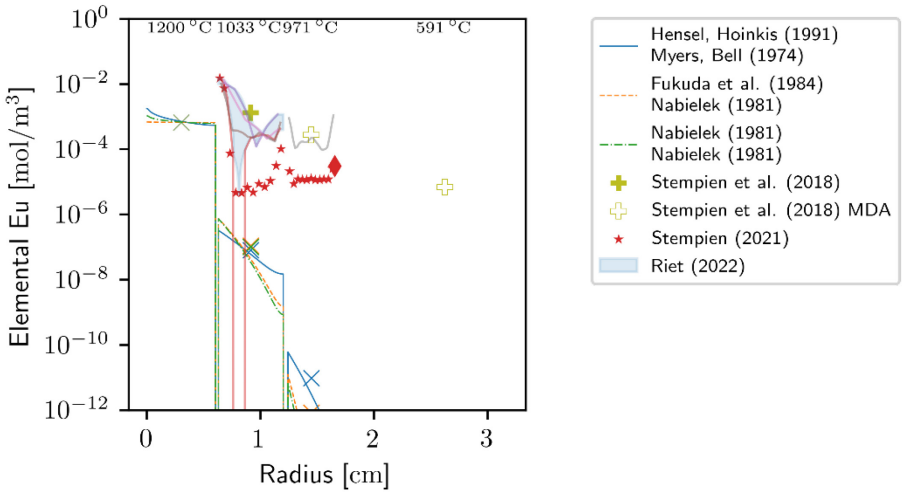

Figure 16. Capsule 3 europium concentration profile. Model predictions using literature transport parameters for strontium are compared against available measurements. An open symbol denotes a value derived from an MDA.

3.4 Capsule 4

Capsule 4 is a FB with a matrix IR and outer and sink rings made from PCEA. Capsule 4 had compact burnups of 13.98–14.41% FIMA, with compact fast neutron fluences of 4.74–4.92 (10^{25} n/m^2, E > 0.18 MeV) at the end of irradiation (Collin et al. 2018). The time-average peak temperature within the compacts was 1084°C. The TAVA temperatures of the compacts, inner, outer, and sink rings were 1008, 820, 708, and 582°C, respectively (Hawkes 2016) and the calculated axial variation in temperature was less than 165°C for the compact, 88°C for the IR and 18°C for the OR.

Capsule 4 was the only FB in the AGR-3/4 experiment that was disassembled and analyzed. Capsules 4 and 5 were the only two capsules where the fuel compacts were stuck in the IRs and had to be forced out using a press in the hot cell (Stempien et al. 2016). Both capsules had similar irradiation conditions (e.g., temperature and fluence), both had rings constructed from the same materials, but one was a FB and one was a standard capsule. Therefore, comparisons between Capsules 4 and 5 may prove meaningful. Thus, it was decided in 2022 that the Capsule 4 rings should be subjected to destructive physical sampling in an attempt to determine whether evidence of axial gas-gap transport seen in other capsules is also present in a FB capsule with its sealed OR. Data from that additional experimental work will be available at the end of 2022.

3.4.1 Cesium

The model predictions for cesium in Capsule 4 are fairly consistent with each other, and are consistent with the experimentally determined inventories. However, the radial profile of the IR (faint line in Figure 17) generated from PGS reconstructions is steeper than the model-predicted value, indicating potentially slower in-graphite transport, but faster transport around the rings. The elevated concentration of cesium measured in the sink ring is consistent with this concept.

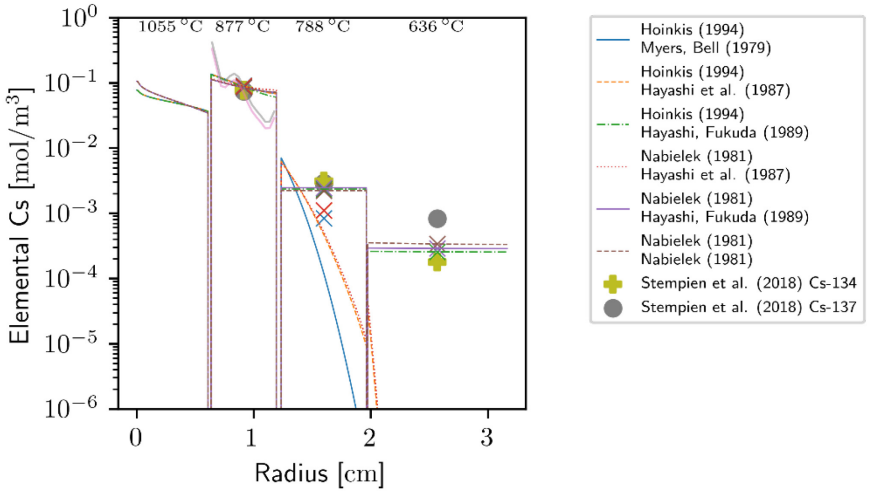

Figure 17. Capsule 4 cesium concentration profile. Model predictions using literature transport parameters are compared against available measurements.

3.4.2 Silver

The total amount of modeled silver transport to the sink ring in Capsule 4 is within an order of magnitude of what was found experimentally, as shown in Figure 18, with much closer agreement for transport into the IR and OR.

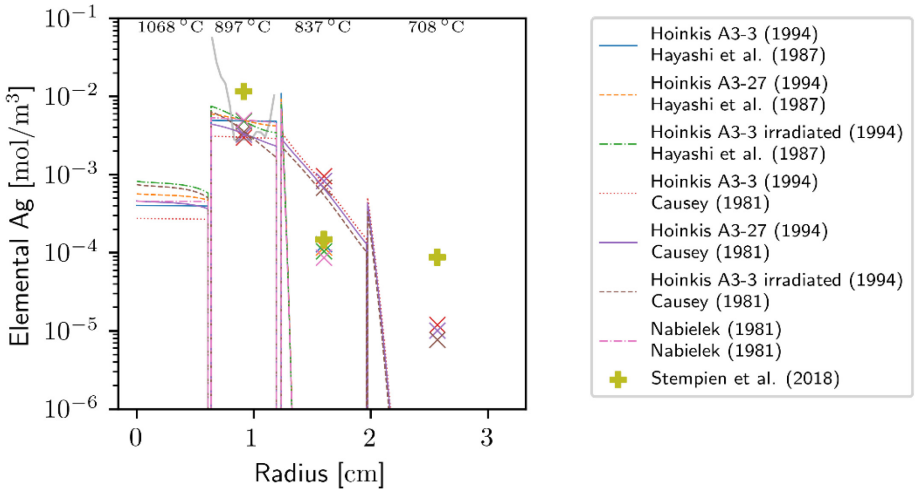

Figure 18. Capsule 4 silver concentration profile. Model predictions using literature transport parameters are compared against available measurements.

3.4.3 Strontium

Strontium transport to Capsule 4's sink ring is strongly underpredicted. As shown in Figure 19, the predicted concentration of the IR's inner surface is lower than the experimentally observed concentration within the sink ring. Once radiochemical analyses of the physical sampling of the Capsule 4 IR and OR have been completed, Sr-90 profiles in those rings can be added to this plot and estimates of the total Sr-90 inventory in the IR and ORs can be made.

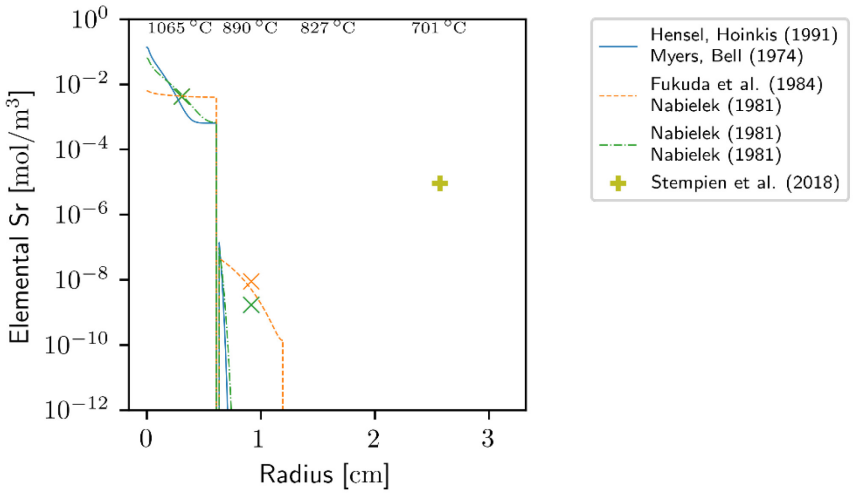

Figure 19. Capsule 4 strontium concentration profile. Model predictions using literature transport parameters are compared against available measurements.

3.4.4 Europium

Europium transport to the IR of Capsule 4 is underpredicted based on tomographic data, which are notably near to the average ring concentration based on MDAs from the gamma scans (Riet 2022), as shown in Figure 20.

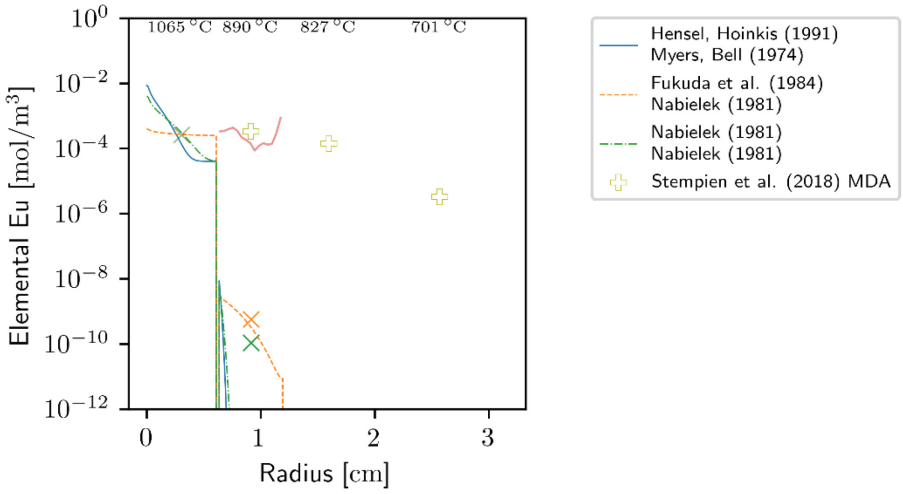

Figure 20. Capsule 4 europium concentration profile. Model predictions using literature transport parameters for strontium are compared against available measurements. Open symbols denote values derived from MDAs.

3.5 Capsule 5

Capsule 5 is a standard capsule with a matrix IR and PCEA outer and sink rings. The fuel in Capsule 5 had compact burnups of 14.74–14.98% FIMA, with compact fast neutron fluences of 5.14–5.23 (10^{25} n/m^2, E > 0.18 MeV) at the end of irradiation (Collin et al. 2018). The time-average peak temperature within the compacts was 1102°C. The TAVA temperatures of the compacts, inner, outer, and sink rings

were 1015, 800, 677, and 546°C, respectively (Hawkes 2016), and the calculated axial variation in temperature was less than 219°C for the compacts, 96°C for the IR, and 27°C for the OR. As stated earlier, Capsules 4 and 5 were the only two capsules where the fuel compacts were stuck in the IRs and had to be forced out using a press in the hot cell (Stempien et al. 2016). Compact 5-4, the uppermost compact in Capsule 5, underwent R-DLBL (see Section 2.3), and those data are included here via triangle symbols. Three radial segments and the central core of the compact were analyzed from the Compact 5-4 R-DLBL.

3.5.1 Cesium

The modeled and experimentally measured cesium concentrations through Capsule 5 are shown in Figure 21. Using literature parameters, the model seems to reasonably approximate transport through the OR and estimate the sink ring average concentration to within an order of magnitude, though the actual mechanism for transport seems to be more complicated than the simple diffusion processes to which the model is currently limited. The measured, steep IR profile would seem to indicate slower transport than predicted by the model, while the increased concentration of cesium in the sink ring relative to the model indicates more overall transport. The measured high concentrations of cesium on the IR's inner surface and the inner and outer surfaces of the OR suggest transport phenomena not captured in the model were active.

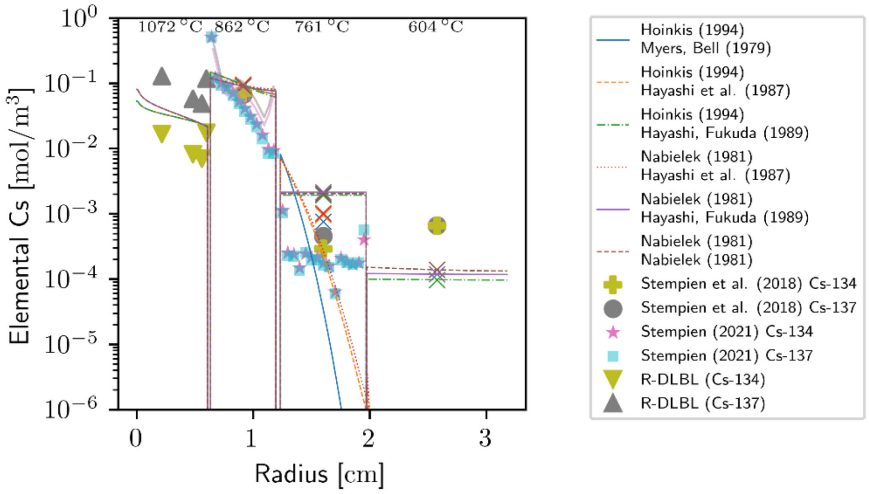

Figure 21. Capsule 5 cesium concentration profile. Model predictions using literature transport parameters are compared against available measurements. The Cs-134 and Cs-137 inventory measurements in the sink ring are within 1% of each other and the markers overlap.

3.5.2 Silver

Experimental measurements of silver transport in Capsule 5 are not entirely self-consistent. The magnitude of the concentrations from the tomographic radial concentration profile for the IR is consistent with the modeled concentrations, though the shape of the profile does not resemble a diffusive profile (faint line in Figure 22). In contrast, destructive measurements and total ring inventories show transport that is slower in the IR, but measurements indicate there is more overall transport to the sink ring than the models predict. Of the measured values, the destructive measurements and overall inventories are likely to be more accurate than the tomographic reconstruction, as they are consistent with each other. Figure 46 of the tomographic reconstruction report shows a signal without a clearly discernable pattern, which implies a small signal-to-noise ratio, in turn increasing the likelihood of "salt and pepper" numerical artifacts in the reconstruction (Figure 61 and Figure 75 of the same report) (Riet 2022). The apparent discrepancy between the gamma spectroscopy based total inventory measurement and the destructive

sampling profile in the OR may be explained by a combination of the high inner surface concentration (which is partially obscured by the model prediction lines) and the phenomenon clearly visible in sections 3.3.2, 3.7.2 and 3.10.2 where higher concentrations of silver are observed at the capsule edges (top or bottom) than at the center.

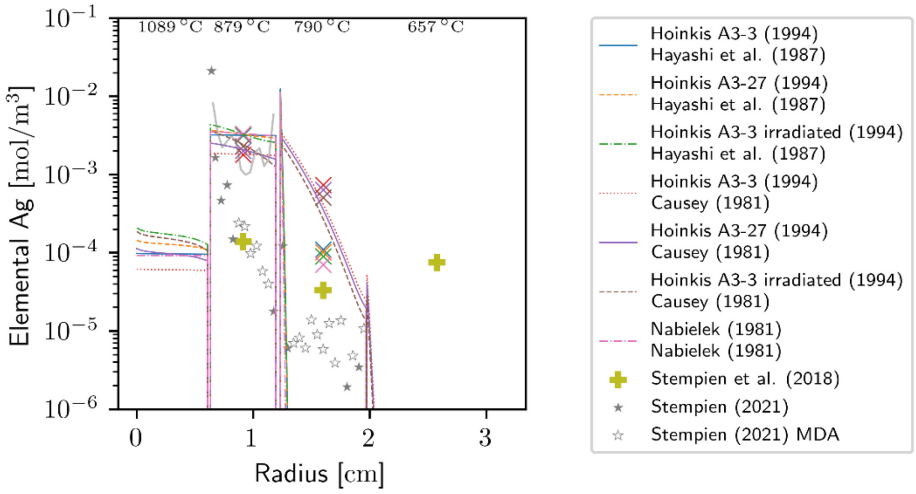

Figure 22. Capsule 5 silver concentration profile. Model predictions using literature transport parameters are compared against available measurements. Open symbols denote values derived from MDAs.

3.5.3 Strontium

The measured transport of strontium in Capsule 5 is not consistent with a 1D radially diffusive mechanism. We observe higher concentrations of strontium within the compact, and relatively constant concentrations of strontium radially through the middle of the OR, suggesting that there may be short-circuit diffusion pathways available, at least to a limiting concentration, after which slower bulk diffusion becomes dominant. Increases in concentration at both the inner and outer edges of the ORs indicate that transport through the rings is not the dominant mode of transport, though we may still be able to estimate the diffusive transport of strontium into the rings by the shape of the profile at the ring edges.

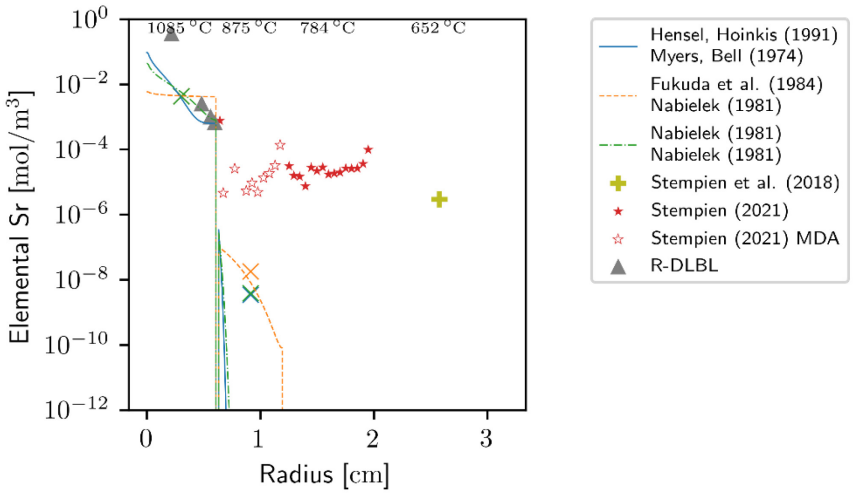

Figure 23. Capsule 5 strontium concentration profile. Model predictions using literature transport parameters are compared against available measurements. Open symbols denote values derived from MDAs.

3.5.4 Europium

The europium concentrations in the compact were modeled using the strontium matrix transport parameters from of Nabielek and Hensel and Hoinkis (Hensel and Hoinkis 1991; IAEA 1997; Nabielek 1981) and are similar to the experimentally measured profile from the Compact 5-4 R-DLBL Figure 24. The model underpredicts the concentrations of europium measured in the IR and OR via the destructive physical sampling method. Outside of the compact, a fast-transport mechanism is indicated by the flat profile of the destructive physical sampling measurements, as shown in Figure 24.

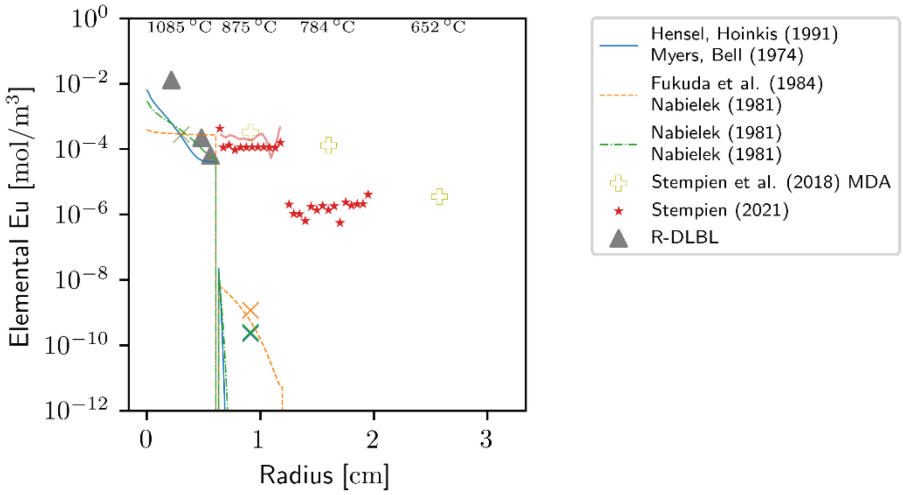

Figure 24. Capsule 5 europium concentration profile. Model predictions using literature transport parameters for strontium are compared against available measurements. Open symbols denote values derived from MDAs.

3.6 Capsule 6

Capsule 6 is a FB capsule with a matrix IR and PCEA outer and sink rings. It was retained intact; therefore, information on the fission product profiles and inventories of the IR and OR is not available. Capsule 6 had compact burnups of 15.21–15.24% FIMA and compact fast neutron fluences of 5.30–5.32 (10^{25} n/m^2, E > 0.18 MeV) at the end of irradiation (Collin et al. 2018). The time-average peak temperature within the compacts was 1133°C. The TAVA temperature of the compacts, inner, outer, and sink rings were 1051, 843, 707, and 603°C, respectively (Hawkes 2016), and the calculated axial variation in temperature was less than 222°C for the compacts, 116°C for the IR, and 27°C for the OR.

3.6.1 Cesium

Using the existing transport parameters from the literature except those of (Hayashi et al. 1987), the model predicts the quantity of cesium transported within Capsule 6 to the sink ring to within a factor of 4 of the measured value, though as shown in Figure 25, the only available experimental data is an overall mass balance of the sink ring.

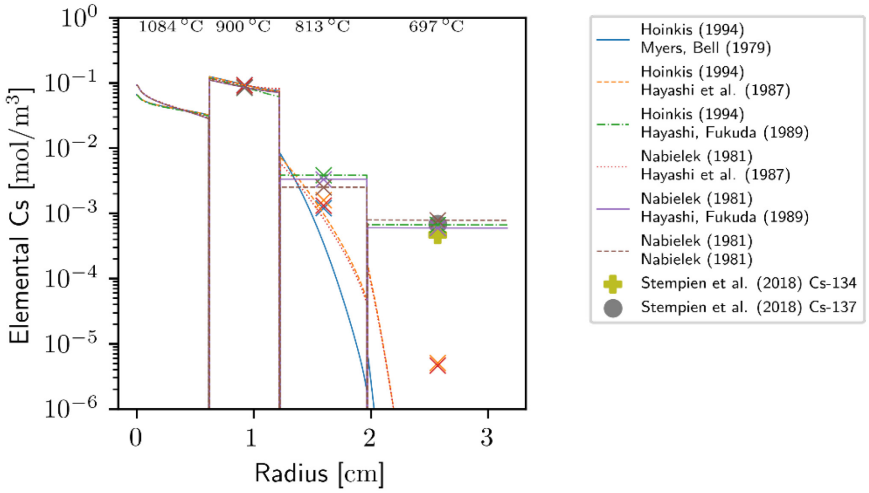

Figure 25. Capsule 6 cesium concentration profile. Model predictions using literature transport parameters are compared against available measurements.

3.6.2 Silver

Given there is only one available measurement to compare against, which is an MDA of the overall concentration of silver in the sink ring and silver transport to the sink ring shown in Figure 26, may be conservatively estimated by the model using transport parameters from the literature. As this comparison relies on an MDA, it is unknown how conservative the estimate is.

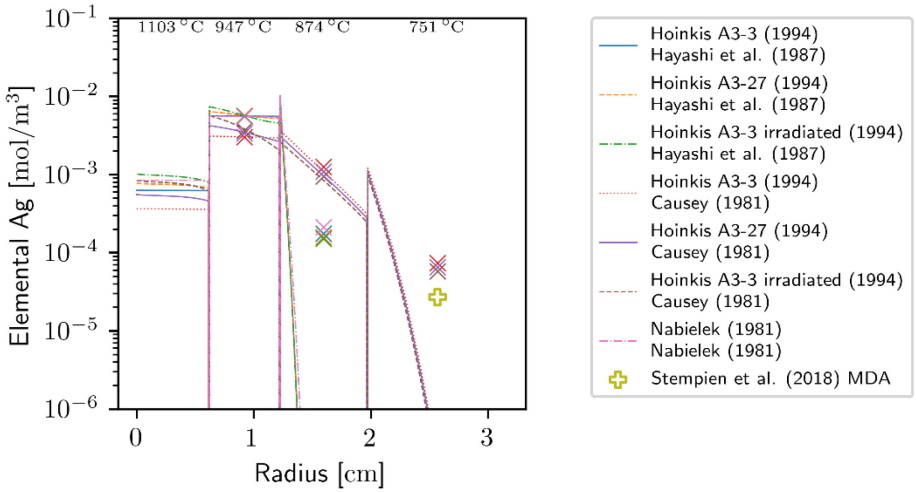

Figure 26. Capsule 6 silver concentration profile. Model predictions using literature transport parameters are compared against available measurements. Open symbols denote a value derived from an MDA.

3.6.3 Strontium

Observed strontium transport to the sink ring is much faster than models based on what the literature predicts for a 1D diffusive model using literature values for transport parameters, shown in Figure 27. Some of the predicted concentrations in the OR are more than six orders of magnitude lower than the observed sink ring concentration.

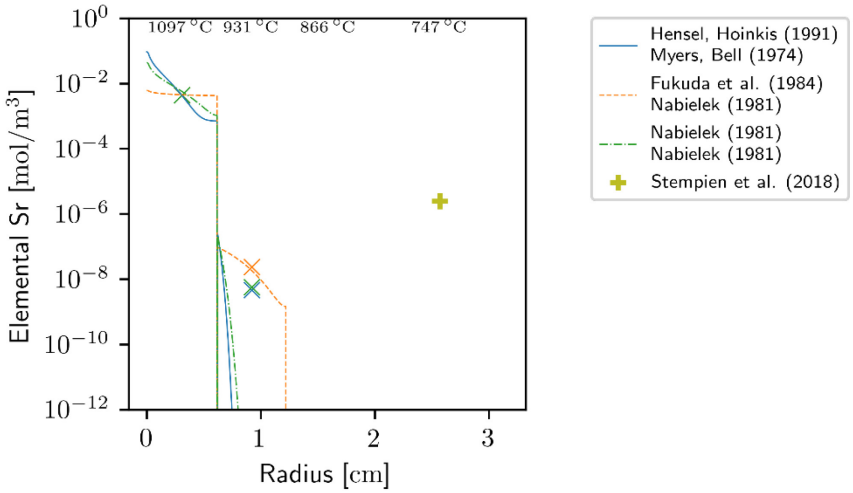

Figure 27. Capsule 6 strontium concentration profile. Model predictions using literature transport parameters are compared against available measurements.

3.6.4 Europium

Figure 28 shows the modeled radial concentration profiles for europium. Again, the strontium transport parameters were used in the absence of available parameters specifically for europium. Only the sink ring of the Capsule 6 FB was measured via gamma spectrometry and destructive burn-leach analyses. No europium-154 was detected in the sink ring; thus, an MDA is shown. There are no available measurement data to compare to in this instance.

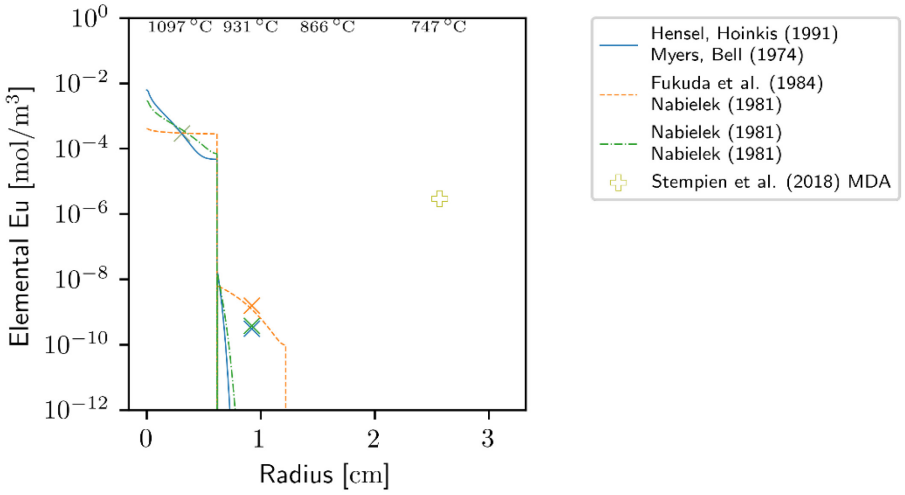

Figure 28. Capsule 6 europium concentration profile. Model predictions using literature transport parameters for strontium are compared against the available measurement. Open symbols denote a value derived from an MDA.

3.7 Capsule 7

Capsule 7 is a standard capsule with a matrix IR and OR, and sink rings made from PCEA. Capsule 7 compacts had burnups of 14.90–15.02% FIMA, with compact fast fluences of 5.24–5.29 (10^{25} n/m^2, E > 0.18 MeV) at the end of irradiation (Collin et al. 2018). The time-average peak temperature within the compacts was 1418°C. The TAVA irradiation temperature of the compacts, inner, outer, and sink rings were 1345, 1151, 1025, and 617°C, respectively (Hawkes 2016), and the calculated axial variation in temperature was less than 192°C for the compacts, 90°C for the IR and 23°C for the OR.

Compact 7-3 underwent R-DLBL which resulted in the analysis of two radial segments, plus the core of the compact that contains the DTF particles (along with the compact matrix and driver particles). The two radial segments had average radii of 5.6 and 4.5 mm. The outermost layer of the radial deconsolidation data has been adjusted to account for what seems to be a single particle failure in the outer layer during the deconsolidation process (not during irradiation) by subtracting the inventory of a single particle from the total.

3.7.1 Cesium

Cesium transport in Capsule 7 is consistent with the model-predicted transport, at least for the rings. Figure 29 shows the experimental and modeled profiles. The measured profile within the capsule seems to have slower overall diffusion with a high surface concentration.

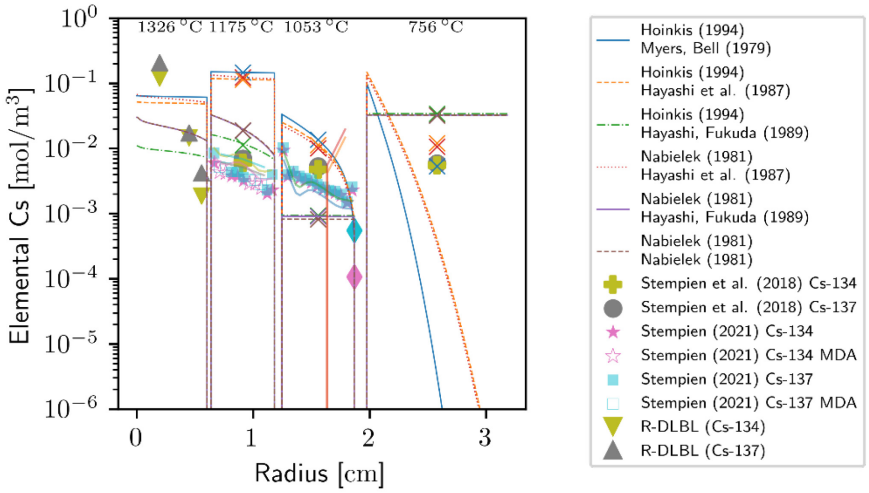

Figure 29. Capsule 7 cesium concentration profile. Model predictions using literature transport parameters are compared against available measurements. The diamond symbols represent the inventory in small nubs on the OR outer surface that were used to center the OR inside the sink ring during irradiation.

3.7.2 Silver

Silver transport through Capsule 7 (Figure 30) presents challenges for interpretation. The radial diffusion models from the literature demonstrate overall transport consistent with the experimentally observed inventories, but the profiles are complicated. The OR of Capsule 7 had nubs to ensure centering inside the sink ring. The concentration of silver in the nubs of Capsule 7's OR was not elevated, suggesting that diffusion through the gas phase around the ring with back-diffusion may not be relevant in this case, an effect which seems to be shared with the cesium results shown in Figure 29.

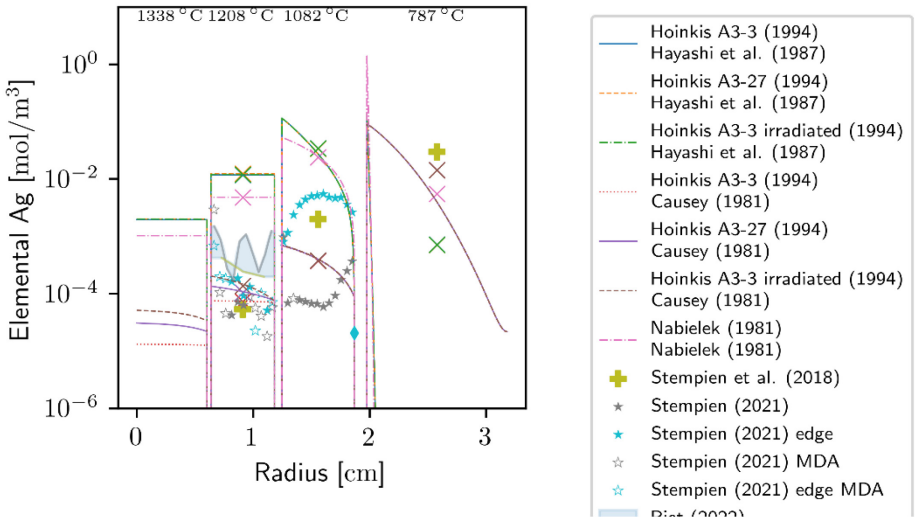

Figure 30. Capsule 7 silver concentration profile. Model predictions using literature transport parameters are compared against available measurements. The diamond symbol represents the inventory in small nubs on the OR outer surface that were used to center the OR inside the sink ring during irradiation.

3.7.3 Strontium

Strontium diffusion in Capsule 7 shown in Figure 31 exhibits smooth concentration profiles, with elevated concentrations at inner and outer surfaces of the rings. The elevated concentration at both surfaces of the capsule indicate transport into the rings from both sides. Within rings, diffusion seems to be the dominant transport mechanism, but within the compact we see elevated concentrations at the outside relative to the center. This is not consistent with a 1D diffusive transport model. The steep measured profiles at the edges of the rings may indicate trapping, or a slow bulk-diffusion pathway relative to a faster effective diffusion pathway in the center of the ring; but, the concentration minimum would be expected to occur further toward the outside of the ring for a typical Arrhenius diffusion model, as transport in the hotter center of the ring should outpace diffusion in the ring's exterior.

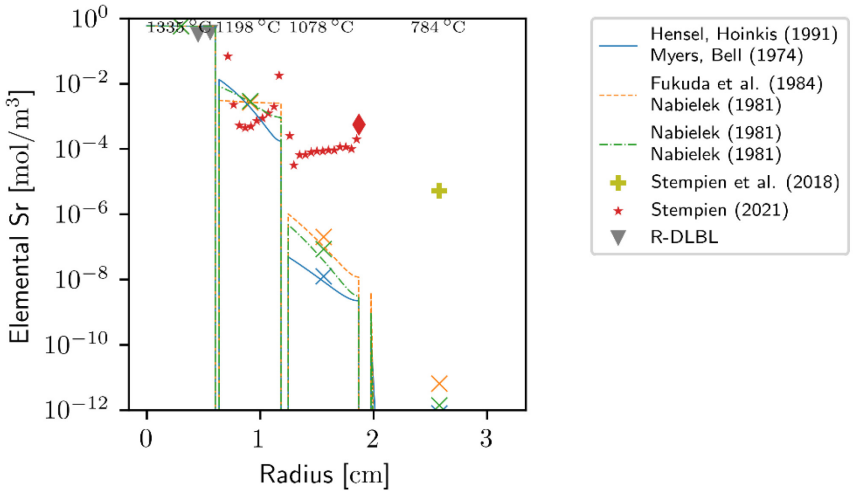

Figure 31. Capsule 7 strontium concentration profile. Model predictions using literature transport parameters are compared against available measurements. The diamond symbol represents the inventory in small nubs on the OR outer surface that were used to center the OR inside the sink ring during irradiation.

3.7.4 Europium

Transport of europium through the compact and IR of Capsule 7 is on the order of magnitude of the model predictions, though the transport to the OR is underpredicted as shown in Figure 32. The overall shape of the observed IR concentration profile is not consistent with a 1D radially diffusive model.

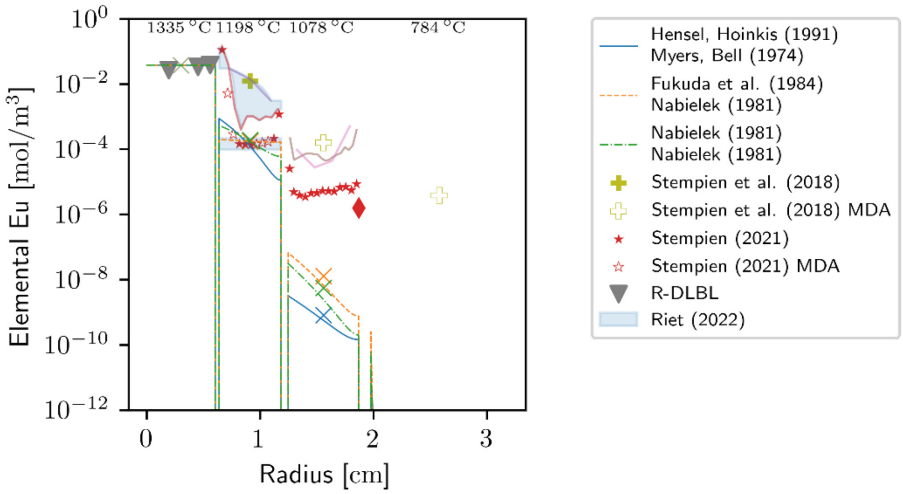

Figure 32. Capsule 7 europium concentration profile. Model predictions using literature transport parameters for strontium are compared against available measurements. The diamond symbol represents the inventory in small nubs on the OR outer surface that were used to center the OR inside the sink ring during irradiation.

3.8 Capsule 8

Capsule 8 is a standard capsule containing the only IG-110 IR used in AGR-3/4, one of two IG-110 ORs (the other was in Capsule 9), and a sink ring made of PCEA. Capsule 8 compacts had burnups of 14.43–14.58% FIMA, with fast neutron fluences of 5.02–5.13 (10^{25} n/m^2, E > 0.18 MeV) at the end of irradiation (Collin et al. 2018). The time-average peak temperature within the compacts was 1257°C. The TAVA irradiation temperature of the compacts, inner, outer, and sink rings were 1190, 1021, 917, and 582°C, respectively (Hawkes 2016), and the calculated axial variation in temperature was less than 141°C for the compacts, 66°C for the IR and 37°C for the OR.

3.8.1 Cesium

The fission product profile of cesium for each ring out to the sink ring in Capsule 8, shown in Figure 33, is lower than was predicted by the model using the literature parameters. Within the sink ring, we observe higher cesium concentrations than any of the literature-based models would predict. This is consistent with the profiles found in other rings and indicates that a low-resistance pathway is available for cesium transport outside of the rings.

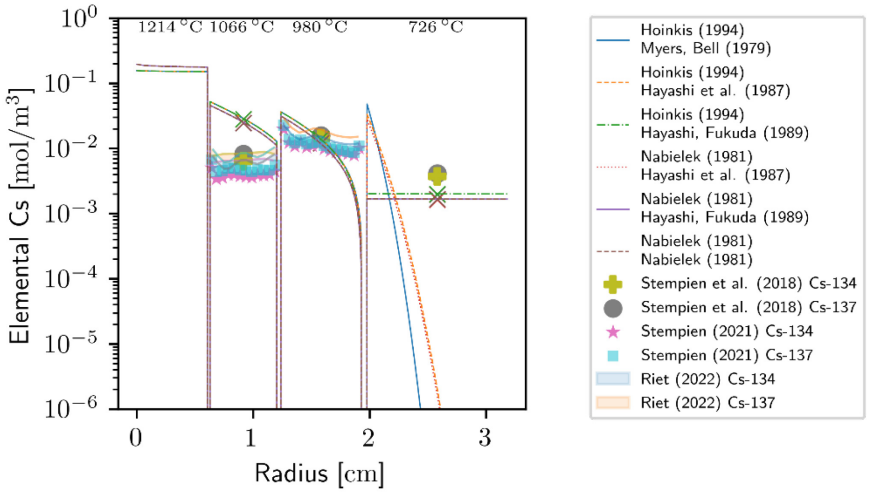

Figure 33. Capsule 8 cesium concentration profile. Model predictions using literature transport parameters are compared against available measurements.

3.8.2 Silver

The final measured radial concentration profile shown in Figure 34 does not follow a diffusive transport model with a source in the compact. The overall transport to the sink ring, however, is in good agreement with several literature parameter-based models.

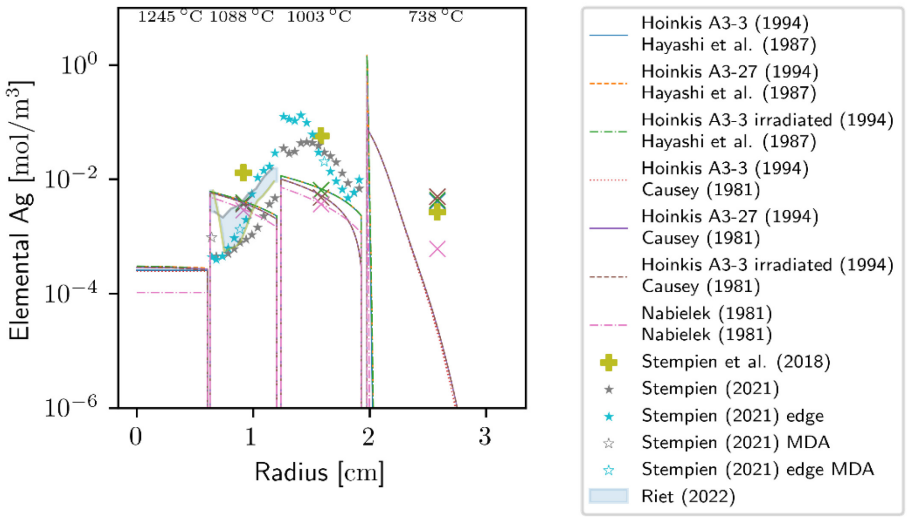

Figure 34. Capsule 8 silver concentration profile. Model predictions using literature transport parameters are compared against available measurements. The open symbol denotes a value derived from an MDA.

3.8.3 Strontium

Strontium transport through Capsule 8 is underpredicted by modeled literature parameters at every experimentally measured location. As can be seen in Figure 35, the measured profiles are smooth, which could imply that radial diffusion is the dominant mode of transport, but the increased concentrations at the outer surface indicate that radial diffusion inward from the outside of the rings toward the center is also a possible mechanism allowed by gas-gap transport around the ring to its outer surface. The very flat

concentration profile in the center of the OR may indicate a fast diffusive regime at low concentrations, or within limited internal geometries such as grain boundaries that would saturate at a lower concentration than is available through the slow diffusion mechanism observed by the slope of the profile at the edges of the rings. See also the discussion in Section 3.3.3.

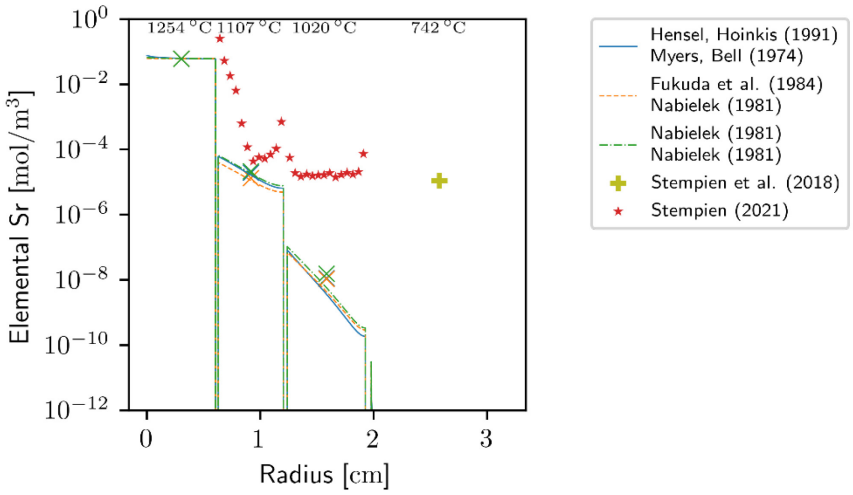

Figure 35. Capsule 8 strontium concentration profile. Model predictions using literature transport parameters are compared against available measurements.

3.8.4 Europium

Europium concentration as a function of radial position in Capsule 8 is shown in Figure 36. The measured concentration profiles have regions that indicate both faster and slower diffusion than the model predicts for any literature parameters. Specifically, for the inner section of the IR, the steep concentration profile would seem to indicate a small diffusive transport coefficient relative to the time available for transport. This is inconsistent with results from the OR. The OR, at approximately 80°C colder than the IR, is expected to have slower diffusion than the IR. This can be seen by the relative slopes of the lines in Figure 36 for any of the modeled literature parameters. The available concentration measurements of the OR suggest, however, that there may be faster (closer to equilibrium) transport through the outside of the OR than the IR. The material composition of Capsule 8 IR and OR is the same (IG-110). Indications from the tomographic scans show that the concentration of both rings vary primarily as a function of radius, not azimuthal angle (Riet 2022), which renders implausible the idea of a hot region in the ring with higher-than-expected transport, or a localized structure such as a single crack which would allow faster diffusion. Furthermore, in the OR, the bulk gamma scans and a number of the physical sampling data points, are derived from MDAs (Stempien et al. 2018; Stempien 2021). This leads to uncertainty as to the concentration profile within the inner section of the OR.

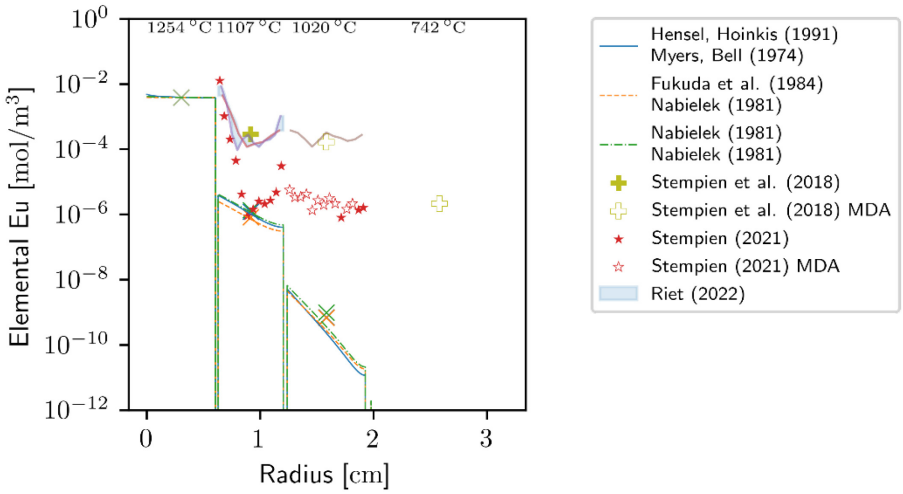

Figure 36. Capsule 8 europium concentration profile. Model predictions using literature transport parameters are compared against available measurements. Open symbols denote values derived from an MDA.

3.9 Capsule 9

Capsule 9 is a FB capsule that was retained intact. Its IR was made of matrix material, its OR was made of IG-110, and its sink ring was PCEA. Capsule 9 compacts had burnups of 13.40-13.87% FIMA, and fast neutron fluences of 4.53-4.76 (10^{25} n/m^2, E > 0.18 MeV) at the end of irradiation (Collin et al. 2018). The time-average peak temperature within the compacts was 1083°C. The TAVA irradiation temperature of the compacts, inner, outer and sink rings were 1008, 822, 698 and 608°C respectively (Hawkes 2016), and the calculated axial variation in temperature was less than 168°C for the compacts, 106°C for the IR and 28°C for the OR. Because the Capsule 9 FB was retained intact data on the IR and ORs are unavailable.

3.9.1 Cesium

Cesium transport to the sink ring in Capsule 9 is underpredicted by literature-based models, as shown in Figure 37. Discussions surrounding the likely phenomena involved can be found in Section 4.1.

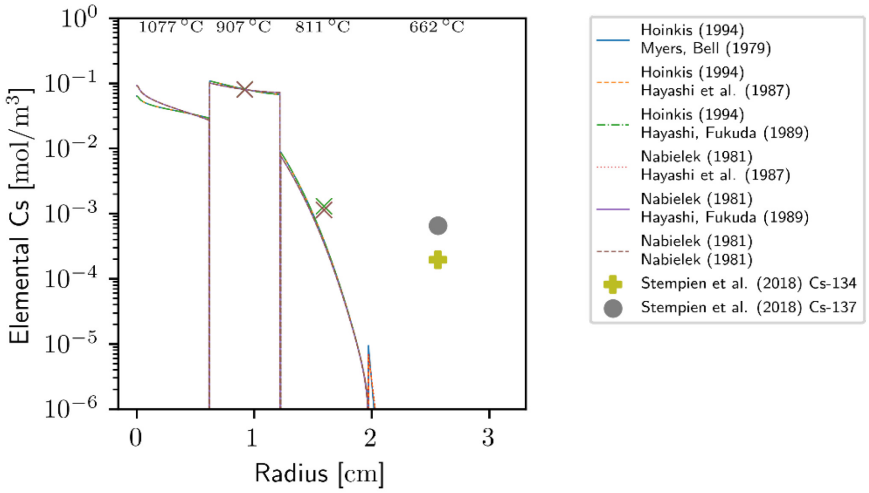

Figure 37. Capsule 9 cesium concentration profile. Model predictions using literature transport parameters are compared against available measurements.

3.9.2 Silver

Silver transport through Capsule 9 has no measured data to validate the model results, though the MDA of Ag-110m in measurements of the sink ring is 10^{-4} mol/m^3, which places an upper bound on the possible concentration in the sink ring, see Figure 38.

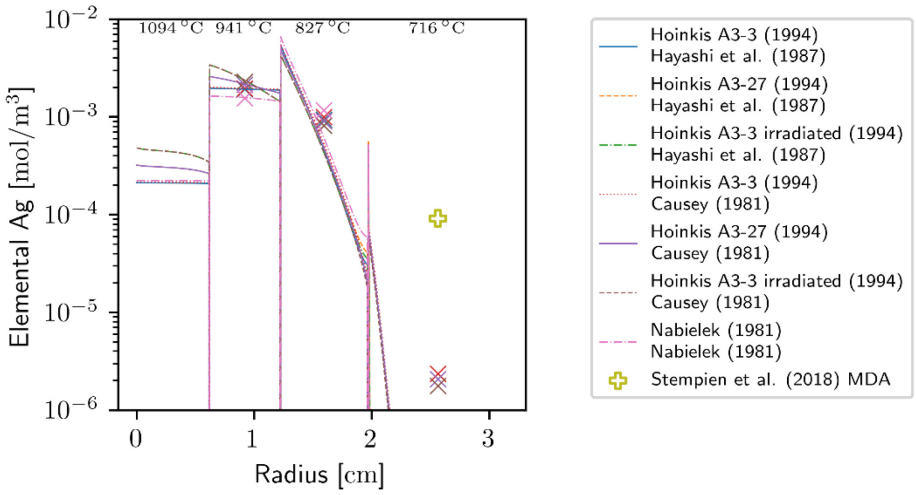

Figure 38. Capsule 9 silver concentration profile. Model predictions using literature transport parameters are compared against available measurements. Open symbols denote values derived from an MDA.

3.9.3 Strontium

Strontium transport through Capsule 9, shown in Figure 39, is not well described by the modeled literature parameters, with the average observed concentration in the sink ring almost two orders of magnitude higher than the modeled IR inner surface concentration.

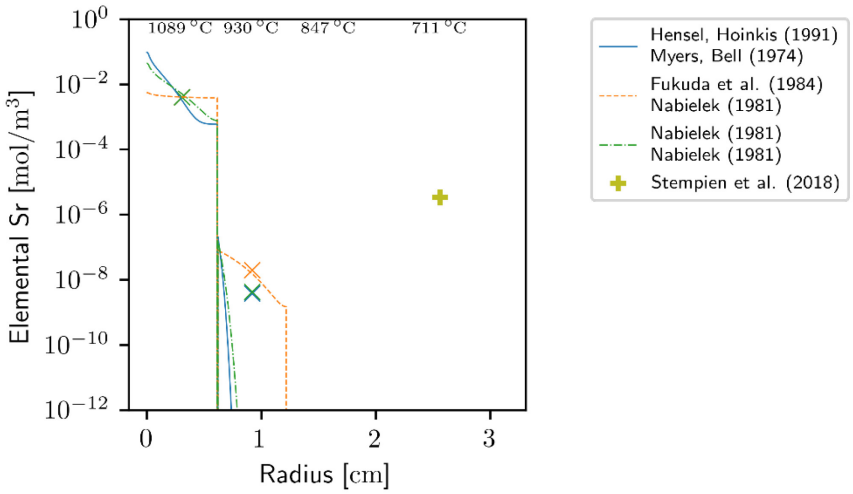

Figure 39. Capsule 9 strontium concentration profile. Model predictions using literature transport parameters are compared against available measurements.

3.9.4 Europium

Figure 40 shows the modeled radial concentration profiles for europium. Again, the strontium transport parameters were used in the absence of available parameters specifically for europium. Only the sink ring of the Capsule 9 FB was measured via gamma spectrometry and destructive burn-leach analyses. No europium-154 was detected in the sink ring; thus, an MDA is shown. There are no available measurement data to compare to in this instance.

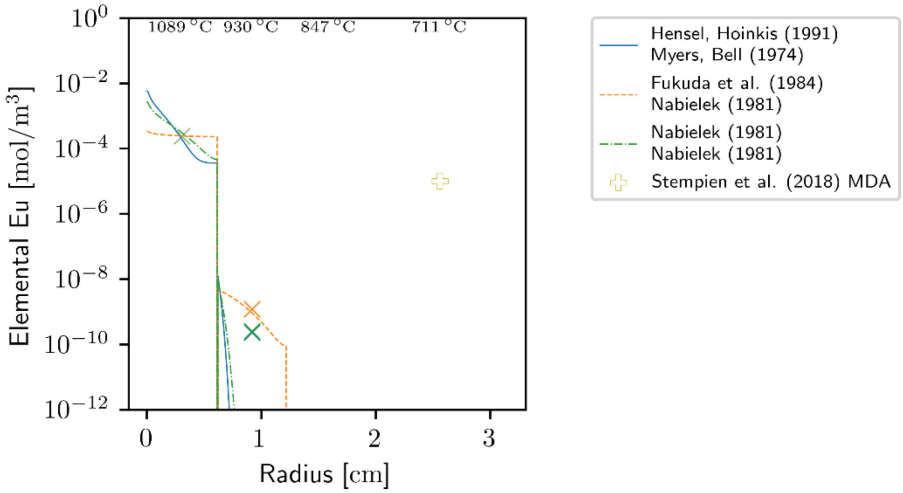

Figure 40. Capsule 9 europium concentration profiles. Model predictions for europium use literature transport parameters from strontium. The open symbol denotes a value derived from an MDA.

3.10 Capsule 10

Capsule 10 is a standard capsule with all rings made from PCEA, similar to Capsule 3. Capsule 10 compacts have burnup of 11.43–12.08% FIMA and compact fast neutron fluences of 3.75–4.12 (10^{25} n/m^2, E > 0.18 MeV) at the end of irradiation (Collin et al. 2018). The time-average peak temperature

within the compacts was 1249°C. The TAVA irradiation temperature of the compacts, inner, outer, and sink rings were 1191, 1038, 971, and 646°C respectively (Hawkes 2016), and the calculated axial variation in temperature was less than 129°C for the compacts, 34°C for the IR and 12°C for the OR.

3.10.1 Cesium

The observed concentration profiles in Capsule 10 are consistent with modeled literature parameters for the inner, outer, and sink rings. The nubs (diamond shape icons in Figure 41) on the outside of the Capsule 10 OR and those on the outside of Capsule 7 are of particular interest, as the outer diameters of the ORs are very similar, but we observe an increase in concentration here at the outside of Capsule 10, but a decrease in concentration at the outside of Capsule 7. The TAVA temperature of the Capsule 10 OR is 68°C cooler than in the Capsule 7 OR.

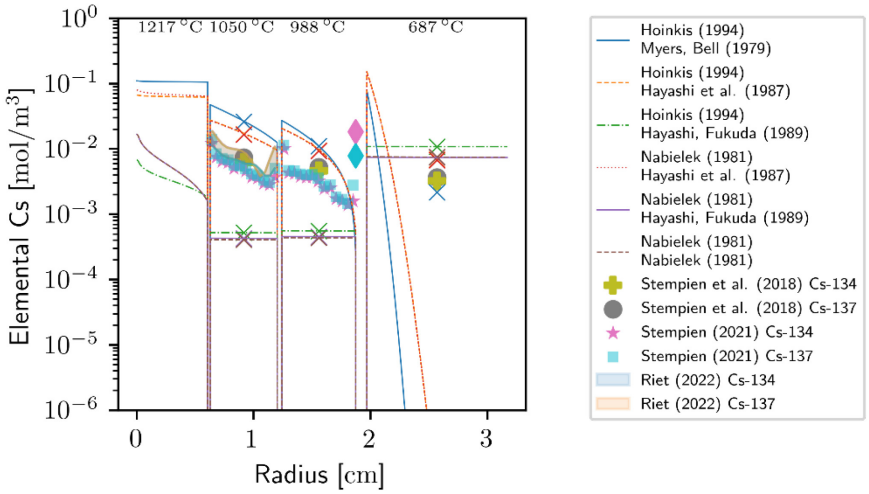

Figure 41. Capsule 10 cesium concentration profile. Model predictions using literature transport parameters are compared against available measurements. The diamond symbols represent the inventory in small nubs on the OR outer surface that were used to center the OR inside the sink ring during irradiation.

3.10.2 Silver

Silver transport through Capsule 10 is generally well represented by modeling it using the parameters from Hoinkis and Causey (Hoinkis 1994; Causey and Wichner 1981). The mechanism of transport is not well understood, though given the complexity of the measured radial concentration profiles in Figure 42, predictions based on the literature diffusion parameters fit the observations more accurately than would reasonably be expected.

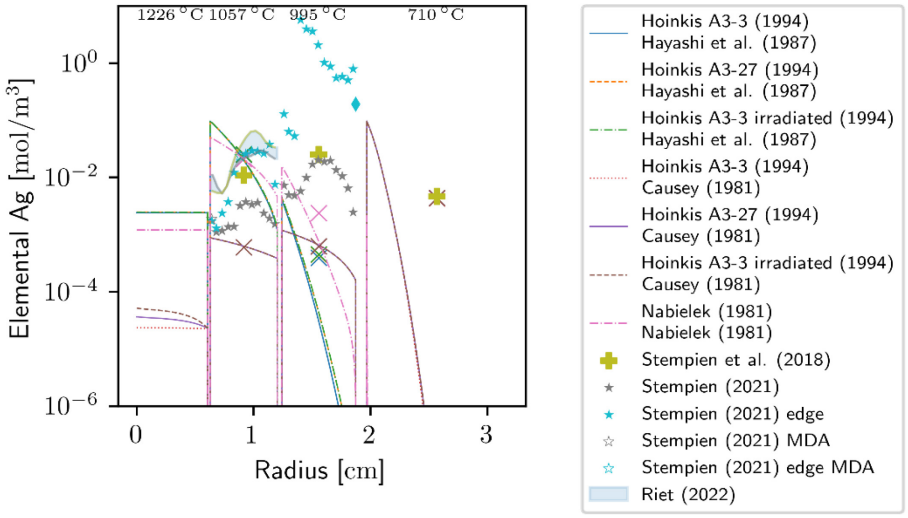

Figure 42. Capsule 10 silver concentration profile. Model predictions using literature transport parameters are compared against available measurements. Open symbols denote values derived from MDAs.

3.10.3 Strontium

Observations of strontium transport through Capsule 10 show that there is much more transport through the rings than the models would predict, as shown in Figure 43. The large, measured concentration of strontium on the inner segments of the IR also indicate that the total modeled release of strontium is too low.

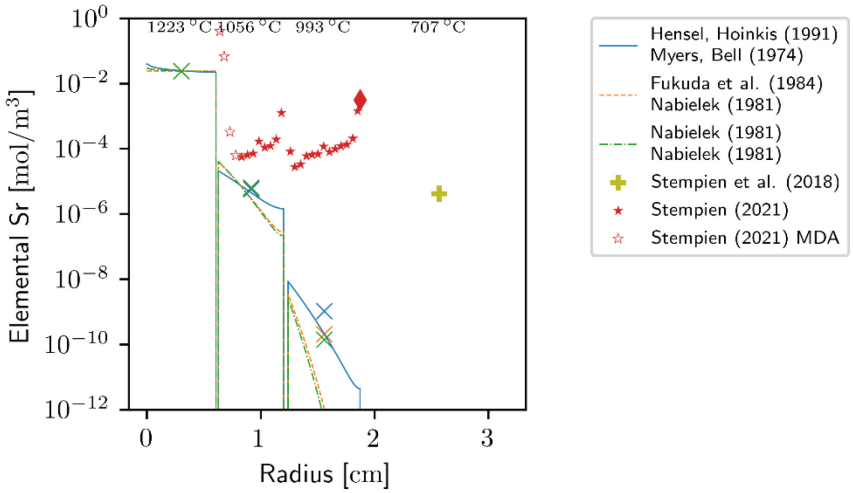

Figure 43. Capsule 10 strontium concentration profile. Model predictions using literature transport parameters are compared against available measurements. The diamond symbol represents the inventory in small nubs on the OR outer surface that were used to center the OR inside the sink ring during irradiation. Open symbols denote values derived from MDAs.

3.10.4 Europium

Europium transport through Capsule 10 has a similar profile to that observed in Capsule 8. Modeled literature parameters underpredicted the amount of transport to the IR and OR. If a diffusive model is assumed, one would expect the smallest concentration gradients to be in regions of fast diffusion, with

large concentration gradients in regions of slow diffusion. Contrary to this expected result, in Figure 41 we observe large concentration gradients on the relatively high-temperature inner sections of the IR, followed by smaller, and inverted, concentration gradients on the outer segments of both the IR and ORs. This implies the necessity of a sensitive and possibly complex model to properly interpret the results.

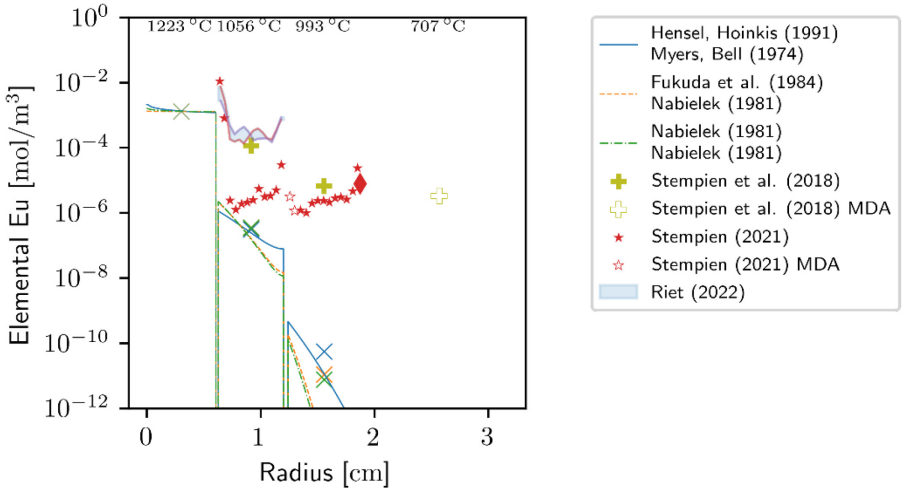

Figure 44. Capsule 10 europium concentration profile. Model predictions using literature transport parameters for strontium are compared against available measurements. Open symbols denote values derived from MDAs.

3.11 Capsule 11

Capsule 11 is a FB with a matrix IR and PCEA outer and sink rings. It was retained intact; therefore, the fission product inventories of the IR and ORs have not been measured. Capsule 11 had compact burnups of 8.42–9.64% FIMA and compact fast neutron fluences of 2.61–3.11 (10^{25} n/m^2, E > 0.18 MeV) at the end of irradiation (Collin et al. 2018). The time-average peak temperature within the compacts was 1280°C. The TAVA irradiation temperature of the compacts, inner, outer and sink rings were 1226, 1124, 966, and 737°C, respectively (Hawkes 2016), and the calculated axial variation in temperature was less than 125°C for the compacts, 77°C for the IR and 16°C for the OR.

3.11.1 Cesium

The limited experimental data available suggest that the literature-based radial diffusion models accurately predict cesium transport through the rings to the sink ring of Capsule 11, as shown in Figure 45.

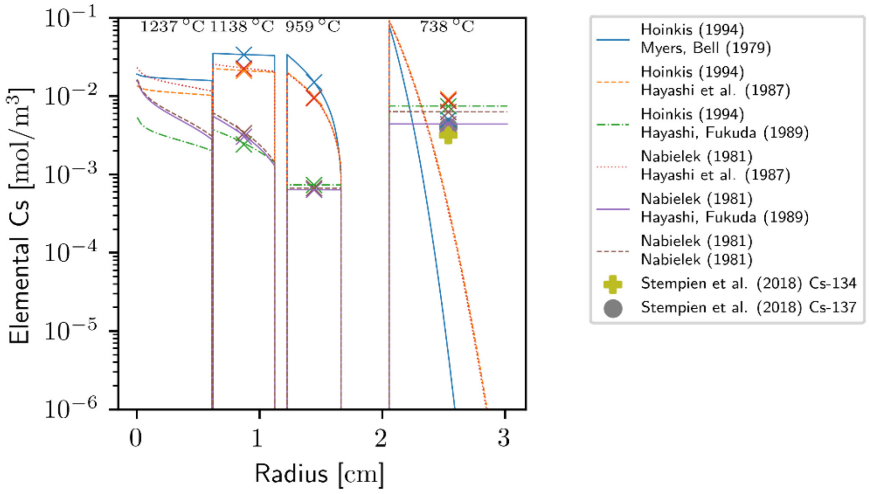

Figure 45. Capsule 11 cesium concentration profile. Model predictions using literature transport parameters are compared against available measurements.

3.11.2 Silver

Silver transport through Capsule 11 to the sink ring may be conservatively predicted by employing the diffusivity from Hoinkis (Causey and Wichner 1981; Hoinkis 1994). Figure 46 shows the predicted silver concentration profiles as a function of radial position.

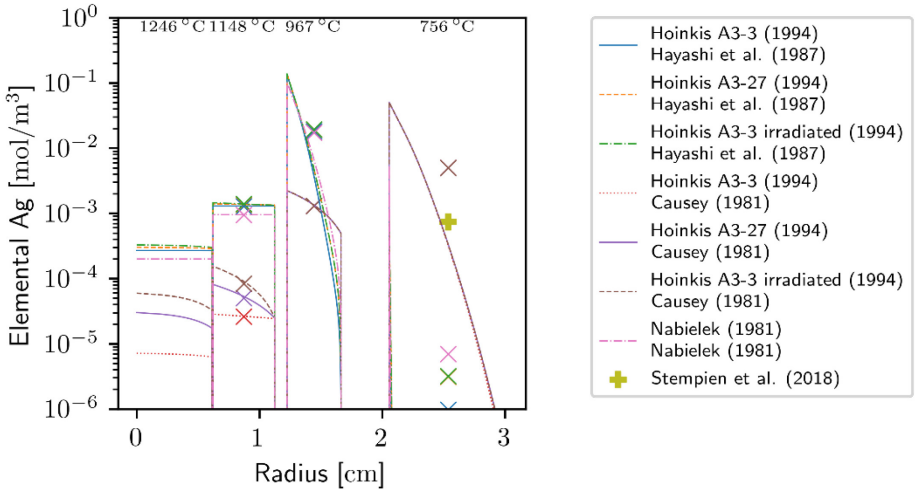

Figure 46. Capsule 11 silver concentration profile. Model predictions using literature transport parameters are compared against available measurements.

3.11.3 Strontium

We observe a much higher strontium concentration in the sink ring of Capsule 11 than is predicted by the modeled literature parameters. Figure 47 shows the predicted profiles and the experimental results.

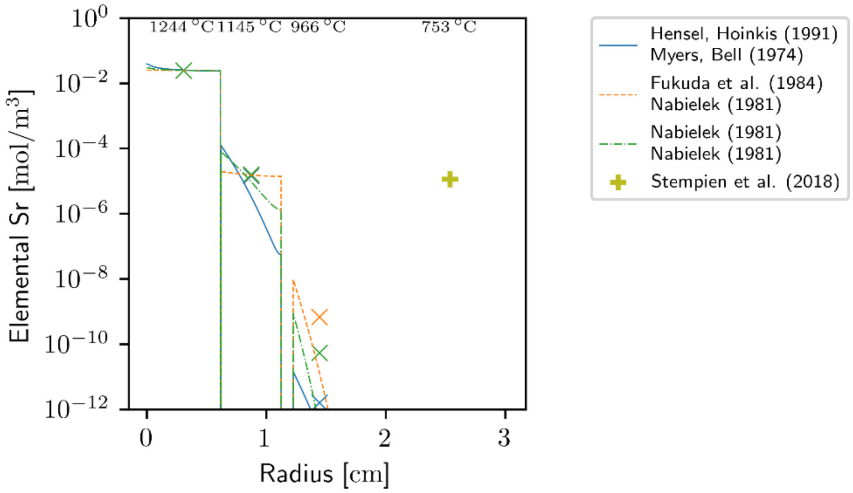

Figure 47. Capsule 11 strontium concentration profile. Model predictions using literature transport parameters are compared against available measurements.

3.11.4 Europium

Figure 48 shows the modeled radial concentration profiles for europium. Again, the strontium transport parameters were used in the absence of available parameters specifically for europium. Only the sink ring of the Capsule 11 FB was measured via gamma spectrometry and destructive burn-leach analyses. No europium-154 was detected in the sink ring; thus, an MDA is shown. There are no available measurement data to compare to in this instance.

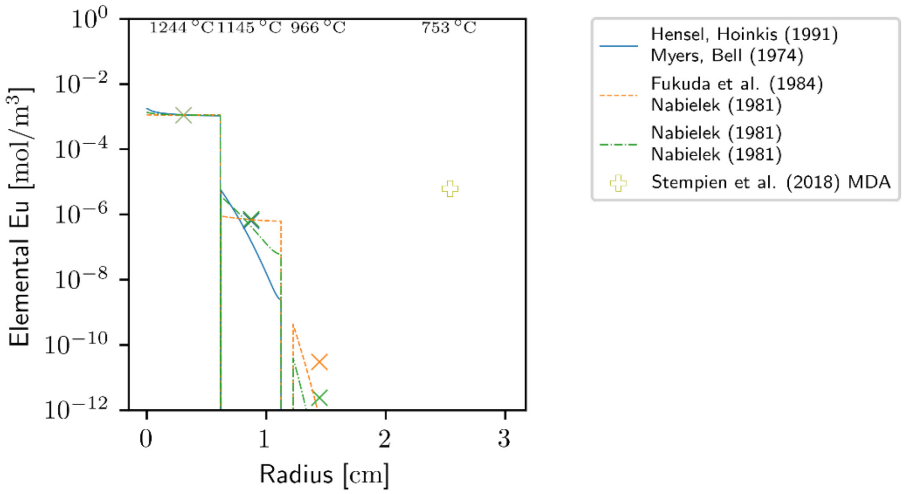

Figure 48. Capsule 11 europium concentration profile. Model predictions for europium used literature transport parameters from strontium. Only the sink ring was measured from this FB, and its europium-154 content was below the MDA. The MDA is depicted using an open symbol.

3.12 Capsule 12

Capsule 12 is a standard capsule composed of a matrix IR and PCEA outer and sink rings. Capsule 12 had compact burnups of 4.85–5.87% FIMA and compact fast neutron fluences of 1.19–1.80 (10^{25} n/m^2, E > 0.18 MeV) at the end of irradiation (Collin et al. 2018). The time-average peak temperature within the compacts was 888°C. The TAVA temperature of the compacts, inner, outer, and sink rings were 854, 782, 741, and 505°C respectively (Hawkes 2016), and the calculated axial variation in temperature was less than 79°C for the compacts, 36°C for the IR and 11°C for the OR.

Data from the R-DLBL of Compact 12-3 are also included here. Note that a thin outer portion of Compact 12-3 accounts for one of the R-DLBL data points. The second R-DLBL data point represents the relatively large center region of the compact that includes the fission product inventory in the compact matrix, driver particles, and the DTF kernels.

3.12.1 Cesium

Cesium transport through Capsule 12, shown in Figure 49, is generally consistent with the model predictions, though predictions of the sink ring inventory underestimate the measured inventory by several orders of magnitude. Given the models predict slightly higher IR fission product inventories than were measured, it is likely the high measured sink ring inventory reflects short-circuit diffusion pathways which allow transport directly to the sink ring. It is worth noting that the measured IR average inventory is very similar to the sink ring average inventory, and that the sink ring average inventory is higher than the IR's minimum internal inventory. The temperature of the sink ring is low enough to allow for condensation of cesium on the sink ring's inner surface, and is outside of the range of applicability for all sets of transport parameters except those of Nabielek (IAEA 1997; Myers and Bell 1979; Hayashi et al. 1987; Hayashi and Fukuda 1989).

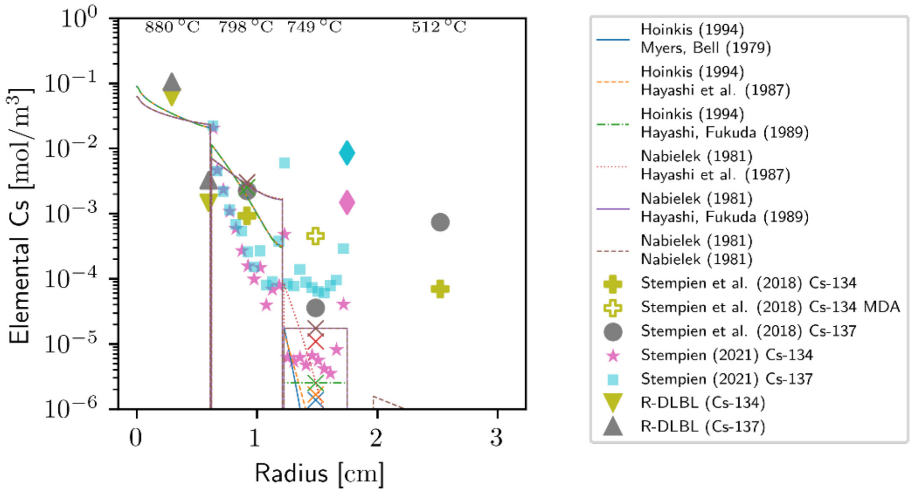

Figure 49. Capsule 12 cesium concentration profile. Model predictions using literature transport parameters are compared against available measurements. The diamond symbols represent the inventory in small nubs on the OR outer surface that were used to center the OR inside the sink ring during irradiation.

3.12.2 Silver

Silver transport through Capsule 12 is shown in Figure 50. Neither destructive physical sampling nor gamma spectroscopy detected an amount of silver above the MDA (Stempien et al. 2018; Stempien 2021).

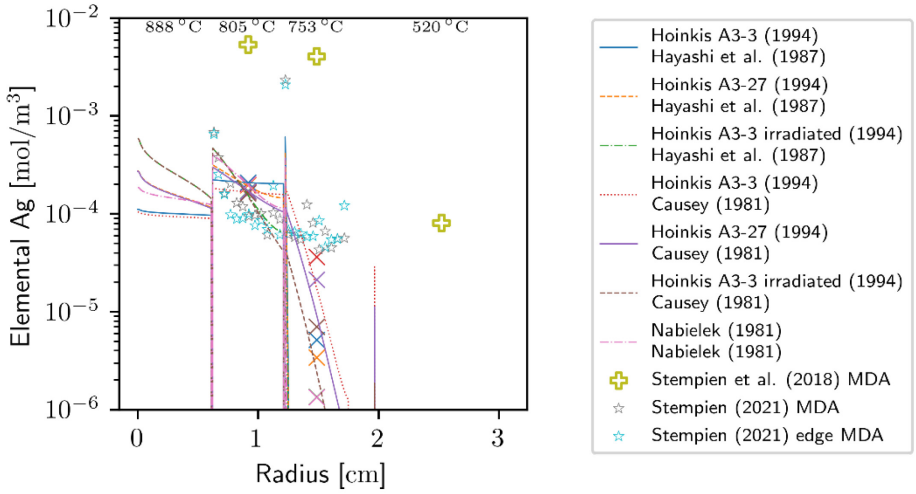

Figure 50. Capsule 12 silver concentration profile. Model predictions using literature transport parameters are compared against available measurements. The diamond symbol represents the inventory in small nubs on the OR outer surface that were used to center the OR inside the sink ring during irradiation. Open symbols denote values derived from an MDA (in this case, all measured values).

3.12.3 Strontium

Strontium transport through Capsule 12 is not well-predicted by the literature-based models, as seen in Figure 51. The R-DLBL of Compact 12-3 provided the concentration at two locations, one near the compact surface and one nearer to the compact center. This center segment includes the fission product inventory in the compact matrix, driver particles, and the DTF kernels. If a smaller center segment could have been obtained closer to the region of the DTF particles (such that it contained less matrix material and driver particles) it is likely that the measured concentration in that case nearer the compact centerline would have been higher, and thus, closer to the predicted value at the compact centerline. While the Sr concentrations in the compact are comparable with the model prediction, the measured Sr concentrations in the rings are much higher than those from the model. The flat profile observed in the OR indicates that there is a fast diffusion regime available to strontium up to a limiting concentration. Elevated concentrations at the outside of the rings indicate a potential short-circuit diffusion pathway around the rings, or a particle buildup at the cooler temperatures of the outside of the rings. Such short-circuit paths are not considered in the current model.

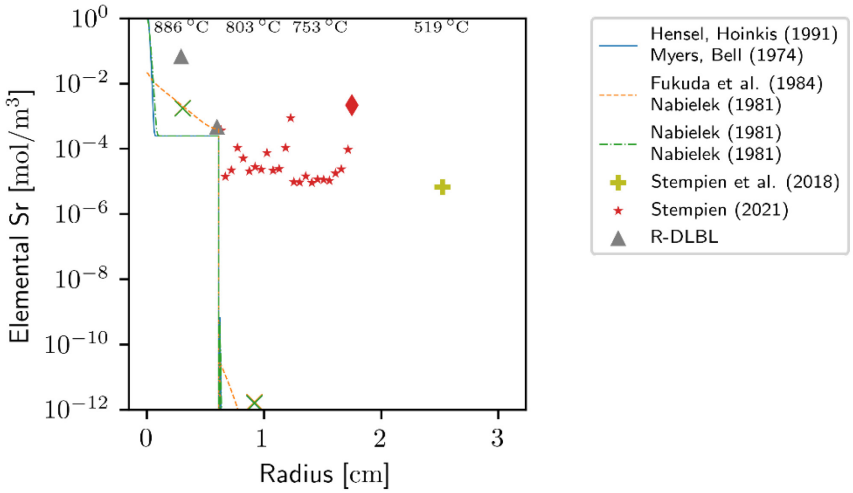

Figure 51. Capsule 12 strontium concentration profile. Model predictions using literature transport parameters are compared against available measurements. The diamond symbol represents the inventory in small nubs on the OR outer surface that were used to center the OR inside the sink ring during irradiation.

3.12.4 Europium

Europium transport through Capsule 12 is shown in Figure 52. The model of Fukuda seems to best follow the observed concentration gradient within the compacts, though the model underestimates the concentration in the compact. In the inner, outer, and sink rings, the model greatly underestimates the measured concentrations.

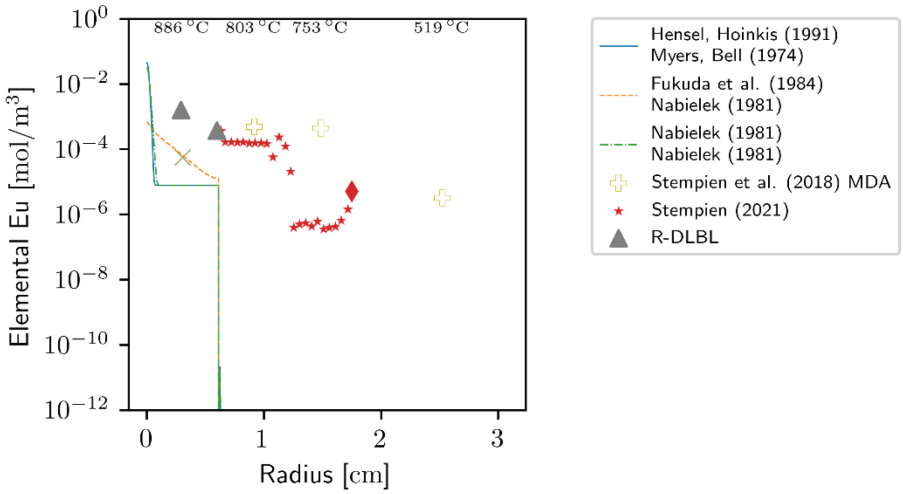

Figure 52. Capsule 12 europium concentration profile. Model predictions using literature transport parameters for strontium are compared against available measurements. The diamond symbol represents the inventory in small nubs on the OR outer surface that were used to center the OR inside the sink ring during irradiation. Open symbols denote values obtained from an MDA.

4. DISCUSSION

The existing AGR-3/4 fission product transport model was compared to the available experimental data for two main reasons. One is to see if the legacy parameters can be reasonably used to predict the observed transport. The second is to assess if the existing model accounts for sufficient transport phenomena to have meaningful predictive power. In cases where the model seems to capture the physical processes well (based on reasonably close comparisons to the measured data), the desire is to extract new diffusivities by fitting the model to the data. In cases where the model does not seem to capture some important physics, it may not be possible to extract such diffusivities unless the model can be improved.

Total capsule inventory measurements and their agreement with model predictions for different isotopes are shown for the IR in Table 5, OR in Table 6, and sink rings in Table 7. IR predictions are generally the most accurate, and we see agreement to within a factor of ten for all measured rings except in Capsules 7 and 10 for cesium. Silver transport was also in agreement to within a factor of ten, except for Capsules 5, 7, and 10. Europium transport was not in agreement with the modeled parameters. Strontium comparisons were made against physical sampling results for the IR and ORs. Transport through the OR was also often in agreement for isotopes of cesium, but silver and europium predictions were not reliable.

Table 5. Calculated to measured ratio of total capsule inventories for the IR of selected capsules. Predictions with agreement to within a factor of ten are highlighted.

		Per Capsule Calculated/Measured Ratio							
Isotope	Reference	1	3	4	5	7	8	10	12
Ag-110m	Hoinkis, E. (1994) Causey, R.A. (1981)	N/A	3.46	0.42	22.99	230.46	0.28	0.06	N/A
	Hoinkis, E. (1994) Hayashi, K. Et Al. (1987)	N/A	3.24	0.43	14.59	1.36	0.30	2.34	N/A
	Nabielek, H. (1981) Nabielek, H. (1981)	N/A	0.11	0.42	23.40	223.03	0.22	1.93	N/A
	Hoinkis, E. (1994) Hayashi, K. Et Al. (1987)	N/A	3.47	0.30	16.62	1.95	0.28	2.30	N/A
	Hoinkis, E. (1994) Causey, R.A. (1981)	N/A	0.11	0.42	23.49	219.33	0.30	0.06	N/A
	Hoinkis, E. (1994) Hayashi, K. Et Al. (1987)	N/A	3.47	0.26	13.06	89.62	0.28	2.34	N/A
Cs-134	Hoinkis, E. (1994) Myers, B.F., Bell, W.E. (1979)	7.64	3.74	1.10	1.29	19.23	4.43	4.21	3.27
	Hoinkis, E. (1994) Hayashi, K. Et Al. (1987)	7.55	3.69	1.10	1.27	3.18	4.43	2.73	3.25
	Hoinkis, E. (1994) Hayashi, K., Fukuda, K. (1989)	4.07	0.15	1.16	1.27	24.65	4.43	0.08	3.30
	Nabielek, H. (1981) Hayashi, K. Et Al. (1987)	7.62	5.74	1.12	1.31	20.66	3.87	2.70	2.75
	Nabielek, H. (1981) Hayashi, K., Fukuda, K. (1989)	2.57	0.15	1.17	1.33	1.89	3.87	0.07	2.78
	Nabielek, H. (1981) Nabielek, H. (1981)	7.02	0.14	1.18	1.34	3.14	3.87	0.07	2.78
Cs-137	Hoinkis, E. (1994) Myers, B.F., Bell, W.E. (1979)	7.64	3.74	1.10	1.29	19.23	4.43	4.21	3.27
	Hoinkis, E. (1994) Hayashi, K. Et Al. (1987)	7.55	3.69	1.10	1.27	3.18	4.43	2.73	3.25
	Hoinkis, E. (1994) Hayashi, K., Fukuda, K. (1989)	4.07	0.15	1.16	1.27	24.65	4.43	0.08	3.30
	Nabielek, H. (1981) Hayashi, K. Et Al. (1987)	7.62	5.74	1.12	1.31	20.66	3.87	2.70	2.75
	Nabielek, H. (1981) Hayashi, K., Fukuda, K. (1989)	2.57	0.15	1.17	1.33	1.89	3.87	0.07	2.78
	Nabielek, H. (1981) Nabielek, H. (1981)	7.02	0.14	1.18	1.34	3.14	3.87	0.07	2.78
Eu-154	Fukuda, K., Et Al. (1984) Nabielek, H. (1981)	0.00	0.00	N/A	N/A	0.02	0.00	0.00	N/A

		Per Capsule Calculated/Measured Ratio							
Isotope	Reference	1	3	4	5	7	8	10	12
	Hensel, W., Hoinkis, E. (1991) Myers, B.F., Bell, W.E. (1974)	0.00	0.00	N/A	N/A	0.02	0.00	0.00	N/A
	Nabielek, H. (1981) Nabielek, H. (1981)	0.00	0.00	N/A	N/A	0.01	0.00	0.00	N/A
Sr-90	Fukuda, K., Et Al. (1984) Nabielek, H. (1981)	N/A	0.36	N/A	N/A	76.39	4.14	81.70	N/A
	Hensel, W., Hoinkis, E. (1991) Myers, B.F., Bell, W.E. (1974)	N/A	0.27	N/A	N/A	82.25	6.09	73.06	N/A
	Nabielek, H. (1981) Nabielek, H. (1981)	N/A	0.34	N/A	N/A	83.57	6.77	81.91	N/A

Table 6. Calculated to measured ratio of ring inventories for the OR of selected capsules. Predictions with agreement to within a factor of ten are highlighted.

		Per Capsule Calculated/Measured Ratio						
Isotope	Reference	1	3	4	5	7	8	10
Ag-110m	Hoinkis, E. (1994) Causey, R.A. (1981)	N/A	0.01	0.79	3.31	16.92	0.08	0.02
	Hoinkis, E. (1994) Hayashi, K. Et Al. (1987)	N/A	0.10	0.58	19.15	0.19	0.11	0.02
	Nabielek, H. (1981) Nabielek, H. (1981)	N/A	0.04	0.87	3.06	17.01	0.06	0.09
	Hoinkis, E. (1994) Hayashi, K. Et Al. (1987)	N/A	0.01	4.60	15.27	0.19	0.08	0.02
	Hoinkis, E. (1994) Causey, R.A. (1981)	N/A	0.04	0.70	2.72	17.07	0.11	0.02
	Hoinkis, E. (1994) Hayashi, K. Et Al. (1987)	N/A	0.01	6.47	22.05	11.90	0.08	0.02
Cs-134	Hoinkis, E. (1994) Myers, B.F., Bell, W.E. (1979)	9.63	2.61	0.72	6.64	2.35	0.99	2.41
	Hoinkis, E. (1994) Hayashi, K. Et Al. (1987)	11.92	2.57	0.80	7.01	0.17	0.98	2.04
	Hoinkis, E. (1994) Hayashi, K., Fukuda, K. (1989)	5.06	0.22	0.36	7.36	2.85	0.98	0.12
	Nabielek, H. (1981) Hayashi, K. Et Al. (1987)	14.07	3.28	0.76	3.52	2.09	0.84	2.01
	Nabielek, H. (1981) Hayashi, K., Fukuda, K. (1989)	3.08	0.23	0.35	3.31	0.19	0.84	0.10

		Per Capsule Calculated/Measured Ratio						
Isotope	Reference	1	3	4	5	7	8	10
	Nabielek, H. (1981) Nabielek, H. (1981)	19.34	0.21	0.27	2.61	0.19	0.84	0.09
Cs-137	Hoinkis, E. (1994) Myers, B.F., Bell, W.E. (1979)	9.63	2.61	0.72	6.64	2.35	0.99	2.41
	Hoinkis, E. (1994) Hayashi, K. Et Al. (1987)	11.92	2.57	0.80	7.01	0.17	0.98	2.04
	Hoinkis, E. (1994) Hayashi, K., Fukuda, K. (1989)	5.06	0.22	0.36	7.36	2.85	0.98	0.12
	Nabielek, H. (1981) Hayashi, K. Et Al. (1987)	14.07	3.28	0.76	3.52	2.09	0.84	2.01
	Nabielek, H. (1981) Hayashi, K., Fukuda, K. (1989)	3.08	0.23	0.35	3.31	0.19	0.84	0.10
	Nabielek, H. (1981) Nabielek, H. (1981)	19.34	0.21	0.27	2.61	0.19	0.84	0.09
Eu-154	Fukuda, K., Et Al. (1984) Nabielek, H. (1981)	N/A	N/A	N/A	N/A	N/A	N/A	0.00
	Hensel, W., Hoinkis, E. (1991) Myers, B.F., Bell, W.E. (1974)	N/A	N/A	N/A	N/A	N/A	N/A	0.00
	Nabielek, H. (1981) Nabielek, H. (1981)	N/A	N/A	N/A	N/A	N/A	N/A	0.00
Sr-90	Fukuda, K., Et Al. (1984) Nabielek, H. (1981)	N/A	0.0001	N/A	N/A	3.00	0.69	0.0016
	Hensel, W., Hoinkis, E. (1991) Myers, B.F., Bell, W.E. (1974)	N/A	0.0014	N/A	N/A	0.19	0.72	0.0081
	Nabielek, H. (1981) Nabielek, H. (1981)	N/A	0.00006	N/A	N/A	1.27	0.99	0.0011

Table 7. Ratio of calculated to measured inventories for the sink ring of selected capsules. Predictions in agreement to within a factor of ten are highlighted.

		Per Capsule Calculated/Measured Ratio										
Isotope	Reference	1	2	3	4	5	6	7	8	10	11	12
Ag 110m	Hoinkis, E. (1994) Causey, R.A. (1981)	0.09	N/A	0.00	0.00	0.00	N/A	0.02	1.86	0.93	0.00	N/A
	Hoinkis, E. (1994) Hayashi, K. Et Al. (1987)	0.00	N/A	0.00	0.00	0.01	N/A	0.48	1.62	0.00	6.72	N/A
	Nabielek, H. (1981) Nabielek, H. (1981)	0.00	N/A	0.28	0.00	0.00	N/A	0.02	0.23	0.00	0.00	N/A
	Hoinkis, E. (1994) Hayashi, K. Et Al. (1987)	0.00	N/A	0.00	0.09	0.00	N/A	0.48	1.86	0.00	0.01	N/A
	Hoinkis, E. (1994) Causey, R.A. (1981)	0.07	N/A	0.28	0.00	0.00	N/A	0.02	1.62	0.93	0.00	N/A
	Hoinkis, E. (1994) Hayashi, K. Et Al. (1987)	0.00	N/A	0.00	0.14	0.01	N/A	0.18	1.85	0.00	6.73	N/A
Cs 134	Hoinkis, E. (1994) Myers, B.F., Bell, W.E. (1979)	0.01	8.37	1.82	1.90	0.15	0.01	2.17	0.53	0.68	1.38	0.01
	Hoinkis, E. (1994) Hayashi, K. Et Al. (1987)	0.13	0.42	1.77	1.62	0.21	0.00	5.87	0.53	2.14	2.74	0.01
	Hoinkis, E. (1994) Hayashi, K., Fukuda, K. (1989)	1.19	8.23	3.48	0.00	0.18	1.27	0.97	0.54	3.37	2.35	0.00
	Nabielek, H. (1981) Hayashi, K. Et Al. (1987)	0.18	8.29	0.68	1.44	0.00	1.68	1.93	0.45	2.09	2.88	0.00
	Nabielek, H. (1981) Hayashi, K., Fukuda, K. (1989)	0.56	0.08	3.81	0.00	0.00	0.01	6.19	0.45	2.30	1.58	0.00
	Nabielek, H. (1981) Nabielek, H. (1981)	9.34	0.44	3.50	0.00	0.00	1.42	5.88	0.44	2.34	1.98	0.00
Cs 137	Hoinkis, E. (1994) Myers, B.F., Bell, W.E. (1979)	0.01	8.37	1.82	1.90	0.15	0.01	2.17	0.53	0.68	1.38	0.01
	Hoinkis, E. (1994) Hayashi, K. Et Al. (1987)	0.13	0.42	1.77	1.62	0.21	0.00	5.87	0.53	2.14	2.74	0.01
	Hoinkis, E. (1994) Hayashi, K., Fukuda, K. (1989)	1.19	8.23	3.48	0.00	0.18	1.27	0.97	0.54	3.37	2.35	0.00

		Per Capsule Calculated/Measured Ratio										
Isotope	Reference	1	2	3	4	5	6	7	8	10	11	12
	Nabielek, H. (1981)											
	Hayashi, K. Et Al. (1987)	0.18	8.29	0.68	1.44	0.00	1.68	1.93	0.45	2.09	2.88	0.00
	Nabielek, H. (1981)											
	Hayashi, K., Fukuda, K. (1989)	0.56	0.08	3.81	0.00	0.00	0.01	6.19	0.45	2.30	1.58	0.00
	Nabielek, H. (1981)											
	Nabielek, H. (1981)	9.34	0.44	3.50	0.00	0.00	1.42	5.88	0.44	2.34	1.98	0.00
	Fukuda, K., Et Al. (1984)											
Eu 154	Nabielek, H. (1981)	N/A	N/A	N/A	N/A	N/A	N/A	N/A	N/A	N/A	N/A	N/A
	Hensel, W., Hoinkis, E. (1991)											
	Myers, B.F., Bell, W.E. (1974)	N/A	N/A	N/A	N/A	N/A	N/A	N/A	N/A	N/A	N/A	N/A
	Nabielek, H. (1981)											
	Nabielek, H. (1981)	N/A	N/A	N/A	N/A	N/A	N/A	N/A	N/A	N/A	N/A	N/A
	Fukuda, K., Et Al. (1984)											
Sr 90	Nabielek, H. (1981)	0.00	0.00	0.00	0.00	0.00	0.00	0.00	0.00	0.00	0.00	0.00
	Hensel, W., Hoinkis, E. (1991)											
	Myers, B.F., Bell, W.E. (1974)	0.00	0.00	0.00	0.00	0.00	0.00	0.00	0.00	0.00	0.00	0.00
	Nabielek, H. (1981)											
	Nabielek, H. (1981)	0.00	0.00	0.00	0.00	0.00	0.00	0.00	0.00	0.00	0.00	0.00

4.1 Cesium

Cesium transport through the capsules seems to be generally in line with modeled literature parameters, though we observe indications of short-circuit diffusion pathways. One short-circuit pathway currently being considered is species diffusion *around* the ring rather than through it, diffusing through the gas gap at the top and bottom edges of the ring. This would result in an increase of concentration on both sides of the ring relative to the bulk. Many of the rings and capsules exhibit smooth concentration profiles that have a clear and consistent gradient across the ring, which may allow diffusivity to be extracted via fitting to the measured concentration profiles if the right boundary conditions can be obtained. The shape of the available compact transport profiles seems to indicate slower diffusion at high temperatures in the compacts than the models would account for, though the transport to the rings is faster than the models predict. Where there is a discrepancy between Cs-134 and Cs-137, Cs-134 is thought to be a more reliable indicator of cesium concentration because it does not have a gaseous precursor and it has a much shorter half-life, which lowers the risk of picking up hot-cell contamination.

The modeled parameters seem to have a generally bi-modal distribution of concentration profiles, with some parameter sets resulting in very flat, fast-diffusing radial transport profiles and others resulting in a set of concentration profiles which are generally compatible with each other.

4.2 Silver

Silver transport in graphite and the graphitic matrix is difficult to interpret, and silver transport is fast relative to other fission product species. The predicted transport profiles are generally in agreement with observed measurements on a total inventory basis. The overall ring inventories from PGS are consistently higher than those obtained by destructive sampling in the center of the ring, indicating that silver may transport or collect at the top and bottom edges more readily than in the center of the rings, a phenomenon noted by Hayashi in 1987 (Hayashi et al. 1987). This phenomenon is also clearly evident in the axial scan profiles for Ag-110 shown in Figures 35-37 of Appendix A of (Riet 2022).

For Capsule 1, the higher-than-expected concentrations in each ring could be due to an underestimation of silver transport at low temperatures and at low concentrations. For example, the referenced paper from Hoinkis (Hoinkis 1994) used a loading of 10^{-4} atomic %, approximately two orders of magnitude higher than the 10^{-6} atomic % measured in the IR. Concentration-dependent diffusivity has been observed in cesium and strontium; however, it is not significant until 2.6×10^{-4} atomic % for cesium and 12.6×10^{-4} atomic % for strontium. Though transport properties can differ in the types of graphites used historically and those in the AGR program, we do not observe significant differences in transport between the isostatically pressed IG-110 and extruded PCEA. The magnitude of impact due to different graphite constructions is likely to be small.

It would be advisable to use the transport models with caution, as all the underlying physics are clearly not captured in the current transport model.

4.3 Strontium

Strontium transport is not well-predicted by the models using literature parameters for any capsule under study. Some of the discrepancy between literature-based predictions and experimental observations may be explained by short-circuit diffusion pathways, which would allow for the observed high concentrations at the outer edges of the rings. Furthermore, the literature parameters for diffusion of strontium seem to overpredict diffusivity in the compact of Capsule 5, so the temperature dependence of the diffusivity should be in question. Furthermore, as discussed in the report on physical sampling of the rings (Stempien 2021), there is evidence of significant Sr-90 transport via a gaseous precursor (Kr-90) and a highly volatile intermediate (Rb-90). However, the similarity in the shapes of the Eu-154 and Sr-90 profiles across rings in all capsules suggests that the dominant mechanism of Sr-90 transport is similar to that of Eu-154, and therefore, the transport of short-lived Sr-90 precursors is not a major effect (Stempien 2021).

4.4 Europium

Using the available strontium transport parameters to model europium transport (for which there are no available parameters) generally compares reasonably to measured concentrations within the few compacts subjected to R-DLBL thus far. In the hottest AGR-3/4 capsule, Capsule 7, the model does a reasonable job in comparison to the measured concentrations in the compact and IR. In Capsule 7, the shape of the predicted OR profile is similar to the shape of the profile from destructive sampling although the model underpredicts the concentrations there by factors in excess of an order of magnitude. In fact, the accuracy of the model predictions for the concentration profiles in the IRs and ORs of Capsules 8 and 10 is similar to that observed for Capsule 7. The modeled europium transport through Capsule 3 is in better agreement with experimental results than the modeled transport of strontium through Capsule 3, though transport to the rings is still underpredicted. Of the capsules where significant PIE measurements are available for comparison to the model, the model most underestimated europium transport to the Capsule 12 rings (which had the coldest irradiation temperatures).

5. CONCLUSIONS AND FUTURE WORK

Transport parameters collected over decades and compiled in IAEA TECDOC-978 were used in a transport model of the AGR-3/4 experiment, and the results of the modeling effort were compared to PIE measurements of the AGR-3/4 experiment. For overall silver transport, the agreement between the model and results may be adequate (in that the inventory in the outermost ring of the experiment is often reasonably well-predicted) but misses important characteristics of the underlying concentration profiles. Transport for cesium is accurate to within approximately one order of magnitude for all the capsules except Capsule 12, which was the coldest capsule, though the overall mobility of cesium was greater than expected. Many of the concentration profiles exhibited characteristics that indicate fast-transport pathways that circumvent the rings. It will be the subject of a future work to attempt to fit these profiles and account for the short-circuit diffusion pathways, such as accounting for gas gaps in a 2D model. Additionally, more results from R-DLBL of AGR-3/4 compacts can be considered in this analysis as they become available.

This simple model using literature transport parameters does not capture the transport of europium or strontium to within acceptable limits, and the prediction of silver transport may be described as serendipitous. More detailed models accounting for possible short-circuit diffusion pathways, possibly including gas gaps or grain boundary transport, and the process of obtaining best-fit diffusion parameters for these elements, are the subject of future work.

Destructive physical sampling of the IR and OR from the Capsule 4 FB was performed, but the radiochemical results from that work are not available as of this writing. It will be informative to compare the measured Capsule 4 concentration profiles with those of standard capsules. It is possible the FB capsules, like Capsule 4, experienced different or less short-circuit transport in the gas gaps between rings than the standard capsules. This could lend the Capsule 4 measurements to closer comparisons with the 1D transport in the current AGR-3/4 model.

6. REFERENCES

Causey, Rion A, and R. P. Wichner. 1981. “Silver Transport in H-451 Graphite.” In Colloquium on the Transport of Fission Products in Matrix and Graphite. Oak Ridge National Laboratory.

Collin, Blaise P. 2015a. “AGR-3/4 Irradiation Experiment Test Plan.” Idaho National Laboratory Report, no. PLN-3867: INL/MIS-11-22351.

Collin, Blaise P., Paul A. Demkowicz, David A. Petti, Grant L. Hawkes, Joe Palmer, Binh T. Pham, Dawn M. Scates, and James W. Sterbentz. 2018. “The AGR-3/4 Fission Product Transport Irradiation Experiment.” Nuclear Engineering and Design 327 (December 2017): 212–27. https://doi.org/10.1016/j.nucengdes.2017.12.016.

Collin, Blaise P. 2015b. “AGR-3/4 Irradiation Test Final As-Run Report.” Idaho National Laboratory, INL/EXT-15-35550. https://inldigitallibrary.inl.gov/sites/sti/sti/6305200.pdf.

Demkowicz, Paul Andrew, John D. Hunn, Robert N. Morris, Isabella J. van Rooyen, Tyler J. Gerczak, Jason M. Harp, and Scott A. Ploger. 2015. “AGR-1 Post Irradiation Examination Final Report.” Idaho National Laboratory Report, INL/EXT-15-36407. https://www.osti.gov/biblio/1236801%0Ahttps://www.osti.gov/servlets/purl/1236801.

Fukuda, Kousaku, Tomotsugu Sawai, and Katsuichi Ikawa. 1984. “Diffusion of Fission Products in Matrix Graphite for VHTR Fuel Compacts.” Journal of Nuclear Science and Technology 21 (2): 126–32. https://doi.org/10.1080/18811248.1984.9731023.

Harp, Jason M, John D Stempien, and Paul A Demkowicz. 2020. “Gamma Spectrometry Examination of the AGR-3/4 Irradiation.” Idaho National Laboratory Report, INL/EXT-20-58254.

Hawkes, Grant L. 2016. “AGR-3/4 Daily As-Run Thermal Analyses.” Idaho National Laboratory, ECAR-2807.

Hayashi, Kimio, and Kousaku Fukuda. 1989. “Diffusion Coefficients of Cesium in Un-Irradiated Graphite and Comparison with Those Obtained from in-Pile Experiments.” Journal of Nuclear Materials 168 (3): 328–36. https://doi.org/10.1016/0022-3115(89)90599-0.

Hayashi, Kimio, F. Kobayashi, K. Minato, K. Ikawa, and K. Fukuda. 1987. “In-Pile Release Behavior of Metallic Fission Products in Graphite Materials of an Htgr Fuel Assembly.” Journal of Nuclear Materials 149 (1): 57–68. https://doi.org/10.1016/0022-3115(87)90498-3.

Hensel, W., and E. Hoinkis. 1991. “The Diffusion of Sr in the Graphitic Matrix A3-3 in Vacuum and in the Presence of Hydrogen.” Journal of Nuclear Materials 184 (2): 88–96. https://doi.org/10.1016/0022-3115(91)90498-V.

Hoinkis, E. 1983. “The Determination of Diffusion Coefficients of Cesium and Silver by the Release Method in As-Received, Oxidized and Neutron Irradiated Graphitic Matrix.” In Transport of Fission Products in Matrix and Graphite HMI-B 372, 77–106.

Hoinkis, E. 1994. “The Diffusion of Silver in the Graphitic Matrices A3-3 and A3-27.” Journal of Nuclear Materials 209 (2): 132–47. https://doi.org/10.1016/0022-3115(94)90288-7.

Hunn, John D., and Andrew K. Kercher. 2006. “Results from ORNL Characterization of Nominal 350 Um LEUCO Kernels from the BWXT G73V-20-69303 Composite.” Oak Ridge National Laboratory, ORNL/TM-2006/552.

Hunn, John D., Richard A. Lowden, James H. Miller, Brian C. Jolly, Michael P. Trammell, Andrew K. Kercher, Fred C. Montgomery, and Chinthaka M. Silva. 2014. “Fabrication and Characterization of Driver-Fuel Particles, Designed-to-Fail Fuel Particles, and Fuel Compacts for the US AGR-3/4 Irradiation Test.” Nuclear Engineering and Design 271: 123–30.

https://doi.org/10.1016/j.nucengdes.2013.11.020.

Hunn, John D., Michael P. Trammell, and Fred C. Montgomery. 2011. “Data Compilation for AGR-3/4 Matrix Ring Blank Lot ARB-B1.” Oak Ridge National Laboratory, ORNL/TM-2011/272.

Hunn, John D, and Richard A Lowden. 2007. “Data Compilation for AGR-3/4 Driver Fuel Coated Particle Composite LEU03-09T Revision 0.” Oak Ridge National Laboratory 27: ORNL/TM-2007/019.

Hunn, John D, and James H Miller. 2009. “Data Compilation for AGR-3/4 Designed-to-Fail (DTF) Fuel Particle Batch LEU04-02DTF” 27: ORNL/TM-2008/193.

IAEA. 1997. “Fuel Performance and Fission Product Behaviour in Gas Cooled Reactors.” International Atomic Energy Agency Report, IAEA-TECDOC-978.

Kercher, Andrew K., Brian C. Jolly, Fred C. Montgomery, G. W. Chinthaka, M. Silva, and John D. Hunn. 2011. “Data Compilation for AGR-3/4 Particle Batch LEU03-07DTF.” Oak Ridge National Laboratory, no. April: ORNL/TM-2011/109.

Mitchell, Travis R., and Paul A. Demkowicz. 2020. “Technical Program Plan for INL Advanced Reactor Technologies; Technology Development Office / Advanced Gas Reactor Fuel Development and Qualification Program PLN-3636.”

Myers, B. F., and W. E. Bell. 1979. “Cesium Transport Data for HTGR Systems.” General Atomics Report, GA-A13990.

Myers, B F, and W E Bell. 1974. “Strontium Transport Data for Htgr Systems.” General Atomics Report, GA-A13168.

Nabielek, H. 1981. “Fission Product Data from the British HTR Work.” Transport of Fission Products in Matrix and Graphite HMI-B 372, not published in proceedings.

Riet, Adriaan A. 2022. “Reconstruction of Fission Product Distribution from Tomographic Scans in TRISO Fuel Graphitic Matrix and Nuclear Grade Graphites.” Idaho National Laboratory, INL/RPT-22-67635.

Skerjanc, William F. 2016. “AGR-3/4 Irradiation Test Predictions Using PARFUME.” Idaho National Laboratory Report, INL/EXT-16-38280.

Stempien, John D. 2017. “Radial Deconsolidation and Leach-Burn-Leach of AGR-3/4 Compacts 3-3, 12-1 and 12-3.” Idaho National Laboratory Report, INL/EXT-17-43182.

Stempien, John D. 2021. “Measurement of Fission Product Concentration Profiles in AGR-3/4 TRISO Fuel Graphitic Matrix and Nuclear Graphites,” INL/EXT-21-62863.

Stempien, John D, Paul A Demkowicz, Jason M Harp, and Philip L Winston. 2018. “AGR-3/4 Experiment Preliminary Mass Balance.” Idaho National Laboratory, INL/EXT-18-46049.

Stempien, John D, Francine J Rice, Phil L Winston, and Jason M Harp. 2016. “AGR-3/4 Irradiation Test Train Disassembly and Component Metrology First Look Report.” Idaho National Laboratory, INL/EXT-16-38005.

Sterbentz, James W. 2015. “JMOCUP As-Run Daily Physics Depletion Calculation for the AGR-3/4 TRISO Particle Experiment in ATR Northeast Flux Trap.” Idaho National Laboratory, ECAR 2753.

Walton, Kyle L., Nathan S. Jacobson, Benjamin A. Kowalski, John D. Brockman, and Sudarshan K. Loyalka. 2021. “Sorption Isosteres and Isotherms of Silver on NBG-17 Graphite.” Journal of Nuclear Materials 557: 153264. https://doi.org/10.1016/j.jnucmat.2021.153264.

Appendix A
Custom MOOSE InterfaceKernel

There is not currently a Freundlich Isotherm interfacekernel in MOOSE, so the following class was developed to handle the interfacial conditions. The contribution to the residual from this class is the test function multiplied by the imbalance between the left hand side and right hand side of (4) in Section 2.4. The class definition is found in FreundlichPenaltyInterface.h and the implementation is found in FreundlichPenaltyInterface.C

Class definition (FreundlichPenaltyInterface.h):

```
#include "ADInterfaceKernel.h"

class FreundlichPenaltyInterface : public ADInterfaceKernel
{
public:
  static InputParameters validParams();
  FreundlichPenaltyInterface(const InputParameters &);

protected:
  virtual ADReal computeQpResidual(Moose::DGResidualType type) override;
  const ADMaterialProperty<Real> & _A;
  const ADMaterialProperty<Real> & _B;
  const ADMaterialProperty<Real> & _D;
  const ADMaterialProperty<Real> & _E;
  const ADMaterialProperty<Real> & _d1;
  const ADMaterialProperty<Real> & _d2;
  const ADMaterialProperty<Real> & _diff;
  const ADMaterialProperty<Real> & _diff_neighbor;
  const Real & _Rgas;
  const ADMaterialProperty<Real> & _carbon_density;
  const Real & _penalty;
  unsigned int _T_var;
  const VariableValue & _temperature;
};
```

Class implementation (FreundlichPenaltyInterface.C):

```
#include "FreundlichPenaltyInterface.h"

registerMooseObject("sorptiontestApp", FreundlichPenaltyInterface);

InputParameters
FreundlichPenaltyInterface::validParams()
{
  InputParameters params = ADInterfaceKernel::validParams();
  params.addParam<MaterialPropertyName>(
      "As",
      "As",
      " Temperature independent coefficient of concentration proportionality, intercept term");
```

```
  params.addParam<MaterialPropertyName>("Bs",
                                        "Bs",
                                        " Temperature-dependent coefficient of "
                                        "concentration-pressure proportionality, intercept term");
  params.addParam<MaterialPropertyName>(
      "Ds",
      "Ds",
      " Temperature independent coefficient of concentration-pressure proportionality order");
  params.addParam<MaterialPropertyName>(
      "Es",
      "Es",
      " Temperature dependence of order of proportion between temperature and concentration");
  params.addParam<MaterialPropertyName>(
      "d1s", "d1s", " Temperature independent coefficient of transition concentration.");
  params.addParam<MaterialPropertyName>(
      "d2s", "d2s", " Temperature dependence of transition concentration.");
  params.addParam<MaterialPropertyName>("rho", "rho", " Density of solid phase [g/cm^3]");
  params.addParam<MaterialPropertyName>("diffusivity", "D", " Diffusivity of solid phase [m/s^2]");
  params.addParam<MaterialPropertyName>("d_vapor", "D", " Diffusivity of vapor phase [m/s^2]");
  params.addParam<MaterialPropertyName>("rho", "rho", " Density of solid phase [g/cm^3]");
  params.addParam<Real>("Rgas", 8.314462, " Ideal gas constant");
  params.addParam<Real>("penalty", 1, " penalty associated with concentration imbalance");
  params.addRequiredCoupledVar("T", "Temperature");

  return params;
}

FreundlichPenaltyInterface::FreundlichPenaltyInterface(const InputParameters & parameters)
  : ADInterfaceKernel(parameters),
    _A(getADMaterialProperty<Real>("As")),
    _B(getADMaterialProperty<Real>("Bs")),
    _D(getADMaterialProperty<Real>("Ds")),
    _E(getADMaterialProperty<Real>("Es")),
    _d1(getADMaterialProperty<Real>("d1s")),
    _d2(getADMaterialProperty<Real>("d2s")),
    _diff(getADMaterialProperty<Real>("diffusivity")),
    _diff_neighbor(getADMaterialProperty<Real>("d_vapor")),
    _Rgas(getParam<Real>("Rgas")),
    _carbon_density(getADMaterialProperty<Real>("rho")),
    _penalty(getParam<Real>("penalty")),
    _T_var(coupled("T")),
    _temperature(coupledValue("T"))
{
}
ADReal
FreundlichPenaltyInterface::computeQpResidual(Moose::DGResidualType type)
{
  ADReal r = 0;
  ADReal ln_trans_conc = ln_trans_conc = _d1[_qp] - _d2[_qp] * _temperature[_qp];
  ADReal subresidual = 0;
  switch (type)
```

```
 {
  case Moose::Element:
    r = log(_u[_qp] / _carbon_density[_qp]) > ln_trans_conc
          ? _test[_i][_qp] *
              (_u[_qp] / _carbon_density[_qp] -
               pow(_neighbor_value[_qp] / exp(_A[_qp] + _B[_qp] / _temperature[_qp]),
                   _temperature[_qp] / (_D[_qp] * _temperature[_qp] + _E[_qp])))
          : _test[_i][_qp] * (-_neighbor_value[_qp] +
                              _u[_qp] / _carbon_density[_qp] *
                                exp((_A[_qp] + _B[_qp] / _temperature[_qp]) +
                                    (_D[_qp] - 1 + _E[_qp] / _temperature[_qp]) *
                                      (_d1[_qp] - _d2[_qp] * _temperature[_qp])));
    subresidual =
      _test[_i][_qp] * -_diff_neighbor[_qp] * _grad_neighbor_value[_qp] * _normals[_qp];
    break;
  case Moose::Neighbor:
    r = log(_u[_qp] / _carbon_density[_qp]) > ln_trans_conc
          ? -_test[_i][_qp] *
              (_u[_qp] / _carbon_density[_qp] -
               pow(_neighbor_value[_qp] / exp(_A[_qp] + _B[_qp] / _temperature[_qp]),
                   _temperature[_qp] / (_D[_qp] * _temperature[_qp] + _E[_qp])))
          : -_test[_i][_qp] * (-_neighbor_value[_qp] +
                               _u[_qp] / _carbon_density[_qp] *
                                 exp((_A[_qp] + _B[_qp] / _temperature[_qp]) +
                                     (_D[_qp] - 1 + _E[_qp] / _temperature[_qp]) *
                                       (_d1[_qp] - _d2[_qp] * _temperature[_qp])));
    subresidual = _test_neighbor[_i][_qp] * -_diff[_qp] * _grad_u[_qp] * _normals[_qp];
    break;
 }
 return r; // + subresidual;
}
```

In addition, a custom “Arrhenius diffusion material” was added to the MOOSE model in order to facilitate temperature-dependent diffusivity, as follows:

Class definition (ADArrheniusDiffusionMaterial.h):

```
#pragma once

#include "ADMaterial.h"
#include "MooseTypes.h"

// Forward Declarations
class Function;

/**
 * Simple material with diffusivity (D) defined using an Arrhenius relation.
 */
class ADArrheniusDiffusionMaterial : public ADMaterial
{
public:
```

```
  static InputParameters validParams();

  ADArrheniusDiffusionMaterial(const InputParameters & parameters);

protected:
  virtual void computeProperties();

  const ADVariableValue & _ad_temperature;

  const Real _my_pre_exponential;
  const Real _my_activation_energy;
  const Real _my_ideal_gas_constant;
  const MaterialPropertyName _diffusivity_name;
  ADMaterialProperty<Real> & _pre_exponential;

  ADMaterialProperty<Real> & _activation_energy;
  ADMaterialProperty<Real> & _ideal_gas_constant;
  ADMaterialProperty<Real> & _diffusivity;

private:
  void setDerivatives(ADReal & prop, Real dprop_dT, const ADReal & ad_T);
};
```

Class implementation (ADArrheniusDiffusionMaterial.C)

```
#include "ADArrheniusDiffusionMaterial.h"
#include "Function.h"

#include "libmesh/quadrature.h"

registerMooseObject("sorptiontestApp", ADArrheniusDiffusionMaterial);

InputParameters
ADArrheniusDiffusionMaterial::validParams()
{
  InputParameters params = Material::validParams();

  params.addRequiredCoupledVar("temp", "Coupled Temperature");

  params.addRequiredParam<Real>("pre_exponential", "The pre-exponential term");

  params.addRequiredParam<Real>("activation_energy", "Activation energy for diffusion");
  params.addParam<Real>("ideal_gas_constant", 8.31446261815324, "Ideal gas constant");
  params.addParam<MaterialPropertyName>(
      "diffusivity_name", "D", "The name of the diffusivity variable");
  params.addClassDescription("Material model to compute diffusivity using an Arrhenius method");

  return params;
}
```

```
ADArrheniusDiffusionMaterial::ADArrheniusDiffusionMaterial(const InputParameters & parameters)
  : Material(parameters),

    _ad_temperature(adCoupledValue("temp")),
    _my_pre_exponential(isParamValid("pre_exponential") ? getParam<Real>("pre_exponential") : 0),
    _my_activation_energy(isParamValid("activation_energy") ? getParam<Real>("activation_energy")
                                                : 0),
    _my_ideal_gas_constant(isParamValid("ideal_gas_constant") ? getParam<Real>("ideal_gas_constant")
                                                  : 8.31466261815324),
    _diffusivity_name(isParamValid("diffusivity_name")
                      ? getParam<MaterialPropertyName>("diffusivity_name")
                      : "diffusivity"),
    _pre_exponential(declareADProperty<Real>("pre_exponential")),
    _activation_energy(declareADProperty<Real>("activation_energy")),
    _ideal_gas_constant(declareADProperty<Real>("ideal_gas_constant")),
    _diffusivity(declareADProperty<Real>(_diffusivity_name))
{
}

void
ADArrheniusDiffusionMaterial::setDerivatives(ADReal & prop, Real dprop_dT, const ADReal & ad_T)
{
  if (ad_T < 0)
    prop.derivatives() = 0;
  else
    prop.derivatives() = dprop_dT * ad_T.derivatives();
}

void
ADArrheniusDiffusionMaterial::computeProperties()
{
  /// TODO: Set diffusivity here

  for (unsigned int qp(0); qp < _qrule->n_points(); ++qp)
  {
    Real qp_temperature = 0;
    qp_temperature = MetaPhysicL::raw_value(_ad_temperature[qp]);
    if (qp_temperature < 0)
    {
      std::stringstream msg;
      msg << "WARNING:  In ADArrheniusDiffusionMaterial:  negative temperature!\n"
          << "\tResetting to zero.\n"
          << "\t_qp: " << qp << "\n"
          << "\ttemp: " << qp_temperature << "\n"
          << "\telem: " << _current_elem->id() << "\n"
          << "\tproc: " << processor_id() << "\n";
      mooseWarning(msg.str());
      qp_temperature = 0;
    }
    _pre_exponential[qp] = _my_pre_exponential;
    _ideal_gas_constant[qp] = _my_ideal_gas_constant;
```

```
    _activation_energy[qp] = _my_activation_energy;
    _diffusivity[qp] = _pre_exponential[qp] * exp(_activation_energy[qp] /
                                        (_ideal_gas_constant[qp] * _ad_temperature[qp]));
  }
}
```

Sample input file

```
[Mesh]
 [./fullgrid]
 type = CartesianMeshGenerator
 dim = 1
 dx = '2.37055148e-06 6.82524987e-06 1.7796352e-05 3.64871904e-05 4.80413124e-05 3.64871904e-05
1.7796352e-05 6.82524987e-06 2.37055148e-06 1.60745265e-06 1.67108422e-06 1.73719671e-06
1.80588376e-06 1.87724229e-06 1.95137262e-06 2.02837853e-06 2.10836734e-06 2.19145009e-06
2.27774154e-06 2.36736033e-06 2.46042904e-06 2.55707432e-06 2.65742695e-06 2.76162197e-06
2.86979873e-06 2.98210102e-06 3.09867715e-06 3.21968e-06 3.34526715e-06 3.47560092e-06
3.61084848e-06 3.75118186e-06 3.89677807e-06 4.0478191e-06 4.204492e-06 4.36698892e-06
4.53550708e-06 4.71024884e-06 4.89142169e-06 5.07923821e-06 5.27391605e-06 5.47567791e-06
5.68475144e-06 5.90136918e-06 6.12576842e-06 6.35819111e-06 6.59888369e-06 6.84809689e-06
7.10608552e-06 7.37310824e-06 7.64942725e-06 7.93530801e-06 8.23101884e-06 8.53683055e-06
8.85301598e-06 9.1798495e-06 9.51760649e-06 9.8665627e-06 1.02269937e-05 1.05991739e-05
1.09833762e-05 1.13798708e-05 1.17889243e-05 1.2210799e-05 1.26457516e-05 1.30940321e-05
1.35558826e-05 1.40315362e-05 1.45212152e-05 1.50251302e-05 1.55434782e-05 1.60764409e-05
1.66241833e-05 1.71868517e-05 1.77645719e-05 1.83574473e-05 1.89655565e-05 1.95889519e-05
2.02276568e-05 2.08816636e-05 2.15509312e-05 2.2235383e-05 2.29349043e-05 2.36493397e-05
2.43784911e-05 2.5122115e-05 2.58799201e-05 2.66515649e-05 2.74366553e-05 2.82347427e-05
2.90453213e-05 2.98678263e-05 3.07016319e-05 3.15460496e-05 3.24003267e-05 3.32636447e-05
3.41351182e-05 3.50137944e-05 3.58986523e-05 3.67886023e-05 3.7682487e-05 3.85790811e-05
3.94770929e-05 4.03751653e-05 4.12718779e-05 4.21657496e-05 4.30552411e-05 4.39387584e-05
4.4814657e-05 4.56812462e-05 4.65367939e-05 4.73795326e-05 4.82076651e-05 4.90193711e-05
4.98128141e-05 5.05861494e-05 5.13375314e-05 5.20651218e-05 5.27670988e-05 5.34416651e-05
5.40870572e-05 5.47015547e-05 5.5283489e-05 5.5831253e-05 5.63433094e-05 5.68181999e-05
5.72545539e-05 5.76510962e-05 5.80066552e-05 5.83201698e-05 5.85906963e-05 5.88174139e-05
5.89996307e-05 5.91367874e-05 5.92284614e-05 5.92743695e-05 5.92743695e-05 5.92284614e-05
5.91367874e-05 5.89996307e-05 5.88174139e-05 5.85906963e-05 5.83201698e-05 5.80066552e-05
5.76510962e-05 5.72545539e-05 5.68181999e-05 5.63433094e-05 5.5831253e-05 5.5283489e-05
5.47015547e-05 5.40870572e-05 5.34416651e-05 5.27670988e-05 5.20651218e-05 5.13375314e-05
5.05861494e-05 4.98128141e-05 4.90193711e-05 4.82076651e-05 4.73795326e-05 4.65367939e-05
4.56812462e-05 4.4814657e-05 4.39387584e-05 4.30552411e-05 4.21657496e-05 4.12718779e-05
4.03751653e-05 3.94770929e-05 3.85790811e-05 3.7682487e-05 3.67886023e-05 3.58986523e-05
3.50137944e-05 3.41351182e-05 3.32636447e-05 3.24003267e-05 3.15460496e-05 3.07016319e-05
2.98678263e-05 2.90453213e-05 2.82347427e-05 2.74366553e-05 2.66515649e-05 2.58799201e-05
2.5122115e-05 2.43784911e-05 2.36493397e-05 2.29349043e-05 2.2235383e-05 2.15509312e-05
2.08816636e-05 2.02276568e-05 1.95889519e-05 1.89655565e-05 1.83574473e-05 1.77645719e-05
1.71868517e-05 1.66241833e-05 1.60764409e-05 1.55434782e-05 1.50251302e-05 1.45212152e-05
1.40315362e-05 1.35558826e-05 1.30940321e-05 1.26457516e-05 1.2210799e-05 1.17889243e-05
1.13798708e-05 1.09833762e-05 1.05991739e-05 1.02269937e-05 9.8665627e-06 9.51760649e-06
9.1798495e-06 8.85301598e-06 8.53683055e-06 8.23101884e-06 7.93530801e-06 7.64942725e-06
7.37310824e-06 7.10608552e-06 6.84809689e-06 6.59888369e-06 6.35819111e-06 6.12576842e-06
5.90136918e-06 5.68475144e-06 5.47567791e-06 5.27391605e-06 5.07923821e-06 4.89142169e-06
```

4.71024884e-06 4.53550708e-06 4.36698892e-06 4.204492e-06 4.0478191e-06 3.89677807e-06
3.75118186e-06 3.61084848e-06 3.47560092e-06 3.34526715e-06 3.21968e-06 3.09867715e-06
2.98210102e-06 2.86979873e-06 2.76162197e-06 2.65742695e-06 2.55707432e-06 2.46042904e-06
2.36736033e-06 2.27774154e-06 2.19145009e-06 2.10836734e-06 2.02837853e-06 1.95137262e-06
1.87724229e-06 1.80588376e-06 1.73719671e-06 1.67108422e-06 1.60745265e-06 4.2623079e-08
4.43103284e-08 4.60633616e-08 4.78846616e-08 4.97767986e-08 5.17424322e-08 5.37843142e-08
5.5905291e-08 5.81083061e-08 6.03964029e-08 6.27727271e-08 6.52405293e-08 6.78031673e-08
7.04641093e-08 7.32269355e-08 7.60953414e-08 7.90731396e-08 8.21642623e-08 8.53727637e-08
8.8702822e-08 9.21587414e-08 9.57449542e-08 9.94660223e-08 1.03326639e-07 1.0733163e-07
1.11485956e-07 1.1579471e-07 1.20263124e-07 1.24896562e-07 1.29700526e-07 1.34680653e-07
1.39842714e-07 1.45192614e-07 1.50736391e-07 1.56480208e-07 1.62430359e-07 1.6859326e-07
1.74975444e-07 1.81583561e-07 1.88424365e-07 1.95504717e-07 2.02831569e-07 2.10411959e-07
2.18253003e-07 2.2636188e-07 2.34745826e-07 2.43412116e-07 2.52368052e-07 2.61620946e-07
2.71178103e-07 2.81046803e-07 2.91234278e-07 3.01747695e-07 3.12594124e-07 3.23780519e-07
3.35313685e-07 3.47200252e-07 3.59446642e-07 3.72059031e-07 3.8504332e-07 3.98405088e-07
4.12149559e-07 4.26281553e-07 4.40805444e-07 4.55725112e-07 4.71043893e-07 4.86764526e-07
5.028891e-07 5.19419e-07 5.36354845e-07 5.53696434e-07 5.71442678e-07 5.89591544e-07
6.08139991e-07 6.270839e-07 6.46418018e-07 6.66135887e-07 6.86229783e-07 7.0669065e-07
7.27508043e-07 7.48670061e-07 7.70163294e-07 7.91972766e-07 8.14081885e-07 8.36472396e-07
8.59124335e-07 8.82016001e-07 9.0512392e-07 9.28422825e-07 9.5188564e-07 9.75483481e-07
9.99185652e-07 1.02295967e-06 1.04677127e-06 1.07058448e-06 1.09436164e-06 1.11806347e-06
1.14164915e-06 1.16507642e-06 1.18830167e-06 1.21128008e-06 1.23396571e-06 1.2563117e-06
1.27827039e-06 1.29979352e-06 1.32083238e-06 1.34133808e-06 1.36126166e-06 1.38055439e-06
1.39916795e-06 1.41705469e-06 1.43416785e-06 1.45046182e-06 1.46589234e-06 1.4804168e-06
1.49399445e-06 1.5065866e-06 1.51815693e-06 1.52867161e-06 1.53809959e-06 1.54641271e-06
1.55358597e-06 1.55959759e-06 1.56442924e-06 1.56806607e-06 1.5704969e-06 1.57171419e-06
1.57171419e-06 1.5704969e-06 1.56806607e-06 1.56442924e-06 1.55959759e-06 1.55358597e-06
1.54641271e-06 1.53809959e-06 1.52867161e-06 1.51815693e-06 1.5065866e-06 1.49399445e-06
1.4804168e-06 1.46589234e-06 1.45046182e-06 1.43416785e-06 1.41705469e-06 1.39916795e-06
1.38055439e-06 1.36126166e-06 1.34133808e-06 1.32083238e-06 1.29979352e-06 1.27827039e-06
1.2563117e-06 1.23396571e-06 1.21128008e-06 1.18830167e-06 1.16507642e-06 1.14164915e-06
1.11806347e-06 1.09436164e-06 1.07058448e-06 1.04677127e-06 1.02295967e-06 9.99185652e-07
9.75483481e-07 9.5188564e-07 9.28422825e-07 9.0512392e-07 8.82016001e-07 8.59124335e-07
8.36472396e-07 8.14081885e-07 7.91972766e-07 7.70163294e-07 7.48670061e-07 7.27508043e-07
7.0669065e-07 6.86229783e-07 6.66135887e-07 6.46418018e-07 6.270839e-07 6.08139991e-07
5.89591544e-07 5.71442678e-07 5.53696434e-07 5.36354845e-07 5.19419e-07 5.028891e-07
4.86764526e-07 4.71043893e-07 4.55725112e-07 4.40805444e-07 4.26281553e-07 4.12149559e-07
3.98405088e-07 3.8504332e-07 3.72059031e-07 3.59446642e-07 3.47200252e-07 3.35313685e-07
3.23780519e-07 3.12594124e-07 3.01747695e-07 2.91234278e-07 2.81046803e-07 2.71178103e-07
2.61620946e-07 2.52368052e-07 2.43412116e-07 2.34745826e-07 2.2636188e-07 2.18253003e-07
2.10411959e-07 2.02831569e-07 1.95504717e-07 1.88424365e-07 1.81583561e-07 1.74975444e-07
1.6859326e-07 1.62430359e-07 1.56480208e-07 1.50736391e-07 1.45192614e-07 1.39842714e-07
1.34680653e-07 1.29700526e-07 1.24896562e-07 1.20263124e-07 1.1579471e-07 1.11485956e-07
1.0733163e-07 1.03326639e-07 9.94660223e-08 9.57449542e-08 9.21587414e-08 8.8702822e-08
8.53727637e-08 8.21642623e-08 7.90731396e-08 7.60953414e-08 7.32269355e-08 7.04641093e-08
6.78031673e-08 6.52405293e-08 6.27727271e-08 6.03964029e-08 5.81083061e-08 5.5905291e-08
5.37843142e-08 5.17424322e-08 4.97767986e-08 4.78846616e-08 4.60633616e-08 4.43103284e-08
4.2623079e-08 1.09889445e-06 1.13085482e-06 1.16373107e-06 1.19754865e-06 1.23233364e-06
1.26811282e-06 1.30491363e-06 1.34276422e-06 1.38169347e-06 1.42173097e-06 1.46290707e-06
1.50525287e-06 1.54880023e-06 1.59358182e-06 1.63963111e-06 1.68698238e-06 1.73567074e-06
1.78573216e-06 1.83720344e-06 1.89012228e-06 1.94452728e-06 2.0004579e-06 2.05795455e-06

2.11705856e-06 2.17781219e-06 2.24025866e-06 2.30444217e-06 2.37040786e-06 2.4382019e-06
2.50787142e-06 2.57946457e-06 2.65303053e-06 2.72861948e-06 2.80628264e-06 2.88607226e-06
2.96804163e-06 3.05224508e-06 3.13873801e-06 3.22757683e-06 3.31881902e-06 3.41252309e-06
3.5087486e-06 3.60755614e-06 3.70900732e-06 3.81316477e-06 3.92009213e-06 4.02985403e-06
4.14251605e-06 4.25814475e-06 4.37680761e-06 4.49857302e-06 4.62351025e-06 4.75168939e-06
4.88318137e-06 5.01805787e-06 5.15639131e-06 5.29825479e-06 5.44372203e-06 5.59286731e-06
5.74576545e-06 5.90249169e-06 6.06312165e-06 6.22773127e-06 6.39639667e-06 6.56919411e-06
6.74619988e-06 6.92749021e-06 7.11314115e-06 7.30322845e-06 7.49782746e-06 7.69701297e-06
7.9008591e-06 8.10943917e-06 8.32282549e-06 8.54108925e-06 8.76430034e-06 8.99252716e-06
9.22583644e-06 9.46429304e-06 9.70795977e-06 9.95689713e-06 1.02111631e-05 1.0470813e-05
1.07358991e-05 1.10064705e-05 1.12825726e-05 1.15642473e-05 1.18515323e-05 1.2144461e-05
1.24430622e-05 1.27473598e-05 1.30573722e-05 1.33731125e-05 1.36945879e-05 1.4021799e-05
1.43547403e-05 1.4693399e-05 1.50377551e-05 1.5387781e-05 1.5743441e-05 1.61046912e-05
1.64714787e-05 1.68437416e-05 1.72214086e-05 1.76043983e-05 1.79926194e-05 1.83859698e-05
1.87843367e-05 1.91875958e-05 1.95956113e-05 2.00082357e-05 2.0425309e-05 2.08466589e-05
2.12721003e-05 2.17014351e-05 2.21344519e-05 2.25709259e-05 2.30106188e-05 2.34532784e-05
2.38986388e-05 2.434642e-05 2.47963283e-05 2.52480557e-05 2.57012806e-05 2.61556674e-05
2.66108669e-05 2.70665162e-05 2.75222394e-05 2.79776474e-05 2.84323387e-05 2.88858993e-05
2.93379036e-05 2.97879147e-05 3.02354849e-05 3.06801565e-05 3.11214624e-05 3.1558927e-05
3.19920667e-05 3.24203912e-05 3.28434037e-05 3.3260603e-05 3.36714834e-05 3.40755364e-05
3.44722518e-05 3.48611188e-05 3.52416271e-05 3.56132682e-05 3.5975537e-05 3.63279326e-05
3.66699602e-05 3.7001132e-05 3.73209686e-05 3.76290009e-05 3.79247709e-05 3.82078331e-05
3.84777565e-05 3.87341249e-05 3.89765394e-05 3.92046185e-05 3.94180003e-05 3.96163432e-05
3.97993271e-05 3.99666544e-05 4.01180514e-05 4.02532687e-05 4.03720826e-05 4.04742954e-05
4.05597364e-05 4.06282625e-05 4.06797583e-05 4.07141372e-05 4.07313412e-05 4.07313412e-05
4.07141372e-05 4.06797583e-05 4.06282625e-05 4.05597364e-05 4.04742954e-05 4.03720826e-05
4.02532687e-05 4.01180514e-05 3.99666544e-05 3.97993271e-05 3.96163432e-05 3.94180003e-05
3.92046185e-05 3.89765394e-05 3.87341249e-05 3.84777565e-05 3.82078331e-05 3.79247709e-05
3.76290009e-05 3.73209686e-05 3.7001132e-05 3.66699602e-05 3.63279326e-05 3.5975537e-05
3.56132682e-05 3.52416271e-05 3.48611188e-05 3.44722518e-05 3.40755364e-05 3.36714834e-05
3.3260603e-05 3.28434037e-05 3.24203912e-05 3.19920667e-05 3.1558927e-05 3.11214624e-05
3.06801565e-05 3.02354849e-05 2.97879147e-05 2.93379036e-05 2.88858993e-05 2.84323387e-05
2.79776474e-05 2.75222394e-05 2.70665162e-05 2.66108669e-05 2.61556674e-05 2.57012806e-05
2.52480557e-05 2.47963283e-05 2.434642e-05 2.38986388e-05 2.34532784e-05 2.30106188e-05
2.25709259e-05 2.21344519e-05 2.17014351e-05 2.12721003e-05 2.08466589e-05 2.0425309e-05
2.00082357e-05 1.95956113e-05 1.91875958e-05 1.87843367e-05 1.83859698e-05 1.79926194e-05
1.76043983e-05 1.72214086e-05 1.68437416e-05 1.64714787e-05 1.61046912e-05 1.5743441e-05
1.5387781e-05 1.50377551e-05 1.4693399e-05 1.43547403e-05 1.4021799e-05 1.36945879e-05
1.33731125e-05 1.30573722e-05 1.27473598e-05 1.24430622e-05 1.2144461e-05 1.18515323e-05
1.15642473e-05 1.12825726e-05 1.10064705e-05 1.07358991e-05 1.0470813e-05 1.02111631e-05
9.95689713e-06 9.70795977e-06 9.46429304e-06 9.22583644e-06 8.99252716e-06 8.76430034e-06
8.54108925e-06 8.32282549e-06 8.10943917e-06 7.9008591e-06 7.69701297e-06 7.49782746e-06
7.30322845e-06 7.11314115e-06 6.92749021e-06 6.74619988e-06 6.56919411e-06 6.39639667e-06
6.22773127e-06 6.06312165e-06 5.90249169e-06 5.74576545e-06 5.59286731e-06 5.44372203e-06
5.29825479e-06 5.15639131e-06 5.01805787e-06 4.88318137e-06 4.75168939e-06 4.62351025e-06
4.49857302e-06 4.37680761e-06 4.25814475e-06 4.14251605e-06 4.02985403e-06 3.92009213e-06
3.81316477e-06 3.70900732e-06 3.60755614e-06 3.5087486e-06 3.41252309e-06 3.31881902e-06
3.22757683e-06 3.13873801e-06 3.05224508e-06 2.96804163e-06 2.88607226e-06 2.80628264e-06
2.72861948e-06 2.65303053e-06 2.57946457e-06 2.50787142e-06 2.4382019e-06 2.37040786e-06
2.30444217e-06 2.24025866e-06 2.17781219e-06 2.11705856e-06 2.05795455e-06 2.0004579e-06
1.94452728e-06 1.89012228e-06 1.83720344e-06 1.78573216e-06 1.73567074e-06 1.68698238e-06

1.63963111e-06 1.59358182e-06 1.54880023e-06 1.50525287e-06 1.46290707e-06 1.42173097e-06
1.38169347e-06 1.34276422e-06 1.30491363e-06 1.26811282e-06 1.23233364e-06 1.19754865e-06
1.16373107e-06 1.13085482e-06 1.09889445e-06 1.2443194e-07 1.29357622e-07 1.34475349e-07
1.39792373e-07 1.45316194e-07 1.51054578e-07 1.57015558e-07 1.63207445e-07 1.6963883e-07
1.76318599e-07 1.83255935e-07 1.90460328e-07 1.97941581e-07 2.05709818e-07 2.13775491e-07
2.22149389e-07 2.30842642e-07 2.39866729e-07 2.49233487e-07 2.58955112e-07 2.69044171e-07
2.79513603e-07 2.90376726e-07 3.0164724e-07 3.13339235e-07 3.2546719e-07 3.38045978e-07
3.51090868e-07 3.64617522e-07 3.78642003e-07 3.93180766e-07 4.08250661e-07 4.23868925e-07
4.40053181e-07 4.56821429e-07 4.74192039e-07 4.9218374e-07 5.10815607e-07 5.30107051e-07
5.50077795e-07 5.70747862e-07 5.9213755e-07 6.14267408e-07 6.37158205e-07 6.60830905e-07
6.85306628e-07 7.10606614e-07 7.36752178e-07 7.63764669e-07 7.91665412e-07 8.20475659e-07
8.50216528e-07 8.80908933e-07 9.12573521e-07 9.45230588e-07 9.78900006e-07 1.01360113e-06
1.0493527e-06 1.08617275e-06 1.12407851e-06 1.16308627e-06 1.20321127e-06 1.24446759e-06
1.286868e-06 1.33042383e-06 1.3751448e-06 1.42103892e-06 1.46811229e-06 1.51636896e-06
1.56581072e-06 1.61643699e-06 1.66824459e-06 1.72122759e-06 1.77537711e-06 1.83068112e-06
1.8871243e-06 1.94468778e-06 2.00334901e-06 2.06308156e-06 2.12385494e-06 2.18563441e-06
2.24838081e-06 2.31205042e-06 2.37659481e-06 2.44196068e-06 2.50808975e-06 2.57491867e-06
2.64237892e-06 2.71039671e-06 2.77889302e-06 2.84778352e-06 2.91697859e-06 2.98638341e-06
3.05589795e-06 3.1254172e-06 3.19483118e-06 3.26402525e-06 3.33288024e-06 3.40127279e-06
3.46907557e-06 3.53615772e-06 3.60238515e-06 3.66762105e-06 3.73172628e-06 3.79455995e-06
3.8559799e-06 3.91584332e-06 3.97400734e-06 4.03032968e-06 4.0846693e-06 4.13688706e-06
4.18684648e-06 4.23441436e-06 4.27946155e-06 4.32186363e-06 4.3615016e-06 4.39826259e-06
4.43204049e-06 4.46273659e-06 4.4902602e-06 4.51452918e-06 4.53547046e-06 4.55302054e-06
4.56712583e-06 4.57774305e-06 4.58483948e-06 4.5883932e-06 4.5883932e-06 4.58483948e-06
4.57774305e-06 4.56712583e-06 4.55302054e-06 4.53547046e-06 4.51452918e-06 4.4902602e-06
4.46273659e-06 4.43204049e-06 4.39826259e-06 4.3615016e-06 4.32186363e-06 4.27946155e-06
4.23441436e-06 4.18684648e-06 4.13688706e-06 4.0846693e-06 4.03032968e-06 3.97400734e-06
3.91584332e-06 3.8559799e-06 3.79455995e-06 3.73172628e-06 3.66762105e-06 3.60238515e-06
3.53615772e-06 3.46907557e-06 3.40127279e-06 3.33288024e-06 3.26402525e-06 3.19483118e-06
3.1254172e-06 3.05589795e-06 2.98638341e-06 2.91697859e-06 2.84778352e-06 2.77889302e-06
2.71039671e-06 2.64237892e-06 2.57491867e-06 2.50808975e-06 2.44196068e-06 2.37659481e-06
2.31205042e-06 2.24838081e-06 2.18563441e-06 2.12385494e-06 2.06308156e-06 2.00334901e-06
1.94468778e-06 1.8871243e-06 1.83068112e-06 1.77537711e-06 1.72122759e-06 1.66824459e-06
1.61643699e-06 1.56581072e-06 1.51636896e-06 1.46811229e-06 1.42103892e-06 1.3751448e-06
1.33042383e-06 1.286868e-06 1.24446759e-06 1.20321127e-06 1.16308627e-06 1.12407851e-06
1.08617275e-06 1.0493527e-06 1.01360113e-06 9.78900006e-07 9.45230588e-07 9.12573521e-07
8.80908933e-07 8.50216528e-07 8.20475659e-07 7.91665412e-07 7.63764669e-07 7.36752178e-07
7.10606614e-07 6.85306628e-07 6.60830905e-07 6.37158205e-07 6.14267408e-07 5.9213755e-07
5.70747862e-07 5.50077795e-07 5.30107051e-07 5.10815607e-07 4.9218374e-07 4.74192039e-07
4.56821429e-07 4.40053181e-07 4.23868925e-07 4.08250661e-07 3.93180766e-07 3.78642003e-07
3.64617522e-07 3.51090868e-07 3.38045978e-07 3.2546719e-07 3.13339235e-07 3.0164724e-07
2.90376726e-07 2.79513603e-07 2.69044171e-07 2.58955112e-07 2.49233487e-07 2.39866729e-07
2.30842642e-07 2.22149389e-07 2.13775491e-07 2.05709818e-07 1.97941581e-07 1.90460328e-07
1.83255935e-07 1.76318599e-07 1.6963883e-07 1.63207445e-07 1.57015558e-07 1.51054578e-07
1.45316194e-07 1.39792373e-07 1.34475349e-07 1.29357622e-07 1.2443194e-07 1.21321141e-06
1.26123681e-06 1.31113466e-06 1.36297563e-06 1.41683289e-06 1.47278214e-06 1.53090169e-06
1.59127258e-06 1.65397859e-06 1.71910634e-06 1.78674537e-06 1.8569882e-06 1.92993041e-06
2.00567072e-06 2.08431104e-06 2.16595654e-06 2.25071576e-06 2.33870061e-06 2.4300265e-06
2.52481235e-06 2.62318067e-06 2.72525763e-06 2.83117307e-06 2.94106059e-06 3.05505754e-06
3.17330511e-06 3.29594829e-06 3.42313596e-06 3.55502084e-06 3.69175953e-06 3.83351247e-06
3.98044394e-06 4.13272202e-06 4.29051851e-06 4.45400893e-06 4.62337238e-06 4.79879146e-06

4.98045217e-06 5.16854374e-06 5.3632585e-06 5.56479166e-06 5.77334112e-06 5.98910722e-06
6.2122925e-06 6.44310132e-06 6.68173962e-06 6.92841448e-06 7.18333374e-06 7.44670552e-06
7.71873777e-06 7.99963768e-06 8.28961115e-06 8.5888621e-06 8.89759183e-06 9.21599823e-06
9.54427505e-06 9.88261099e-06 1.02311888e-05 1.05901843e-05 1.09597655e-05 1.13400911e-05
1.17313099e-05 1.2133559e-05 1.2546963e-05 1.29716323e-05 1.34076618e-05 1.38551295e-05
1.43140949e-05 1.47845973e-05 1.52666545e-05 1.57602606e-05 1.62653848e-05 1.6781969e-05
1.73099268e-05 1.7849141e-05 1.83994619e-05 1.89607058e-05 1.95326528e-05 2.01150453e-05
2.07075857e-05 2.13099355e-05 2.19217128e-05 2.25424916e-05 2.31717994e-05 2.38091166e-05
2.44538751e-05 2.51054571e-05 2.57631944e-05 2.64263679e-05 2.7094207e-05 2.77658893e-05
2.84405413e-05 2.91172382e-05 2.97950051e-05 3.04728177e-05 3.1149604e-05 3.18242462e-05
3.24955824e-05 3.31624097e-05 3.38234868e-05 3.44775377e-05 3.51232552e-05 3.57593052e-05
3.63843313e-05 3.69969595e-05 3.7595804e-05 3.81794724e-05 3.87465716e-05 3.92957144e-05
3.98255256e-05 4.03346489e-05 4.08217532e-05 4.128554e-05 4.17247501e-05 4.21381704e-05
4.25246406e-05 4.28830603e-05 4.32123948e-05 4.35116818e-05 4.37800369e-05 4.40166595e-05
4.4220837e-05 4.43919503e-05 4.45294768e-05 4.46329947e-05 4.47021849e-05 4.47368337e-05
4.47368337e-05 4.47021849e-05 4.46329947e-05 4.45294768e-05 4.43919503e-05 4.4220837e-05
4.40166595e-05 4.37800369e-05 4.35116818e-05 4.32123948e-05 4.28830603e-05 4.25246406e-05
4.21381704e-05 4.17247501e-05 4.128554e-05 4.08217532e-05 4.03346489e-05 3.98255256e-05
3.92957144e-05 3.87465716e-05 3.81794724e-05 3.7595804e-05 3.69969595e-05 3.63843313e-05
3.57593052e-05 3.51232552e-05 3.44775377e-05 3.38234868e-05 3.31624097e-05 3.24955824e-05
3.18242462e-05 3.1149604e-05 3.04728177e-05 2.97950051e-05 2.91172382e-05 2.84405413e-05
2.77658893e-05 2.7094207e-05 2.64263679e-05 2.57631944e-05 2.51054571e-05 2.44538751e-05
2.38091166e-05 2.31717994e-05 2.25424916e-05 2.19217128e-05 2.13099355e-05 2.07075857e-05
2.01150453e-05 1.95326528e-05 1.89607058e-05 1.83994619e-05 1.7849141e-05 1.73099268e-05
1.6781969e-05 1.62653848e-05 1.57602606e-05 1.52666545e-05 1.47845973e-05 1.43140949e-05
1.38551295e-05 1.34076618e-05 1.29716323e-05 1.2546963e-05 1.2133559e-05 1.17313099e-05
1.13400911e-05 1.09597655e-05 1.05901843e-05 1.02311888e-05 9.88261099e-06 9.54427505e-06
9.21599823e-06 8.89759183e-06 8.5888621e-06 8.28961115e-06 7.99963768e-06 7.71873777e-06
7.44670552e-06 7.18333374e-06 6.92841448e-06 6.68173962e-06 6.44310132e-06 6.2122925e-06
5.98910722e-06 5.77334112e-06 5.56479166e-06 5.3632585e-06 5.16854374e-06 4.98045217e-06
4.79879146e-06 4.62337238e-06 4.45400893e-06 4.29051851e-06 4.13272202e-06 3.98044394e-06
3.83351247e-06 3.69175953e-06 3.55502084e-06 3.42313596e-06 3.29594829e-06 3.17330511e-06
3.05505754e-06 2.94106059e-06 2.83117307e-06 2.72525763e-06 2.62318067e-06 2.52481235e-06
2.4300265e-06 2.33870061e-06 2.25071576e-06 2.16595654e-06 2.08431104e-06 2.00567072e-06
1.92993041e-06 1.8569882e-06 1.78674537e-06 1.71910634e-06 1.65397859e-06 1.59127258e-06
1.53090169e-06 1.47278214e-06 1.41683289e-06 1.36297563e-06 1.31113466e-06 1.26123681e-06
1.21321141e-06 1.04279376e-06 1.08407311e-06 1.1269619e-06 1.17152086e-06 1.21781289e-06
1.26590304e-06 1.31585865e-06 1.36774935e-06 1.42164715e-06 1.47762652e-06 1.53576442e-06
1.59614036e-06 1.65883651e-06 1.72393771e-06 1.79153156e-06 1.86170847e-06 1.9345617e-06
2.01018748e-06 2.08868498e-06 2.17015643e-06 2.25470713e-06 2.34244552e-06 2.43348321e-06
2.52793502e-06 2.62591902e-06 2.72755656e-06 2.83297228e-06 2.94229412e-06 3.05565337e-06
3.17318461e-06 3.29502577e-06 3.42131804e-06 3.55220588e-06 3.68783698e-06 3.82836219e-06
3.97393546e-06 4.12471373e-06 4.28085688e-06 4.44252756e-06 4.60989108e-06 4.78311524e-06
4.96237012e-06 5.14782795e-06 5.33966278e-06 5.5380503e-06 5.7431675e-06 5.95519238e-06
6.17430358e-06 6.40068e-06 6.63450035e-06 6.87594275e-06 7.12518416e-06 7.38239987e-06
7.64776287e-06 7.9214433e-06 8.20360766e-06 8.49441814e-06 8.79403185e-06 9.10259992e-06
9.42026667e-06 9.74716864e-06 1.00834336e-05 1.04291795e-05 1.07845134e-05 1.11495301e-05
1.15243113e-05 1.1908924e-05 1.23034193e-05 1.27078311e-05 1.31221746e-05 1.35464447e-05
1.3980615e-05 1.44246356e-05 1.48784321e-05 1.53419038e-05 1.58149221e-05 1.62973291e-05
1.67889357e-05 1.72895205e-05 1.77988278e-05 1.83165666e-05 1.88424087e-05 1.93759877e-05
1.99168978e-05 2.04646922e-05 2.10188826e-05 2.1578938e-05 2.21442842e-05 2.27143029e-05

2.32883317e-05 2.38656641e-05 2.44455489e-05 2.50271914e-05 2.56097535e-05 2.6192355e-05
2.67740743e-05 2.73539507e-05 2.79309855e-05 2.85041448e-05 2.90723616e-05 2.96345391e-05
3.01895538e-05 3.0736259e-05 3.12734888e-05 3.18000622e-05 3.23147881e-05 3.28164696e-05
3.33039094e-05 3.37759151e-05 3.42313046e-05 3.46689122e-05 3.50875938e-05 3.54862334e-05
3.58637484e-05 3.62190963e-05 3.65512797e-05 3.68593528e-05 3.71424263e-05 3.7399673e-05
3.76303328e-05 3.78337173e-05 3.80092144e-05 3.81562917e-05 3.82745002e-05 3.83634771e-05
3.84229483e-05 3.845273e-05 3.845273e-05 3.84229483e-05 3.83634771e-05 3.82745002e-05
3.81562917e-05 3.80092144e-05 3.78337173e-05 3.76303328e-05 3.7399673e-05 3.71424263e-05
3.68593528e-05 3.65512797e-05 3.62190963e-05 3.58637484e-05 3.54862334e-05 3.50875938e-05
3.46689122e-05 3.42313046e-05 3.37759151e-05 3.33039094e-05 3.28164696e-05 3.23147881e-05
3.18000622e-05 3.12734888e-05 3.0736259e-05 3.01895538e-05 2.96345391e-05 2.90723616e-05
2.85041448e-05 2.79309855e-05 2.73539507e-05 2.67740743e-05 2.6192355e-05 2.56097535e-05
2.50271914e-05 2.44455489e-05 2.38656641e-05 2.32883317e-05 2.27143029e-05 2.21442842e-05
2.1578938e-05 2.10188826e-05 2.04646922e-05 1.99168978e-05 1.93759877e-05 1.88424087e-05
1.83165666e-05 1.77988278e-05 1.72895205e-05 1.67889357e-05 1.62973291e-05 1.58149221e-05
1.53419038e-05 1.48784321e-05 1.44246356e-05 1.3980615e-05 1.35464447e-05 1.31221746e-05
1.27078311e-05 1.23034193e-05 1.1908924e-05 1.15243113e-05 1.11495301e-05 1.07845134e-05
1.04291795e-05 1.00834336e-05 9.74716864e-06 9.42026667e-06 9.10259992e-06 8.79403185e-06
8.49441814e-06 8.20360766e-06 7.9214433e-06 7.64776287e-06 7.38239987e-06 7.12518416e-06
6.87594275e-06 6.63450035e-06 6.40068e-06 6.17430358e-06 5.95519238e-06 5.7431675e-06
5.5380503e-06 5.33966278e-06 5.14782795e-06 4.96237012e-06 4.78311524e-06 4.60989108e-06
4.44252756e-06 4.28085688e-06 4.12471373e-06 3.97393546e-06 3.82836219e-06 3.68783698e-06
3.55220588e-06 3.42131804e-06 3.29502577e-06 3.17318461e-06 3.05565337e-06 2.94229412e-06
2.83297228e-06 2.72755656e-06 2.62591902e-06 2.52793502e-06 2.43348321e-06 2.34244552e-06
2.25470713e-06 2.17015643e-06 2.08868498e-06 2.01018748e-06 1.9345617e-06 1.86170847e-06
1.79153156e-06 1.72393771e-06 1.65883651e-06 1.59614036e-06 1.53576442e-06 1.47762652e-06
1.42164715e-06 1.36774935e-06 1.31585865e-06 1.26590304e-06 1.21781289e-06 1.17152086e-06
1.1269619e-06 1.08407311e-06 1.04279376e-06 2.81289169e-06 2.92652018e-06 3.04466946e-06
3.16751363e-06 3.29523303e-06 3.42801442e-06 3.56605115e-06 3.70954333e-06 3.85869805e-06
4.01372957e-06 4.17485946e-06 4.34231684e-06 4.51633854e-06 4.69716926e-06 4.88506181e-06
5.08027724e-06 5.28308503e-06 5.49376325e-06 5.71259874e-06 5.93988725e-06 6.17593358e-06
6.42105171e-06 6.67556495e-06 6.93980605e-06 7.21411723e-06 7.49885035e-06 7.7943669e-06
8.10103805e-06 8.4192447e-06 8.74937739e-06 9.09183634e-06 9.44703132e-06 9.81538156e-06
1.01973156e-05 1.0593271e-05 1.10036944e-05 1.14290409e-05 1.18697738e-05 1.23263643e-05
1.27992911e-05 1.32890395e-05 1.37961014e-05 1.43209741e-05 1.48641596e-05 1.54261641e-05
1.60074967e-05 1.66086687e-05 1.7230192e-05 1.78725781e-05 1.8536337e-05 1.92219751e-05
1.99299941e-05 2.06608891e-05 2.14151464e-05 2.21932419e-05 2.29956387e-05 2.38227847e-05
2.46751102e-05 2.55530251e-05 2.64569164e-05 2.73871446e-05 2.83440414e-05 2.93279053e-05
3.03389991e-05 3.13775455e-05 3.24437239e-05 3.35376658e-05 3.46594511e-05 3.58091039e-05
3.69865877e-05 3.81918015e-05 3.94245746e-05 4.06846625e-05 4.1971742e-05 4.32854063e-05
4.46251608e-05 4.59904179e-05 4.73804929e-05 4.87945991e-05 5.02318438e-05 5.16912242e-05
5.31716233e-05 5.46718067e-05 5.61904191e-05 5.77259816e-05 5.92768896e-05 6.08414108e-05
6.24176839e-05 6.40037184e-05 6.55973942e-05 6.71964633e-05 6.87985507e-05 7.04011576e-05
7.20016644e-05 7.35973357e-05 7.51853252e-05 7.67626828e-05 7.83263614e-05 7.98732262e-05
8.14000638e-05 8.29035929e-05 8.43804763e-05 8.58273333e-05 8.72407534e-05 8.86173106e-05
8.99535789e-05 9.12461479e-05 9.24916399e-05 9.36867261e-05 9.48281448e-05 9.59127187e-05
9.69373721e-05 9.78991492e-05 9.87952311e-05 9.96229524e-05 0.000100379818 0.000101063518
0.000101671944 0.000102203201 0.000102655618 0.000103027766 0.000103318458 0.000103526765
0.000103652018 0.000103693814 0.000103652018 0.000103526765 0.000103318458 0.000103027766
0.000102655618 0.000102203201 0.000101671944 0.000101063518 0.000100379818 9.96229524e-05
9.87952311e-05 9.78991492e-05 9.69373721e-05 9.59127187e-05 9.48281448e-05 9.36867261e-05

```
9.24916399e-05 9.12461479e-05 8.99535789e-05 8.86173106e-05 8.72407534e-05 8.58273333e-05
8.43804763e-05 8.29035929e-05 8.14000638e-05 7.98732262e-05 7.83263614e-05 7.67626828e-05
7.51853252e-05 7.35973357e-05 7.20016644e-05 7.04011576e-05 6.87985507e-05 6.71964633e-05
6.55973942e-05 6.40037184e-05 6.24176839e-05 6.08414108e-05 5.92768896e-05 5.77259816e-05
5.61904191e-05 5.46718067e-05 5.31716233e-05 5.16912242e-05 5.02318438e-05 4.87945991e-05
4.73804929e-05 4.59904179e-05 4.46251608e-05 4.32854063e-05 4.1971742e-05 4.06846625e-05
3.94245746e-05 3.81918015e-05 3.69865877e-05 3.58091039e-05 3.46594511e-05 3.35376658e-05
3.24437239e-05 3.13775455e-05 3.03389991e-05 2.93279053e-05 2.83440414e-05 2.73871446e-05
2.64569164e-05 2.55530251e-05 2.46751102e-05 2.38227847e-05 2.29956387e-05 2.21932419e-05
2.14151464e-05 2.06608891e-05 1.99299941e-05 1.92219751e-05 1.8536337e-05 1.78725781e-05
1.7230192e-05 1.66086687e-05 1.60074967e-05 1.54261641e-05 1.48641596e-05 1.43209741e-05
1.37961014e-05 1.32890395e-05 1.27992911e-05 1.23263643e-05 1.18697738e-05 1.14290409e-05
1.10036944e-05 1.0593271e-05 1.01973156e-05 9.81538156e-06 9.44703132e-06 9.09183634e-06
8.74937739e-06 8.4192447e-06 8.10103805e-06 7.7943669e-06 7.49885035e-06 7.21411723e-06
6.93980605e-06 6.67556495e-06 6.42105171e-06 6.17593358e-06 5.93988725e-06 5.71259874e-06
5.49376325e-06 5.28308503e-06 5.08027724e-06 4.88506181e-06 4.69716926e-06 4.51633854e-06
4.34231684e-06 4.17485946e-06 4.01372957e-06 3.85869805e-06 3.70954333e-06 3.56605115e-06
3.42801442e-06 3.29523303e-06 3.16751363e-06 3.04466946e-06 2.92652018e-06 2.81289169e-06 '
 [../]
 [./fuel]
 type = SubdomainBoundingBoxGenerator
 bottom_left = '0 0 0'
 top_right = '0.000175 0 0'
 block_name = 'DTF'
 input = fullgrid
 block_id = 1
 [../]
 [./drvfuel]
 type = SubdomainBoundingBoxGenerator
 bottom_left = '0.000175 0 0'
 top_right = '0.006117431 0 0'
 block_id = 2
 block_name = 'DRV'
 input = fuel
 [../]
 [./iring]
 type = SubdomainBoundingBoxGenerator
 bottom_left = '0.006275 0 0'
 top_right = '0.011805 0 0'
 block_id = 3
 block_name = 'IR'
 input = drvfuel
 [../]
 [./oring]
 type = SubdomainBoundingBoxGenerator
 bottom_left = '0.012265 0 0'
 top_right = '0.01675 0 0'
 block_id = 4
 block_name = 'OR'
 input = iring
 [../]
```

```
[./sinkring]
type = SubdomainBoundingBoxGenerator
bottom_left = '0.020605 0 0'
top_right = '0.030795 0 0'
block_id = 5
block_name = 'SR'
input = oring
[../]
[./compair]
type = SubdomainBoundingBoxGenerator
bottom_left = '0.006117431 0 0'
top_right = '0.006275 0 0'
block_name = 'COMPAIR'
block_id = 6
input = sinkring
[../]
[./irair]
type = SubdomainBoundingBoxGenerator
bottom_left = '0.011805 0 0'
top_right = '0.012265 0 0'
block_name = 'INOUTAIR'
block_id = 7
input = compair
[../]
[./orair]
type = SubdomainBoundingBoxGenerator
bottom_left = '0.01675 0 0'
top_right = '0.020605 0 0'
block_name = 'SINKAIR'
block_id = 8
input = irair
[../]
 [./comptoair]
type = SideSetsAroundSubdomainGenerator
input = orair
block = 'DRV'
normal = '1 0 0'
new_boundary = 'comp_boundary'
[../]
[./airtoir]
type = SideSetsAroundSubdomainGenerator
input = comptoair
block = 'IR'
normal = '-1 0 0'
new_boundary = 'IR_left_boundary'
[../]
[./irtoair]
type = SideSetsAroundSubdomainGenerator
input = airtoir
block = 'IR'
normal = '1 0 0'
```

```
new_boundary = 'IR_right_boundary'
[../]
[./airtoor]
type = SideSetsAroundSubdomainGenerator
input = irtoair
block = 'OR'
normal = '-1 0 0'
new_boundary = 'OR_left_boundary'
[../]
[./ortosr]
type = SideSetsAroundSubdomainGenerator
input = airtoor
block = 'OR'
normal = '1 0 0'
new_boundary = 'OR_right_boundary'
[../]
[./airtosr]
type = SideSetsAroundSubdomainGenerator
input = ortosr
block = 'SR'
normal = '-1 0 0'
new_boundary = 'SR_left_boundary'
[../]
[./rename_left_right]
type = RenameBoundaryGenerator
old_boundary = 'left right'
new_boundary = 'center outer'
input = airtosr
[../]
[]

[Problem]
type = FEProblem
coord_type = RZ
rz_coord_axis = Y
[]
[Variables]
[./concentration]
block = 'DTF DRV IR OR SR'
[../]
[./partial_pressure]
block = 'COMPAIR INOUTAIR SINKAIR'
[../]
[./temperature]
[../]
[]

[ICs]
[./ppressure_ic]
type = ConstantIC
variable = partial_pressure
```

```
value = 0
[../]
[./concentration_ic]
type = ConstantIC
variable = concentration
value = 0
[../]
[./temp_ic]
type = ConstantIC
variable = temperature
value = 900
[../]
[]

[Kernels]
[./vapor_diffusion]
type=ADMatDiffusion
variable=partial_pressure
block = 'COMPAIR INOUTAIR SINKAIR'
[../]
[./pressuredt]
type = ADTimeDerivative
variable = partial_pressure
block = 'COMPAIR INOUTAIR SINKAIR'
[../]
[./solid_diffusion]
type=ADMatDiffusion
variable=concentration
block = 'DTF DRV IR OR SR'
[../]
[./diffusiondt]
type = ADTimeDerivative
variable = concentration
block = 'DTF DRV IR OR SR'
[../]
[./heat_conduction]
type = ADHeatConduction
variable = temperature
[../]
[./heat_source]
type = HeatSource
function = volumetric_heat
block = 'DTF DRV'
variable = temperature
[../]
[./conc_source]
type = ADBodyForce
variable = concentration
block = 'DTF'
function = DTFMassIsotope
[../]
```

```
 [./conc_drv_source]
 type = ADBodyForce
 variable = concentration
 block = 'DRV'
 function = DRVMassIsotope
 [../]
 []

 [InterfaceKernels]
 [./compboundaryd]
 type = FreundlichPenaltyInterface
 variable = concentration
 T = temperature
 neighbor_var=partial_pressure
 boundary = comp_boundary
 penalty = 100.000000
 [../]
 [./irboundaryd]
 type = FreundlichPenaltyInterface
 variable = concentration
 T = temperature
 neighbor_var=partial_pressure
 boundary = IR_left_boundary
  penalty = 100.000000
[../]
 [./irrboundaryd]
 type = FreundlichPenaltyInterface
 variable = concentration
 T = temperature
 neighbor_var=partial_pressure
 boundary = IR_right_boundary
  penalty = 100.000000
[../]
 [./orboundaryd]
 type = FreundlichPenaltyInterface
 variable = concentration
 T = temperature
 neighbor_var=partial_pressure
 boundary = OR_left_boundary
  penalty = 100.000000
[../]
 [./orrboundaryd]
 type = FreundlichPenaltyInterface
 variable = concentration
 T = temperature
 neighbor_var=partial_pressure
 boundary = OR_right_boundary
  penalty = 100.000000
[../]
 [./srboundaryd]
 type = FreundlichPenaltyInterface
```

```
 variable = concentration
 T = temperature
 neighbor_var=partial_pressure
 boundary = SR_left_boundary
  penalty = 100.000000
[../]
 []

 [BCs]
 [./templeft]
 type = ADNeumannBC
 variable = temperature
 boundary = center
 [../]
 [./compactrighttemp]
 type = FunctionDirichletBC
 variable = temperature
 boundary = comp_boundary
 function = Tco
 [../]
 [./irlefttemp]
 type = FunctionDirichletBC
 variable = temperature
 boundary = IR_left_boundary
 function = Tii
 [../]
 [./irrighttemp]
 type = FunctionDirichletBC
 variable = temperature
 boundary = IR_right_boundary
 function = Tio
 [../]
 [./orlefttemp]
 type = FunctionDirichletBC
 variable = temperature
 boundary = OR_left_boundary
 function = Toi
 [../]
 [./orrighttemp]
 type = FunctionDirichletBC
 variable = temperature
 boundary = OR_right_boundary
 function = Too
 [../]
 [./sinklefttemp]
 type = FunctionDirichletBC
 variable = temperature
 boundary = SR_left_boundary
 function = Tsi
 [../]
 [./sinkrighttemp]
```

```
type = FunctionDirichletBC
boundary = outer
variable = temperature
function = Tso
[../]
[./concout]
type = ADNeumannBC
variable = concentration
boundary = outer
value = 0
[../]
[]

[Materials]
[./DTFdiff]
type = ADGenericConstantMaterial
prop_names = 'thermal_conductivity'
prop_values = '2592000'
block = 'DTF DRV IR OR SR'
[../]

  [./Matrix_D]
     type = ADArrheniusDiffusionMaterial
     temp = temperature
     pre_exponential = 7.5168e+12
     activation_energy = -414000
     block = 'DTF DRV IR '
  [../]
  [./MatrixSolubility]
     type = ADGenericConstantMaterial
     prop_names = 'As Bs Ds Es d1s d2s rho'
     prop_values = '1.253000 -0.134300 -5.594000 -0.157900 6.305000 0.004345 1.600000'
     block = 'DTF DRV IR '
  [../]

  [./PCEA_D]
     type = ADArrheniusDiffusionMaterial
     temp = temperature
     pre_exponential = 1.3824e+07
     activation_energy = -364000
     block = 'OR SR'
  [../]
  [./PCEASolubility]
     type = ADGenericConstantMaterial
     prop_names = 'As Bs Ds Es d1s d2s rho'
     prop_values = '1.253000 -0.134300 -5.594000 -0.157900 6.305000 0.004345 1.840000'
     block = 'OR SR'
  [../][./Airdiff]
type = ADGenericConstantMaterial
prop_names = 'D thermal_conductivity'
prop_values = '1e-2 1'
```

```
 block = 'COMPAIR INOUTAIR SINKAIR'
 [../]

 []

 [Functions]

[./Tcenter]
 type = ConstantFunction
 value = 1269.385916
 format = columns
 [../]
 [./Tco]
 type = ConstantFunction
 value = 1236.314551
 format = columns
 [../]
 [./Tii]
 type = ConstantFunction
 value = 1177.199015
 format = columns
 [../]
 [./Tio]
  type = ConstantFunction
 value = 1151.648464
 format = columns
 [../]
 [./Toi]
 type = ConstantFunction
 value = 1052.376998
 format = columns
 [../]
 [./Too]
  type = ConstantFunction
 value = 1047.901952
 format = columns
 [../]
 [./Tsi]
 type = ConstantFunction
 value = 831.040073
 format = columns
 [../]
 [./Tso]
  type = ConstantFunction
 value = 820.167282
 format = columns
 [../]
[./volumetric_heat]
 type = PiecewiseLinear
 data_file = 'capsuledata/cap01qdot_units.csv'
 format = columns
```

```
[../]
[./DTFMassIsotope]
type = PiecewiseLinear
data_file = 'capsuledata/cap01AgDTF_units.csv'
format = columns
[../]
[./DRVMassIsotope]
type = PiecewiseLinear
data_file = 'capsuledata/cap01AgDriver_units.csv'
format = columns
[../]
[./dtfunction]
type = PiecewiseLinear
data_file = 'capsuledata/capdtimes_units.csv'
format = columns
[../]
[]

[Executioner]
type = Transient
solve_type = Newton
nl_abs_tol = 1e-10
end_time =  368.923133
petsc_options_iname = '-pc_type -pc_factor_mat_solver_package'
petsc_options_value = 'lu mumps'
[./TimeStepper]
type = FunctionDT
function = dtfunction
[../]
automatic_scaling = 1
[]

[Postprocessors]
[./parpost]
type = ElementIntegralVariablePostprocessor
variable = partial_pressure
block = 'COMPAIR INOUTAIR SINKAIR'
[../]
[./volpost]
type = ElementIntegralVariablePostprocessor
variable = concentration
block = 'DTF DRV IR OR SR'
[../]
[./meshsize]
type =  NumElems
execute_on = FINAL
[../]
[./totalconcentration]
type = ParsedPostprocessor
function = 'volpost + parpost'
pp_names ='parpost volpost'
```

```
[../]
[./DTFtotal]
type = FunctionElementIntegral
function = DTFMassIsotope
block = 'DTF'
[../]
[./DRVtotal]
type = FunctionElementIntegral
function = DRVMassIsotope
block = 'DRV'
[../]
[./SRCtime]
type = ParsedPostprocessor
function = 'DTFtotal + DRVtotal'
pp_names = 'DTFtotal DRVtotal'
[../]
[./timestep_size]
type = TimestepSize
[../]
[./integrated_time]
type = ParsedPostprocessor
function = 'SRCtime * timestep_size'
pp_names = 'SRCtime timestep_size'
[../]
[./SRCtotal]
type = CumulativeValuePostprocessor
postprocessor =integrated_time
[../]

[./irinner]
 type = SideAverageValue
  variable = concentration
  boundary = IR_left_boundary
 [../]
 [./irouter]
  type = SideAverageValue
  variable = concentration
  boundary = IR_right_boundary
 [../]
 [./orinner]
  type = SideAverageValue
  variable = concentration
  boundary = OR_left_boundary
 [../]
 [./orouter]
  type = SideAverageValue
  variable = concentration
  boundary = OR_right_boundary
 [../]
 [./srinner]
  type = SideAverageValue
```

```
  variable = concentration
  boundary = SR_left_boundary
 [../]
 [./srouter]
  type = SideAverageValue
  variable = concentration
  boundary = outer
 [../]
[]

 [Outputs]
 output_linear= false
 output_screen=false
 [./vtk]
 type = VTK
 vtk = true
 postprocessors_as_reporters = true
 execute_on = 'FINAL FAILED'
 [../]
 [./out]
 type = Exodus
 outputs = exodus
 variable = concentration
 output_material_properties = true
 show_material_properties = 'diffusivity'
 execute_on = 'timestep_end nonlinear'
 [../]
 [./csv]
 type = CSV
 execute_on = FINAL
 [../]
 [./csvconc]
  type = CSV
  execute_on =  TIMESTEP_END
  time_column= True
  show = 'irinner irouter orinner orouter srinner srouter integrated_time'
 [../]
 []
```